International
Progress Report

IPR-02-17

# Äspö Hard Rock Laboratory

## Determination of Porosity, Permeability and Diffusivity of rock samples from Äspö HRL using the Helium gas method

Jani Maaranen
Jaana Lehtioksa
Jussi Timonen

University of Jyväskylä
Department of Physics

October 2001

**Svensk Kärnbränslehantering AB**
Swedish Nuclear Fuel
and Waste Management Co
Box 5864
SE-102 40 Stockholm Sweden
Tel +46 8 459 84 00
Fax +46 8 661 57 19

Äspö Hard Rock
Laboratory

| Report no. | No. |
| --- | --- |
| IPR-02-17 | F83K |
| Author | Date |
| Maaranen, Lehtioksa, Timonen | 01-10-01 |
| Checked by | Date |
| Anders Winberg | 02-05-14 |
| Approved | Date |
| Christer Svemar | 02-07-07 |

# Äspö Hard Rock Laboratory

## Determination of Porosity, Permeability and Diffusivity of rock samples from Äspö HRL using the Helium gas method

Jani Maaranen
Jaana Lehtioksa
Jussi Timonen

University of Jyväskylä
Department of Physics

October 2001

*Keywords:* Diffusion, coefficient, Helium-gas method, Permeability, Porosity, Äspö

# Abstract

Sixteen Äspö diorite and granite rock samples from the Äspö Hard Rock Laboratory were measured for their diffusion coefficient, porosity and permeability using the helium gas method. Three of these samples were long, varying in length from 67 to 101 mm, and were later cut into smaller sub-samples on which the same properties were determined. All the long samples and one of the shorter samples contained visible fractures, and the samples broke during the measurements due to mechanical failure. It is difficult to tell if these fractures were caused by the drilling process, or whether they pre-existed in the bedrock. The granite samples contained old and healed fractures that seemed to affect the measured migration properties to some degree, especially when these fractures are subparallel with the core axis, the latter which coincided with the direction of migration. The structure of granite samples was also otherwise oriented (foliation), and an orientation dependence in their migration properties could thus be expected to occur even though this effect could not be observed in the limited set of samples with rather similar structural orientation. Also, the properties of long samples and associated shorter sub-samples were very similar. The observed anomalies in the migration properties were rather small, and for the most part could be explained by the above mentioned structural characteristics. The average values of migration properties of both granite and diorite samples closely coincided with typical values of Swedish and Finnish bedrock measured so far at JYFL, University of Jyväskylä, i.e. the average diffusion coefficient of helium in nitrogen filled samples was $10^{-9}$ $m^2/s$, the average permeability was $2 \cdot 10^{-19}$ $m^2$, and the average porosity was 0.2-0.3% for the two rock types.

# Sammanfattning

Sexton bergprover av Äspödiorit och granit från Äspölaboratoriet analyserades med heliumgasmetoden med avseende på diffusionskoefficient, porositet och permeabilitet. Tre av proverna var långa, 67-101 mm, och sågades senare upp i mindre delar och mättes på nytt. Samtliga långa prover och ett av de korta påvisade tydliga sprickor, och dessa prover gick senare sönder under mätningarna. Det är svårt att säga om dessa sprickor existerade i naturligt i bergproverna, eller om de skapades i samband med borrningen. Granitproverna innehöll äldre och läkta sprickor som verkade påverka mätresultaten i viss mån, speciellt när dessa sprickor var parallella till borrkärnans axel (= migrationsriktningen). För övrigt så innehöll granitproverna en inre struktur (foliation), som borde resultera i ett riktningsberoende i migrationsegenskaperna, även om denna effekt inte tydligt framkom vid analysen av detta bergränsade material med likartade relativ orientering. Det visade sig att egenskaperna mätta på de långa bergproverna överensstämde väl med de mätta på de kortare delproverna. Anomalierna i uppmätta egenskaper var genomgående små, och kunde i de flesta fall förklaras av strukturella skillnader enligt ovan. Medelvärden av uppmätta migrationsegenskaper hos diorit och granitprover befanns överstämma väl med typiska värden hos finsk och svensk bergrund uppmätt vid JYFL (Universitetet i Jyväskylä), dvs. ett medelvärde på diffusionskoefficienten av helium i kvävemättade prover på $10^{-9}$ $m^2/s$, en medelpermeabilitet på $2 \cdot 10^{-19}$ $m^2$, samt en medelporositet på 0.2-0.3% för de två bergarterna.

# Contents

# 1 Introduction

Matrix diffusion and other transport phenomena have been studied in the Department of Physics at the University of Jyväskylä (JYFL) since 1991. The developed helium gas methods offer versatile possibilities for analysis of migration phenomena in fractured and porous media. Porosity, permeability and effective diffusion coefficient are important factors in these phenomena, and they have traditionally been determined by liquid phase experiments. In the gas phase it is possible to make these measurements in a much shorter time scale, although one has to pay attention to problems such as drying of the samples before the measurements. In this method one can also fairly easily identify the samples which include micro-cracks or other defects produced while preparing the samples, which would display non-representative migration characteristics. The samples measured were Äspö diorite and granite bedrock samples, from which the samples porosity, effective diffusion coefficient and permeability were determined.

# 2 Description of samples

All measured samples were cylindrical with a diameter of approximately 35mm and a length of 10-50mm. The rock type of the sample was either granite or diorite. The specifications of the rock type and dimensions of the samples are shown in Table 1.

**Table 1. Sample type and dimensions.**

| type | sample | D [mm] | h [mm] | V [$cm^3$] |
|---|---|---|---|---|
| diorite | ÄD21 | 35.20 | 67.00 | 260.8 |
| diorite | ÄD22 | 35.20 | 67.30 | 262.0 |
| diorite | ÄD4 | 35.20 | 101.30 | 394.3 |
| diorite | D10 | 35.10 | 9.75 | 9.4 |
| diorite | D14 | 35.15 | 10.10 | 9.8 |
| diorite | D27 | 10.30 | 35.10 | 2.9 |
| diorite | D3 | 35.15 | 9.80 | 9.5 |
| diorite | D4 | 35.10 | 20.00 | 19.4 |
| diorite | D5 | 35.10 | 40.10 | 38.8 |
| diorite | D7 | 35.10 | 40.00 | 38.7 |
| granite | G1 | 35.10 | 10.25 | 9.9 |
| granite | G14 | 35.10 | 9.90 | 9.6 |
| granite | G2 | 35.05 | 21.50 | 20.7 |
| granite | G26 | 10.00 | 35.05 | 9.6 |
| granite | G6 | 35.15 | 40.05 | 38.9 |
| granite | G8 | 35.05 | 10.10 | 9.8 |
| diorite | 1 | 35.15 | 26.60 | 25.8 |
| diorite | 2 | 35.15 | 15.40 | 14.9 |
| diorite | 3 | 35.15 | 21.75 | 16.6 |
| diorite | 4 | 31.15 | 35.10 | 26.7 |
| diorite | 5 | 35.15 | 33.90 | 32.9 |
| diorite | 6 | 35.15 | 27.55 | 26.7 |
| diorite | 7 | 35.15 | 19.90 | 19.3 |
| diorite | 8 | 35.15 | 50.70 | 49.2 |

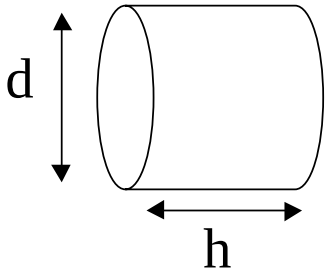

## 2.1 Sample disturbance

During the permeability measurements the long samples ÄD21, ÄD22 and ÄD4 were observed to contain microcracks which lead to breaking of sample ÄD4 in two parts. Measurements of the other two long samples revealed similar kind of fissuring. Due to fissuring samples ÄD21, ÄD22 and ÄD4 were sawn by Posiva in May 2001 such that the widened cracks were excluded from the remaining samples. The sawing of the samples is shown in Figure 1. Sample G1 was damaged during the diffusion measurements and it also contained a visible crack. Due to the shortness of this sample, it could not be sawn into smaller measurable pieces.

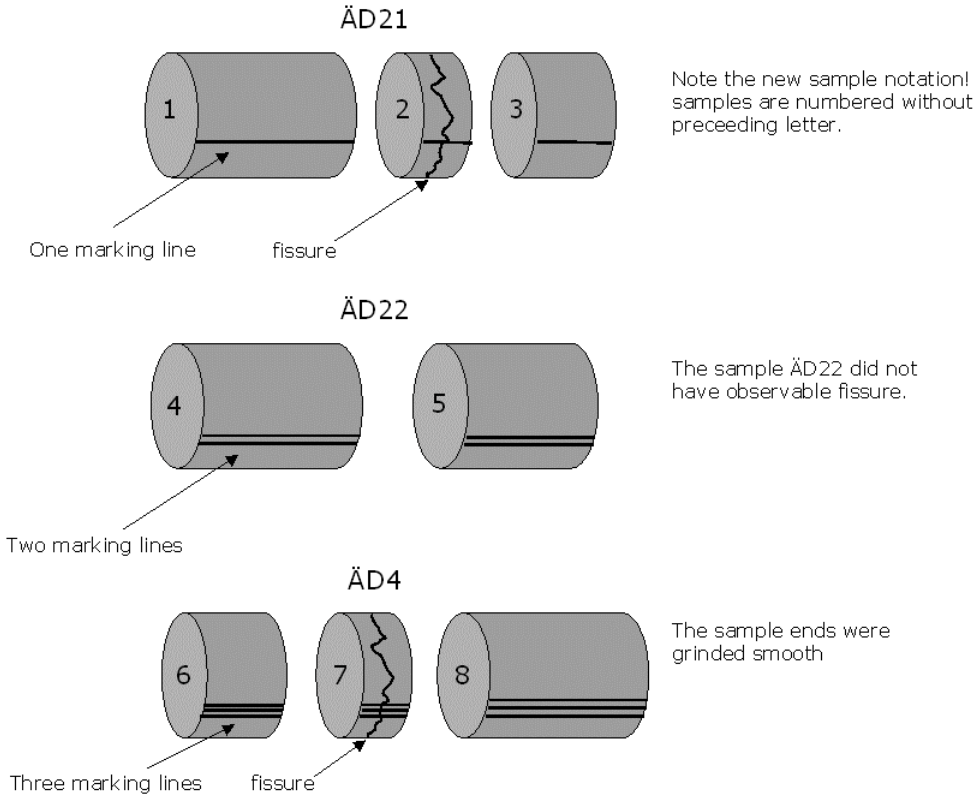


***Figure 1.*** *Segmentation of longer samples using sawing.*

## 2.2 Drying of the samples

All samples were dried in a vacuum oven at a temperature of 55°C prior the measurements. This slightly elevated temperature is not expected to cause any damage in the rock structure. Before drying, samples were carefully cleaned by pressurised air and weighed with a balance. In order to follow the drying process, samples were weighed after suitable intervals. For weighing the temperature of the oven was switched back to room temperature, the oven was filled with nitrogen, and the sample was left in the nitrogen atmosphere for four hours. The purpose of nitrogen saturation of the samples was to decrease the absorption of water vapour from the air. After weighing, vacuum drying was immediately continued. The level and rate of drying were estimated from the weight measurements by using fits by two exponentials to the drying curves. All the drying curves measured are given in Appendix A.

# 3 Diffusion: measurement techniques

The measuring equipment used in the diffusion measurements is shown in Figure 2. In the through-diffusion measurements the injection chamber is first flushed with nitrogen and then evacuated by using a vacuum pump. This is continued until diffusive helium flow from the air inside the sample is stabilised at a very low level. After evacuation the pressure of the injection chamber will be less than 0.08 bar.

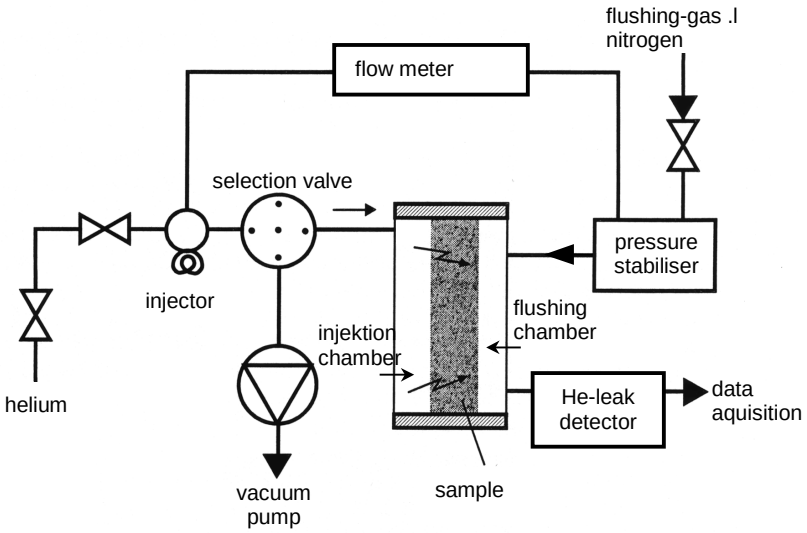


***Figure 2.*** *A schematic picture of the diffusion measurement equipment.*

During the evacuation, helium flows through the injection loop. After the evacuation, the loop containing helium is connected to the injection chamber by using a 6-way valve and an injector valve. At the same time the other end of the loop is connected to nitrogen flow that goes through a pressure stabiliser. Because of this, only the helium in the loop (5 ml) will be injected. Helium is sucked from the loop to the injection chamber by the vacuum. After connecting the loop to the injection chamber, the system is let to stabilise for two minutes. In that time all helium is transferred to the injection chamber, and the valve is turned off. Helium now diffuses through the sample to the flushing chamber, which is continuously flushed with nitrogen. The helium concentration of this nitrogen is then measured with a helium-leak tester. During the through-diffusion, the injection chamber is sealed. The whole through-diffusion measurement takes about 1200 minutes for a sample of length of 10 mm. The purity of the helium used is 99.995% and that of the nitrogen is 99.9%. It is important in the through-diffusion method that there is no pressure difference between the injection and flushing chambers, such that helium migrates through the sample only by diffusion.

The sealing material used in the through-diffusion and permeability measurements is He-tight Terostat by Würth GmbH. Terostat is widely used in vacuum technology, and in these measurements it is used between the cylindrical surface of the sample and the measuring chamber. The flanges including both injection and flushing chambers were

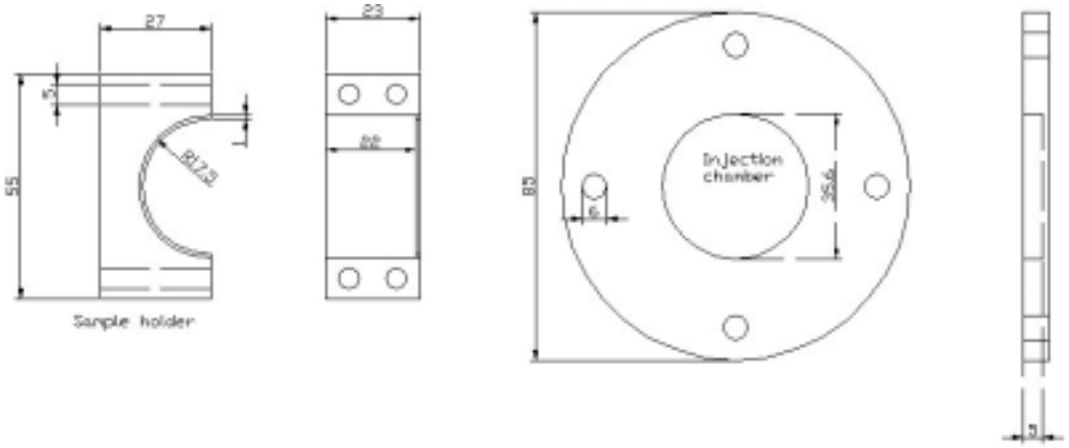


***Figure 3.*** *An example sample holder and injection flange. The length of the aluminium sample holder was made to match the length of the sample.*

made of steel. The sample holders and sample flanges used in all diffusion measurements are shown in Figure 3.

## 3.1 Modelling of the diffusion measurements

Modelling of the through-diffusion measurements is based on the solution of an appropriate diffusion equation. Because of the geometry of the samples and boundary conditions in the transverse directions, one-dimensional approximation can be used. The diffusion equation for the concentration of helium C(x,t) [kg/m$^3$] inside the sample is

$$\frac{\partial C}{\partial t} = \frac{D_e}{\varepsilon_p}\frac{\partial^2 C}{\partial x^2}\ , \qquad (3\text{-}1)$$

where t [s] is time, $D_e$ [m$^2$/s] is the effective diffusion coefficient, $\varepsilon_p$ is the porosity and x is the position inside the sample.

The boundary conditions in the direction of helium transport are such that the concentration of helium in the injection chamber is assumed to decrease according to the diffused amount. It is also assumed that there is no sorption and that the helium concentration at the outer surface of the sample is zero due continuous flushing with nitrogen.

Porosity $\varepsilon_p$ and the effective diffusion coefficient $D_e$ [m$^2$/s] can both be determined from the breakthrough curves of helium by fitting the curves with the relevant solution of Equation (3-1). In this one-dimensional approximation it is in fact possible to derive (Väätäinen et al. 1993, Carslaw 1959) an analytical expression for the mass flow of helium through the sample,

$$\frac{\partial m}{\partial t} = -D_e A \left.\frac{\partial C}{\partial x}\right|_{x=1} \quad [kg/s], \tag{3-2}$$

in the form

$$\frac{1}{m_0}\frac{\partial m}{\partial t} = D_a h \sum_{n=1}^{\infty} \frac{2h\alpha_n e^{-D_a \alpha_n^2 t}}{\sin(\alpha_n l)\left[l\left(\alpha_n^2 + h^2\right) + h\right]}, \tag{3-3}$$

where A[$m^2$] is the cross-sectional area of the sample, $m_o$ [kg] is the mass of the injected helium, $D_a = D_e/\varepsilon_p$ [$m^2$/s] is the apparent diffusion coefficient, $h = \varepsilon_p/s$, s [m] being the average length of the injection cell, $\alpha_n$, n = 1, 2, ..., are the roots of $\alpha\tan(\alpha l) = h$ [l/m], and 1 [m] is the average length of the sample. The average length of the injection cell (s) and the length of the sample (l) are both needed as input parameters.

After fixing the parameters mentioned above, the measured breakthrough curve is fitted by expression by varying the parameters $D_e$ (effective diffusion coefficient) and $\varepsilon_p$ (effective porosity).

# 4 Permeability: measurement techniques

The permeability measurement equipment is similar to that of the diffusion measurements except for the programmable pressure stabiliser in the injection system. The surface of the sample in the injection cell is exposed to an elevated pressure of helium. A constant pressure difference is maintained between the opposite surfaces of the sample. The surface of the sample in the flushing chamber is flushed with nitrogen, and the concentration of helium in the nitrogen is measured. The flow rate of helium through the sample is measured for several pressure differences. For each pressure difference, the flow rate is let to stabilise before reading its value.

## 4.1 Measurement set-ups for permeability determination

In the permeability measurements two types of sample holders were used. The reason for unidentical holders is the observed fissuring of the long (>50mm) samples. As told already in section 1.1, the long samples ÄD21, ÄD22 and ÄD4 were observed to contain microcracks. The fissuring mechanism suggests that these cracks were present in the rock matrix already before the measurements. The first set-up (Figure 4a) used in these measurements introduced a radial compressive force on the cylindrical sample to ensure the sealing. As seen in Figure 4b, Terostat sealing penetrated due this force in the fissure openings causing finally a breaking of the sample.

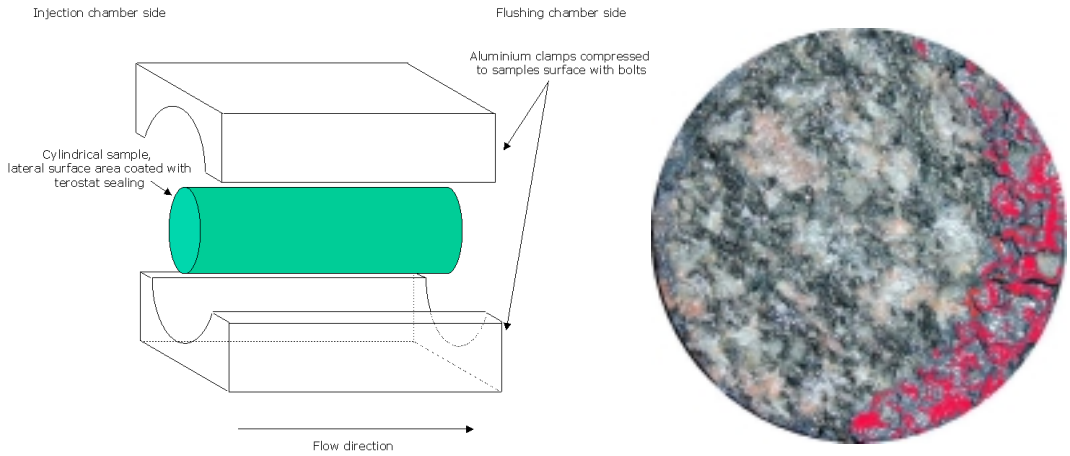


***Figures 4a and 4b.*** *The first measurement set-up for the long samples. The flanges including the injection and flushing chambers are not shown here. In Figure 4b the penetration of Terostat sealing in the fissure openings is illustrated by red colouring. The Figure 4b is from the broken sample ÄD4.*

Because of the Terostat penetration described above, the measuring set-up had to be redesigned. The main aim was to ensure sealing without producing at the same time a substantial compressive force on the sample. To this end the sample was inserted in a socket which shrunk at an elevated temperature. The injection and flushing chamber flanges were made from aluminium such that the socket tightened the flanges against the sample ends.

Terostat was used again for sealing. To shrink the socket it must be heated to a temperature of 100°C for a couple of seconds. During the tests, we made sure that the sample temperature was not elevated appreciably. This was ensured by the low heat conductivity of Terostat. The redesigned measuring set-up for permeability measurements is shown in Figure 5.

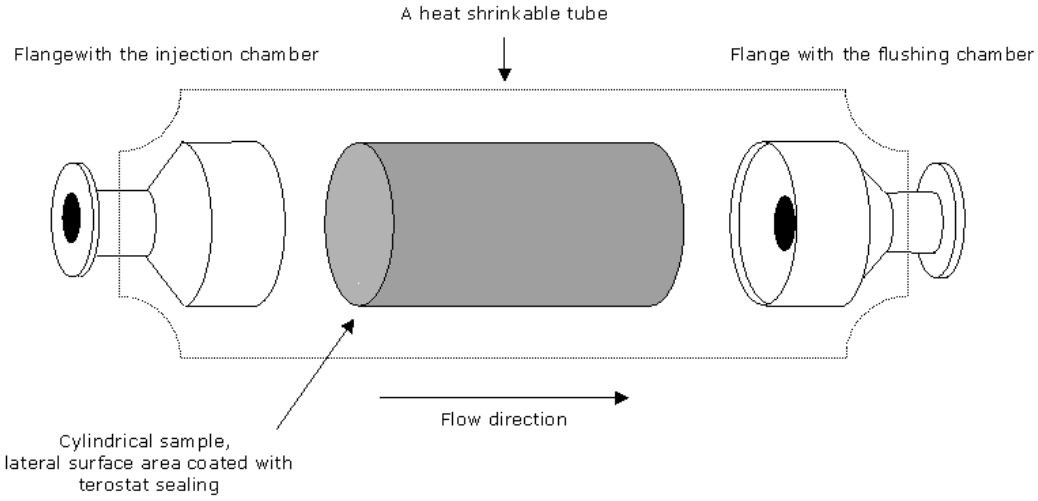


***Figure 5..*** *Redesigned measurement set-up for permeability*

## 4.2 Evaluation of the measured permeability curves

In the case when a pressure difference exists across the sample, helium transport through the sample is mediated by diffusion and also by flow induced by the pressure gradient. According to Fick's and d'Arcy's laws for a compressible fluid, the volume flow of helium through the sample is then given by (Dullien 1979)

$$Q = Q_{diff} + \frac{KA}{\mu l}\frac{\left(p_2^2 - p_1^2\right)}{2p_1} \quad , \qquad (4\text{-}1)$$

where Q [$m^3/s$] is the flow rate through the sample, $Q_{diff}$ [$m^3/s$] is the flow rate due to diffusion only, K [$m^2$] is the permeability coefficient, A [$m^2$] is the cross-sectional area of the sample, $\mu$ [Pa s] is the dynamic viscosity of helium gas, l [m] is the length of the sample, $p_2$ [Pa] is the pressure of helium in the injection cell, and $p_1$ [Pa] is the pressure of helium at the outlet. The total flow rate through the sample is measured for several pressure differences $p_2 - p_1$, and the permeability coefficient is determined from a fit to the measured points by Equation (4-2) (Figures 6a and 6b).

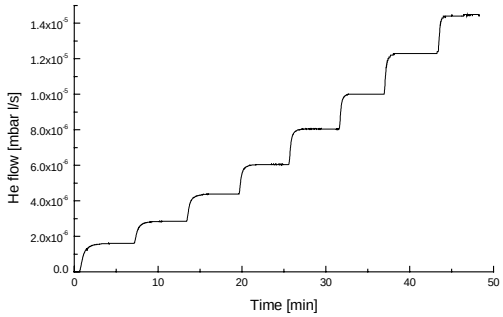


***Figure 6.*** *A measured permeability curve.*

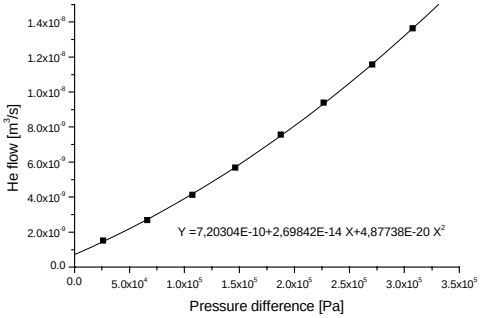


***Figure 6b,*** *Helium flow as a function of pressure difference for the data of Figure 6a, and the curve fitted to the measured points by Equation (4.2-1)*

The measured permeabilities, K [$m^2$], can be used to determine the hydraulic conductivities, $K_H$ [m/s], of the samples. These are given by (Dullien 1979)

$$K_H = \frac{\rho g}{\mu} K , \qquad (4\text{-}2)$$

where $\rho$ is the density of water ($\rho$ = 997.08 kg/$m^3$ at 25°C (Kell 1967)), g is the acceleration of gravity at sea level (g = 9.81 m/$s^2$), and $\mu$ is the dynamic viscosity of water ($\mu = 8.9042*10^{-4}$ kg/ms at 25°C (Weast 1974-1975)).

# 5 Porosity: measurement techniques with a pycnometer

Porosity measurements were carried out using a He-gas pycnometer which is based on the equation of state of ideal gas. Helium gas is used because it is non-reactive and penetrates easily small pores, and because it very accurately fulfils the ideal gas law. Also, a porosity value obtained by helium gas will obviously be closer to that measured in a He-gas diffusion experiment, than a value obtained by using some other media such as water. The values obtained by He-gas pycnometry are complementary to those of the diffusion measurements.

The experimental arrangement of the pycnometer used in the porosity measurements is shown in Figure 7. The volumes of the cells, $V_R$ and $V_S$, are first determined by using calibration samples. A polished aluminium calibration sample of volume $V_N$ is inserted in the sample cell $V_S$, the whole system is evacuated, and the pressure $P_V$ and temperature $T_V$ are measured after stabilisation. The reference cell is then pressurised with helium. The pressure $P_R$ and the temperature $T_R$ are measured after stabilisation, after which the helium is allowed to expand into the measuring chamber. After stabilisation, the resulting pressure $P_S$ and temperature $T_S$ of the whole volume are measured. The unknown volumes in the system can be determined when the volume $V_N$, pressures $P_V$, $P_R$ and $P_S$, and temperatures $T_V$, $T_R$ and $T_S$ are known for at least two calibration samples. The same procedure is then repeated on the sample to be measured.

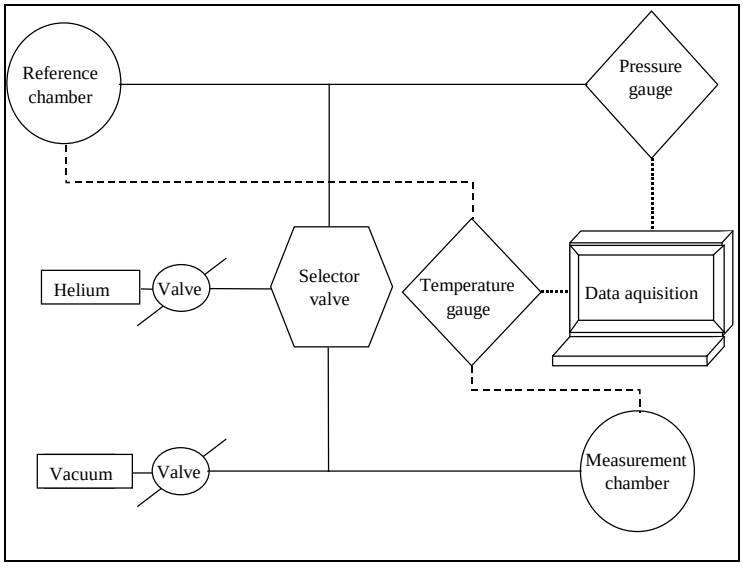


***Figure 7.*** *Experimental set-up of the He-pycnometer.*

## 5.1 Grain volume

According to the ideal-gas law, the porosity of the sample can be determined when the pressures $P_V$, $P_R$ and $P_S$, the temperatures $T_V$, $T_R$ and $T_S$, the volumes of the cells $V_R$ and $V_S$, and the bulk volume of the sample $V_b$ are all known. The porosity $\varepsilon_p$ [%] can then be expressed in the form

$$\varepsilon_p = \frac{V_b - V_g}{V_b} \cdot 100, \tag{5-1}$$

where the grain volume $V_g$ is given by

$$V_g = V_S - V_R \frac{(P_R T_S T_V - P_S T_V T_R)}{(P_S T_V T_R - P_V T_S T_R)}. \tag{5-2}$$

## 5.2 Bulk volume

Bulk volume was measured using the water-immersion method. The sample was weighed in ambient conditions and then in water. The temperature of the water was also measured to determine its density. The density of water $\rho_w$ [kg/m$^3$] as a function of temperature T [°C] is given by [Kell G. S. 1967]

$$\rho_w = 0.99995 + 5.0000 \cdot 10^{-5} \cdot T - 7.5450 \cdot 10^{-6} \cdot T^2 + 3.6131 \cdot 10^{-8} \cdot T^3. \tag{5-3}$$

Using the difference in the two masses and the density of water, the bulk volume of the sample can be determined from

$$V_b = \frac{m_d - m_f}{\rho_w}, \tag{5-4}$$

where $m_d$ is the mass of the sample in ambient conditions [kg], and $m_f$ is the mass of the sample in water [kg].

The masses of the samples were determined with a Metler Toledo AT400 balance. The balance resolution was 0.1 mg and measuring accuracy was 0.2 mg. Deionised water was used in the immersion measurements to reduce bubble formation.

# 6 Error analysis

The error in individual diffusion measurement is reliably under 10% of the measured value for the effective diffusion coefficient and under 50% for effective porosity. These values were obtained by observing the effect of variation in modelling parameters $D_e$ and $\varepsilon_p$ (Figures 8 and 9).

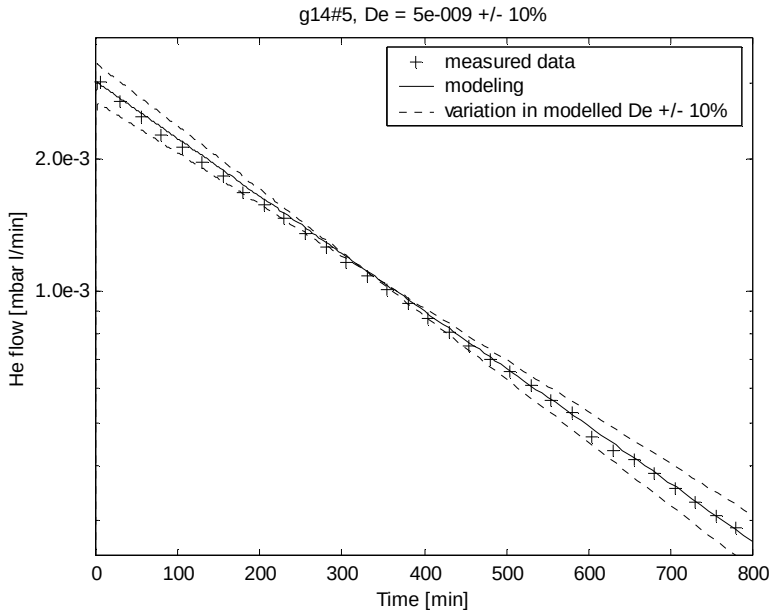


***Figure 8.*** *Typical measured and fitted breakthrough curve together with 10% variations in the fitted effective diffusion coefficient. Note the logarithmic scale on the y-axis.*

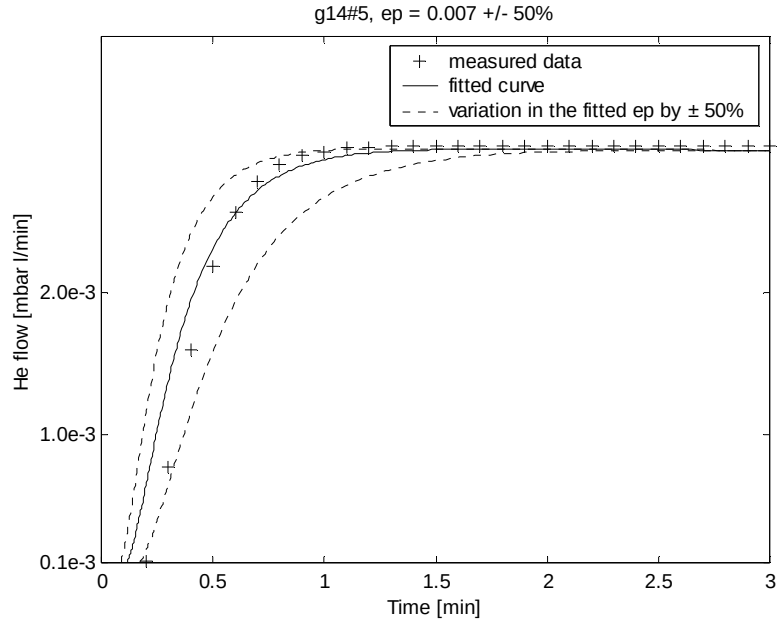


***Figure 9.*** *The early part of the breakthrough curve of Figure 8 which determines the porosity. The effect of porosity variation by ± 50% is also seen in the figure. The y scale is now linear.*

The error in the porosity measurement results done with pycnometer vary depending of the bulk and grain volumes of the sample. This follows from dimensional limitations of the measurement system. For small samples and pore volumes, the uncertainties in the measurable quantities (such as pressure, temperature and chamber volumes) begin to play remarkable role.

The general formula for error propagation in the dependent quantity *q(x,…,z)*, with independent uncertainties *dx ,…,dz* in the measured quantities *x,…,z,* is given by

$$dq = \sqrt{\left(\left(\frac{\partial q}{\partial x}dx\right)^2 + \left(\frac{\partial q}{\partial z}dz\right)^2\right)}. \qquad (6\text{-}1)$$

The effective porosities of the samples were determined from Equation (3-1) where the grain volumes $V_g$ were determined from Equation (5-2).

The uncertainties of the grain volumes were determined from Equation (6-1). The relevant quantities and their uncertainties are explained in Table 2.

**Table 2. Uncertainties of the quantities involved.**

| | | | |
|---|---|---|---|
| Uncertainty of the volume of the measuring cell | d $V_S$ | 0.02 | $cm^3$ |
| Uncertainty of the volume of the reference cell | d $V_R$ | 0.02 | $cm^3$ |
| Uncertainty of the pressure in the reference cell | d $P_R$ | 10 | Pa |
| Uncertainty of the temperature in the reference cell | d $T_R$ | 0.1 | K |
| Uncertainty of the temperature in the measuring cell | d $T_S$ | 0.1 | K |
| Uncertainty of the pressure in the measuring cell | d $P_S$ | 10 | Pa |
| Uncertainty of the pressure in the whole system | d $P_V$ | 10 | Pa |
| Uncertainty of the temperature in the whole system | d $T_V$ | 0.1 | K |
| Uncertainty of sample bulk volume determination | d $V_B$ | * | $cm^3$ |

** Depends on sample's volume*.

Uncertainty of sample bulk volume determination and the uncertainties in volumes $V_s$ and $V_R$ were estimated from the standard deviations in the water immersion volume determination and calibration measurements. All pressures were measured with Beamex PC 106 pressure calibrator. Its accuracy was 10 Pa. Temperature measurements were made by J-type (Iron-Constantan) thermocouples, and the accuracy of the measurements was in 0.1 K in the measuring range 292-298 K due averaging over large number of samples.

The partial differentials involved are given by

$$\frac{\partial V_g}{\partial Vs} \cdot dV_S = dV_S \,, \tag{6-2}$$

$$\frac{\partial V_g}{\partial V_R} \cdot dV_R = \frac{-T_V}{T_R}\left(\frac{P_R T_S - P_S T_R}{P_S T_V - P_V T_S}\right) \cdot dV_R, \tag{6-3}$$

$$\frac{\partial V_g}{\partial P_R} \cdot dP_R = \frac{-V_R T_V T_S}{T_R P_S T_V - P_V T_S T_R} \cdot dP_R, \tag{6-4}$$

$$\frac{\partial V_g}{\partial T_R} \cdot dT_R = \frac{V_R T_V}{T_R^2}\left(\frac{P_R T_S - P_S T_R}{P_S T_V - P_V T_S} + \frac{V_R T_V P_S}{T_R P_S T_V - T_R P_V T_S}\right) \cdot dT_R \,, \tag{6-5}$$

$$\frac{\partial V_g}{\partial T_S} \cdot dT_S = \frac{-V_R T_V}{T_R}\left(\frac{P_R}{P_S T_V - P_V T_S} + \frac{P_V P_R T_S - P_V P_S T_R}{(P_S T_V - P_V T_S)^2}\right) \cdot dT_S \tag{6-6}$$

$$\frac{\partial V_g}{\partial P_S} \cdot dP_S = \frac{-V_R T_V}{T_R}\left(\frac{-T_R}{P_S T_V - P_V T_S} + \frac{T_V P_R T_S - P_S T_R T_V}{(P_S T_V - P_V T_S)^2}\right) \cdot dP_S \,, \tag{6-7}$$

$$\frac{\partial V_g}{\partial P_V} \cdot dP_V = \frac{-V_R T_V}{T_R}\left(\frac{T_S P_R T_S - P_S T_R T_S}{(P_S T_V - P_V T_S)^2}\right) \cdot dP_V \quad \text{and} \tag{6-8}$$

$$\frac{\partial V_g}{\partial T_V} \cdot dT_V = \frac{-V_R}{T_R}\left(\frac{P_R T_S - P_S T_R}{P_S T_V - P_V T_S}\right) + \frac{V_R T_V}{T_R}\left(\frac{P_R T_S P_S - P_S{}^2 T_R}{(P_S T_V - P_V T_S)^2}\right) \cdot dT_V \,. \tag{6-9}$$

The deviation in the porosity results for individual samples was very small. Deviation between successive measurement was typically less than 0.05%. For each sample the measurement was repeated for five times to ensure the reproducibility of the results. The most difficult task in the pycnometer method is to determine the bulk volume $V_b$ and to estimate the uncertainty in measured the $V_b$. This uncertainty is unfortunately the most influential one in the error analysis.

An adequate error analysis for the permeability results is hard to accomplish. The number of individual measurements is small for a statistical error analysis. Unlike in the case of effective diffusion coefficient, permeability is far more sensitive to alterations in the measuring conditions. This leads to larger relative variation in the measured permeability results. However, the permeability results obtained are more accurate than order of magnitude estimates.

# 7 Results

The diffusion and permeability results are averages over at least three independent measurements except for diffusion measurements for samples 1-8. In the case of significant variation in the results of three measurements, further measurements were done to determine a representative mean value. For samples 1-8 measurements were repeated twice. The pycnometer porosity results are given as averages over at least five independent measurements. A summary of the results is shown in Table 3.

**Table 3. Summary of results**

| Sample | Rock type | Volume $V_B$ [$cm^3$] | De [$m^2/s$] ± stdev. of mean | Ep (diff) [%] | N | Ep (pyk) [%] | N | perm [$m^2$] | N |
|---|---|---|---|---|---|---|---|---|---|
| Ä21 | diorite | 260.8 | $(4.40 \pm 0.05)\cdot10^{-10}$ | $0.23 \pm 0.02$ | 5 | ** | | $(9 \pm 5)\cdot10^{-19}$ | 4 |
| ÄD22 | diorite | 262.0 | $(9.50 \pm 0.00)\cdot10^{-10}$ | $0.37 \pm 0.02$ | 5 | ** | | * | |
| ÄD4 | diorite | 394.3 | $4.5\cdot10^{-10}$ **** | 0.5 | 1 | ** | | * | |
| D10 | diorite | 9.4 | $(1.10 \pm 0.05)\cdot10^{-9}$ | $0.25 \pm 0.01$ | 3 | $0.42 \pm 0.15$ | 5 | $(1\cdot1 \pm 0.1)\cdot10^{-19}$ | 3 |
| D15 | diorite | 9.8 | $(1.23 \pm 0.04)\cdot10^{-9}$ | $0.24 \pm 0.01$ | 5 | $0.31 \pm 0.13$ | 5 | $(1.49 \pm 0.06)\cdot10^{-19}$ | 5 |
| D27 | diorite | 9.6 | $(1.32 \pm 0.06)\cdot10^{-9}$ | $0.30 \pm 0.01$ | 3 | $0.34 \pm 0.13$ | 5 | $(1.45 \pm 0.05)\cdot10^{-19}$ | 3 |
| D3 | diorite | 9.5 | $(1.39 \pm 0.13)\cdot10^{-9}$ | $0.28 \pm 0.01$ | 5 | $0.44 \pm 0.13$ | 5 | $(1.6 \pm 0.4)\cdot10^{-19}$ | 4 |
| D4 | diorite | 19.4 | $(1.22 \pm 0.01)\cdot10^{-9}$ | $0.21 \pm 0.01$ | 5 | $0.33 \pm 0.08$ | 5 | $(1.2 \pm 0.1)\cdot10^{-20}$ | 5 |
| D5 | diorite | 38.8 | $(9.6 \pm 0.4)\cdot10^{-10}$ | $0.29 \pm 0.01$ | 5 | $0.22 \pm 0.04$ | 5 | $(3.3 \pm 0.3)\cdot10^{-20}$ | 4 |
| D7 | diorite | 38.7 | $(1.18 \pm 0.01)\cdot10^{-9}$ | $0.26 \pm 0.01$ | 5 | $0.30 \pm 0.05$ | 5 | $(4.4 \pm 0.2)\cdot10^{-19}$ | 4 |
| G1* | granite | 9.9 | $(2.4 \pm 0.3)\cdot10^{-10}$ | $0.13 \pm 0.01$ | 2 | * | | $(8 \pm 7)\cdot10^{-19}$ | 2 |
| G14 | granite | 9.6 | $(3.6\pm 0.1)\cdot10^{-9}$ | $0.17 \pm 0.01$ | 3 | $0.35 \pm 0.16$ | 5 | $(1.3 \pm 0.1)\cdot10^{-19}$ | 3 |
| G2 | granite | 20.7 | $(2.0 \pm 0.5)\cdot10^{-10}$ | $0.20 \pm 0.01$ | 5 | $0.20 \pm 0.05$ | 5 | $(2.8 \pm 0.5)\cdot10^{-21}$ | 4 |
| G26 | granite | 2.8 | $(9.4 \pm 0.2)\cdot10^{-10}$ | $0.20 \pm 0.01$ | 3 | $0.35 \pm 0.16$ | 5 | $(1.4 \pm 0.5)\cdot10^{-20}$ | 3 |
| G6 | granite | 38.9 | $(1.9 \pm 0.05)\cdot10^{-9}$ | $0.19 \pm 0.01$ | 5 | $0.14 \pm 0.05$ | 5 | $(2.3 \pm 0.5)\cdot10^{-20}$ | 5 |
| G8 | granite | 9.8 | $(6.5 \pm 0.00)\cdot10^{-10}$ | $0.14 \pm 0.01$ | 3 | $0.11 \pm 0.07$ | 5 | $(1.2 \pm 0.4)\cdot10^{-20}$ | 3 |
| 1 | diorite | 25.8 | $(1.10 \pm 0.00)\cdot10^{-9}$ | $0.40 \pm 0.00$ | 2 | $0.32 \pm 0.09$ | 5 | $(3.5 \pm 0.5)\cdot10^{-20}$ | 3 |
| 3 | diorite | 16.6 | $(9.80 \pm 0.00)\cdot10^{-10}$ | $0.30 \pm 0.00$ | 2 | $0.11 \pm 0.07$ | 5 | $(1.7 \pm 0.9)\cdot10^{-19}$ | 3 |
| 4 | diorite | 26.7 | $(2.00 \pm 0.00)\cdot10^{-10}$ | $0.20 \pm 0.00$ | 2 | $0.12 \pm 0.08$ | 5 | $(7.1 \pm 0.9)\cdot10^{-20}$ | 3 |
| 5 | diorite | 32.9 | $(5.1 \pm 0.5)\cdot10^{-10}$ | $0.45 \pm 0.15$ | 2 | $0.13 \pm 0.04$ | 5 | $(2.6 \pm 0.3)\cdot10^{-20}$ | 3 |
| 6 | diorite | 26.7 | $(4.5 \pm 0.5)\cdot10^{-10}$ | $0.20 \pm 0.00$ | 2 | $0.23 \pm 0.05$ | 5 | $(9 \pm 4)\cdot10^{-20}$ | 3 |
| 8 | diorite | 49.2 | $(1.4 \pm 0.7)\cdot10^{-9}$ | $0.2 \pm 0.1$ | 2 | $0.13 \pm 0.04$ | 5 | $(2.4 \pm 0.3)\cdot10^{-19}$ | 3 |

* sample G1 was broken during the first measurement

** samples sawed from ÄD21, ÄD22 and ÄD4 which include the major fissure do not allow the determination of migration characteristic by the methods used.

*** The values are from diffusion measurements ÄD21, ÄD22 and ÄD4 before sawing.

Samples G14 and 5 show somewhat anomalous behaviour in their effective diffusion coefficient and pycnometer porosity respectively. These anomalies may result from small statistics, and further measurements are still planned to resolve the issue. Comparison of the pycnometry porosities is given in Figure 10. From this figure we can conclude that, within error bars, the two porosity measurement give consistent values except for Sample 5. A comparison of the measured diffusion coefficients and permeabilities is shown in Figure 11.

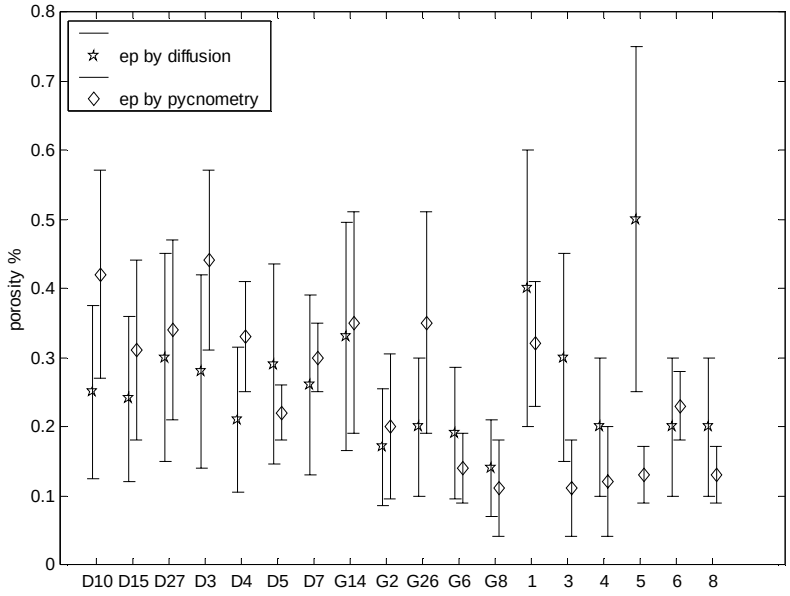


***Figure 10.*** *Comparison between porosities obtained with diffusion and pycnometry measurements.*

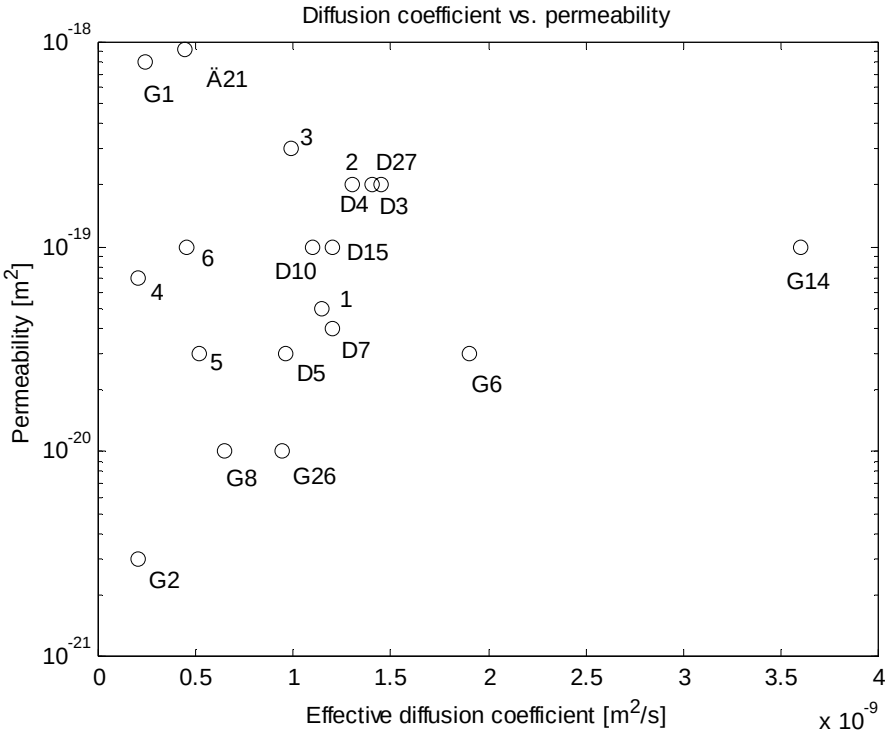


***Figure 11****. Diffusion coefficient as a function of permeability.*

As discussed already above, Sample G14 has a somewhat higher diffusion coefficient that the other samples, which needs clarification. Also, Samples G21 and Ä21 have a somewhat higher permeability. These samples were broken during measurements, and they were successfully measured only once. In Figure 12, we plot the effective diffusion coefficient against the through diffusion porosity. Samples G14, ÄD4 and 5 stand out in this plot as expected and otherwise the results display a fairly consistent trend of increasing diffusion coefficient with increasing porosity.

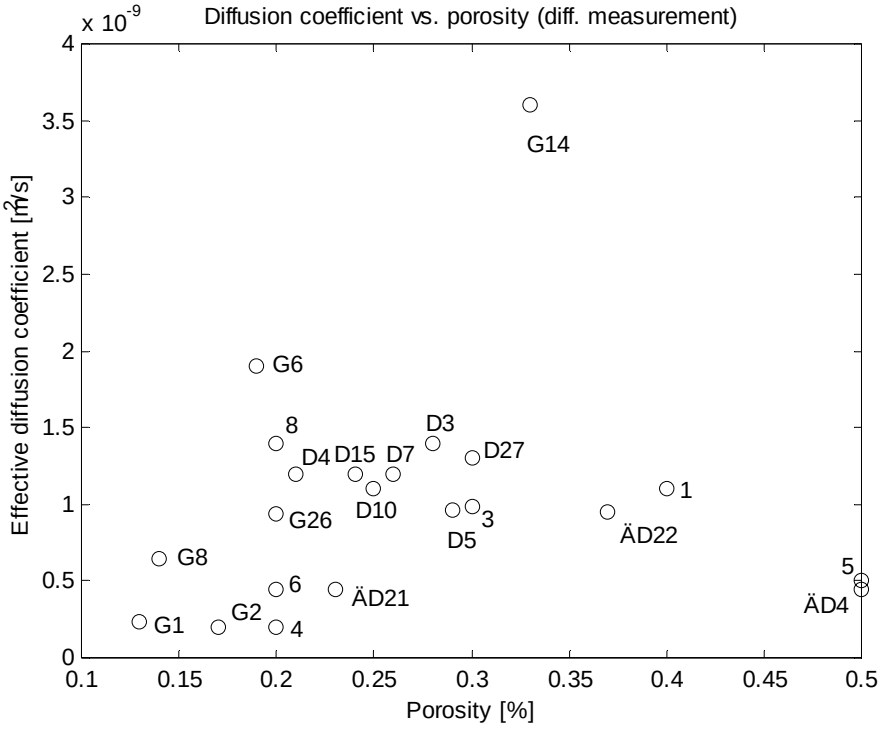


***Figure 12.*** *Diffusion coefficient as a function of porosity as determined by the through-diffusion method.*

In Figure 13, we plot the effective diffusion coefficient as a function of pycnometer porosity as a consistency check for the plot in Figure 12. Even though the mutual order of points is changed, a similar expected trend is observed also in the plot.

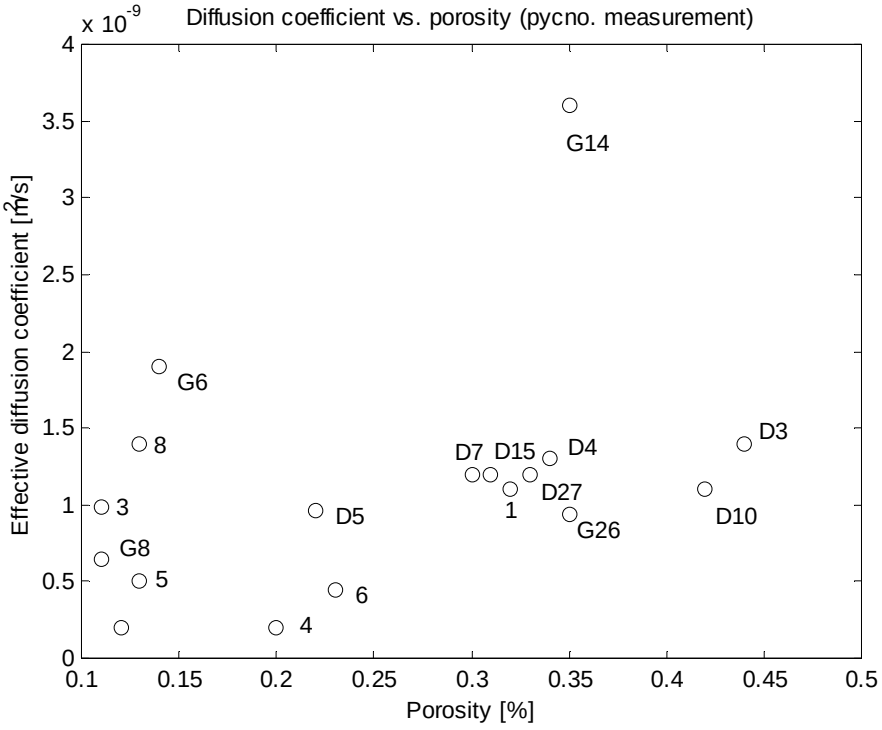


***Figure 13.*** *Diffusion coefficient as a function of porosity as determined by pycnometer.*

In Figure 15, we plot the permeability against the pycnometer porosity. Also this plot shows a consistet increase of permeability with the increasing porosity, with perhaps a somewhat excessive permeability for Samples 3 and 8.

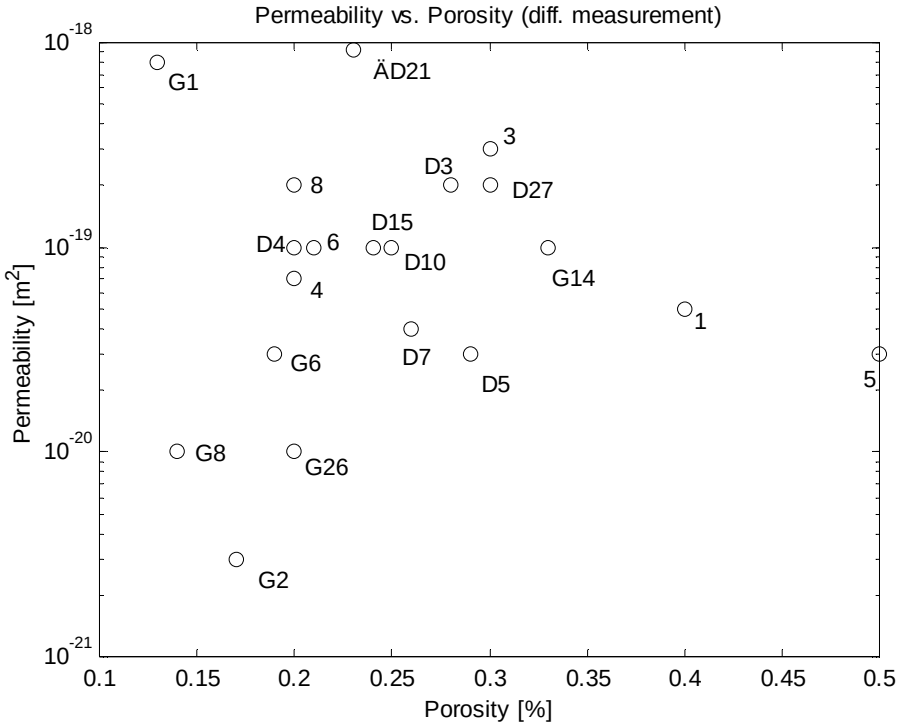


***Figure 14.*** *Permeability as a function of porosity as determined by the through-diffusion method.*

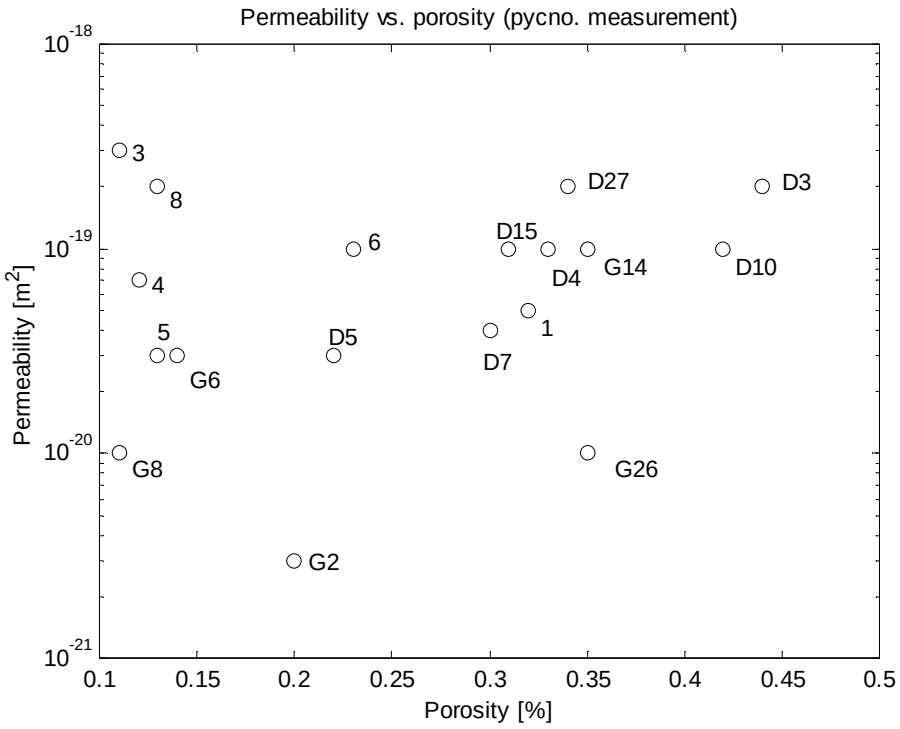


***Figure 15****. Permeability as a function of porosity as determined by pycnometer.*

# 8 Conclusions

## 8.1 Granite

Granite has quartz and feldspar as its main components. Minority (darker) components are usually biotite and amphibole (hornblende), and to even less extent augite and (or) muscovite. Being an abyssal rock, in granite these minerals usually form a non orientated evenly grained rock matrix. This is not however the case in the Äspö granite samples. The Äspö red granite has clear orientation in its structure (Figure 16) as the darker minerals form aligned chists or laminas.

***Figure 16.*** *Typical Äspö granite sample (G2).*

Almost all granite samples include multiple fractures randomly oriented with respect to their chistosity (Figure 17). Furthermore, these fractures typically reach through the sample as seen in Figure 18. They are as dark as the darker minerals of the granite, which could imply that the fractures are not likely results of drilling or other recent activity. They act as migration paths for fluids, and the openings of the samples are filled in time with minerals like biotite. This kind of filling of fracture is not seen in sample G1 that was accidentally broken during the measurements (Figure 19).

***Figure 17.*** *Sample G26 with a main fracture.*

***Figure 18****. Sample G14.*

***Figure 19.*** *Accidentally broken sample G1.*

The somewhat anomalous behaviour regarding the diffusion coefficient of sample G14 can at least partly be explained by the "natural" fracturing that appears in the rock matrix of this sample. As can be seen in Figure 20, this sample contains many fractures, and is in fact the most fractured of the samples.

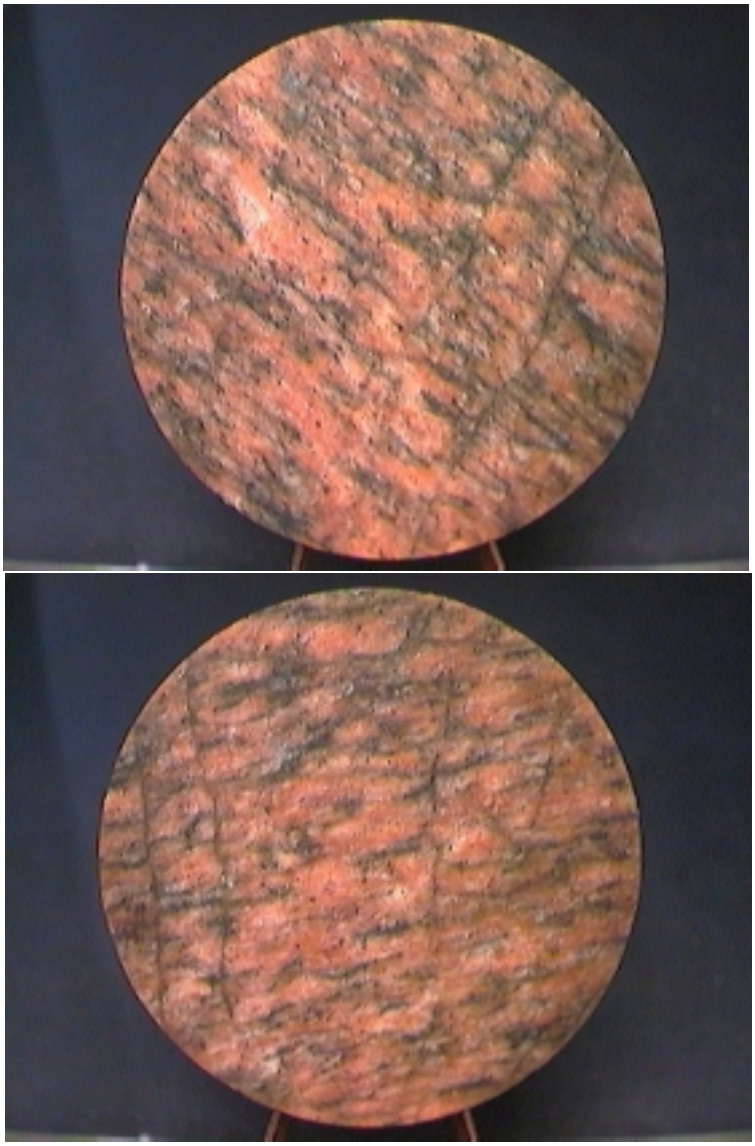

***Figure 20.*** *Both sides of sample G14.*

Independent measurements for sample G14 reveal no substantial deviation, which implies repeatability of the results. Even though most granite samples display clear fissuring, on the average Äspö granite has mean migration characteristics which are very similar to those of typical Finnish and Swedish bedrock.

The average diffusion coefficient of all rock samples measured at JYFL is $6 \cdot 10^{-9}$ $m^2/s$ (N=214) while this average for the Äspö granite samples is $1 \cdot 10^{-19}$ $m^2/s$ (N=6). The mean porosity of Äspö granite samples is 0.2 % and the mean porosity of all samples measured at JYFL is 0.5 %.

Although the granite samples are fractured as described above, their surfaces (after grinding) are smooth, and one cannot locate the fractures in the surface profiles.

## 8.2 Diorite

Diorite is an abyssal rock type like granite. The light coloured minerals are usually plagioclase. The darker minerals are, like in granite, biotite, amphibole (hornblende) and augite (Figure 21). In diorite a noticeable difference from granite is the heterogeneity and granularity of rock. The grains of different minerals are substantially larger than in granite. Unlike in granite, some of the grains can be seen in the surface profile (Figures 7 and 8) after grinding. The regions of lowered height are always made of darker minerals. The somewhat higher porosity of diorite (mean $\varepsilon_p$=0.3%) in comparison with granite (mean $\varepsilon_p$=0.2%) may thus be due to increased surface porosity in the former case. The mean effective diffusion coefficient of the diorite samples is $1 \cdot 10^{-9}$ $m^2/s$ (the same as the granite average). No fracturing like in the granite samples was observed.

***Figure 21.*** *Diorite sample D10.*

The only anomalous measurement result that now remains unexplained is the porosity of sample 5 determined by diffusion. This result may be due to small statistics. Sample 5 was measured only twice and the two results for porosity were 0.3% and 0.6% (c.f. Appendix B). The pycnometer porosity of sample 5 is as small as 0.13 % (Figure 10). A summary of results for the two rock types is shown in Table 4, and a comparison of the Äspö results and those of all results measured at JYFL is shown in Table 5.

**Table 4. Summary of results for different rock types**

| Rock type | De [$m^2/s$] | N | $\varepsilon_p$ [%] Diff | N | $\varepsilon_p$ [%] Pycno | N | k [$m^2$] | N |
|---|---|---|---|---|---|---|---|---|
| Granite | $1 \cdot 10^{-09}$ | 6 | 0.2 | 6 | 0.2 | 5 | $2 \cdot 10^{-19}$ | 6 |
| Diorite | $1 \cdot 10^{-09}$ | 14 | 0.3 | 16 | 0.3 | 13 | $2 \cdot 10^{-19}$ | 14 |

**Table 5. Comparison of the Äspö rock samples and all samples measured to date at JYFL**

| | De [$m^2/s$] | N | $\varepsilon_p$ [%] | N |
|---|---|---|---|---|
| All JYFL | $6 \cdot 10^{-09}$ | 214 | 0.5 | 214 |
| Äspö | $1 \cdot 10^{-09}$ | 23 | 0.3 | 23 |

***Figure 22.*** *Surface profile of granite sample G14.*

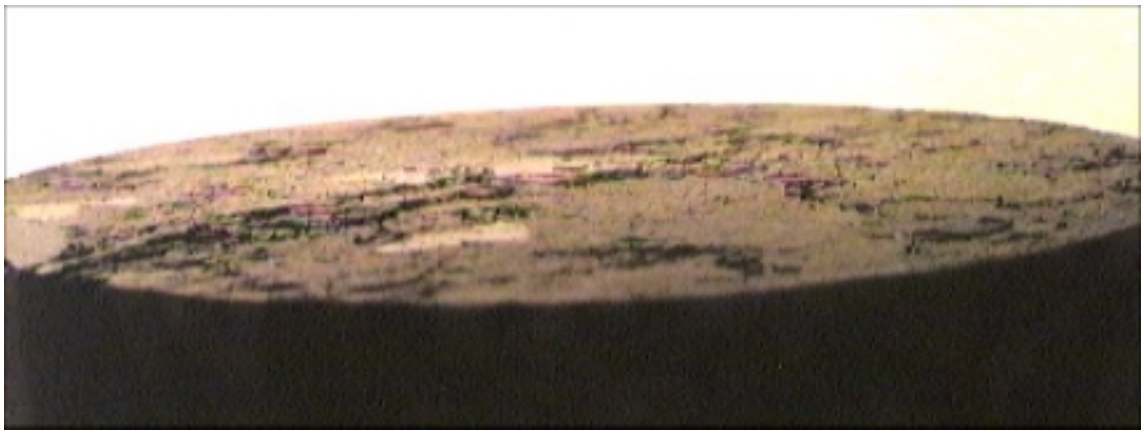

***Figure 23.*** *Surface profile of diorite sample D10.*

# References

**Carslaw, H.S., Jaeger, J.C.**, *Conduction of Heat in Solids*, 2nd. Ed., Oxford University Press, Oxford, 1959

**Dullien, F.A.L**., *Porous Media Fluid Transport and Pore Structure*,Academic Press, Inc., San Diego, California, 1979

**Kell G. S.,** *Precise Presentation of Volume Properties of Water at One Atmosphere,* Journal of Chemical and Engineering Data, Vol.12 (1967) pp.66-69

**Taylor, J.R.**, *An Introduction to Error Analysis*, 2nd. Ed., 1997

**Väätäinen, K., Timonen, J., Hautojärvi, A.**, in *Symp. Scientific Basis for Nuclear Waste Management XVI,* edited by C.G. Interrante & R.T. Pabalan (Mater. Res. Soc. Proc., Pittsburgh, PA, 1993) pp. 851-856

**Weast, R.C.**, (ed.), *Handbook of Chemistry and Physics*, 55th. Ed., p. F49, Chemical Rubber Comppany Press, Cleveland, Ohio, 1974-1975

# APPENDIX A

# Drying curves for analysed samples

APPENDIX A
Drying curves

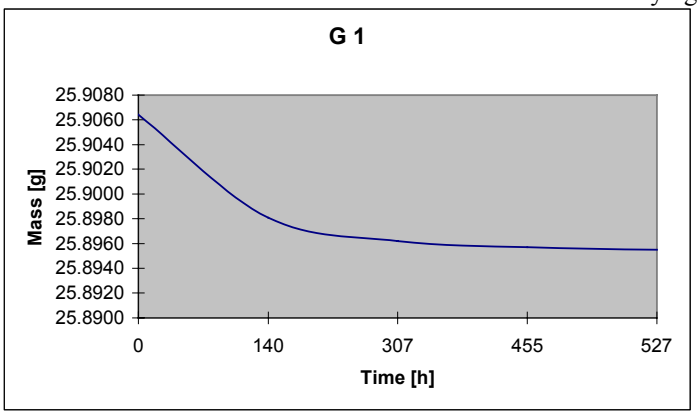


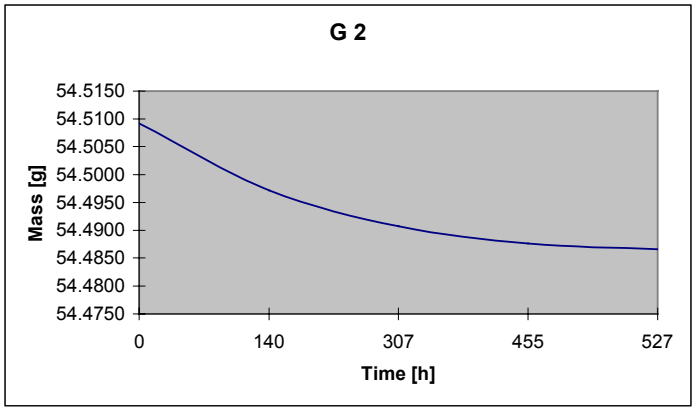


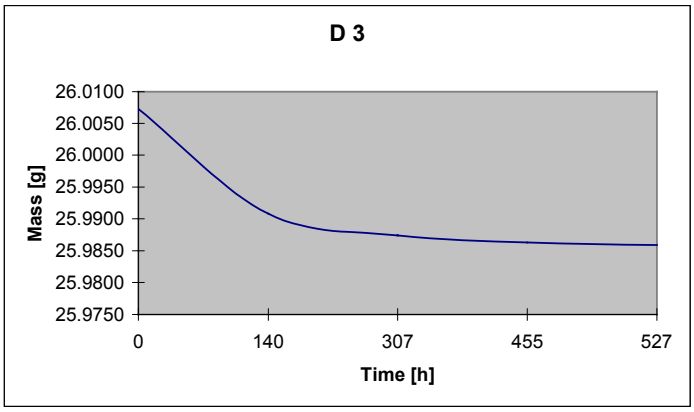


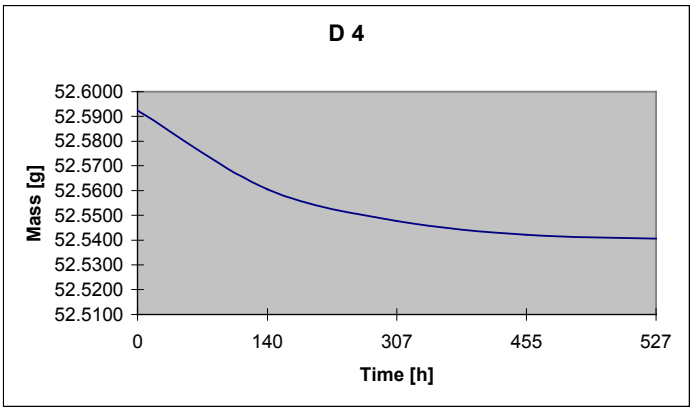


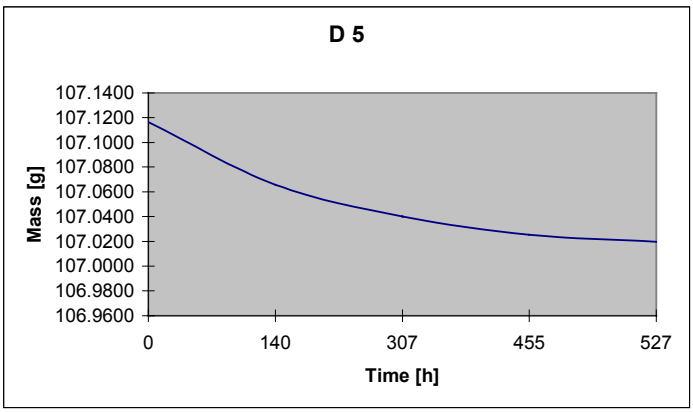


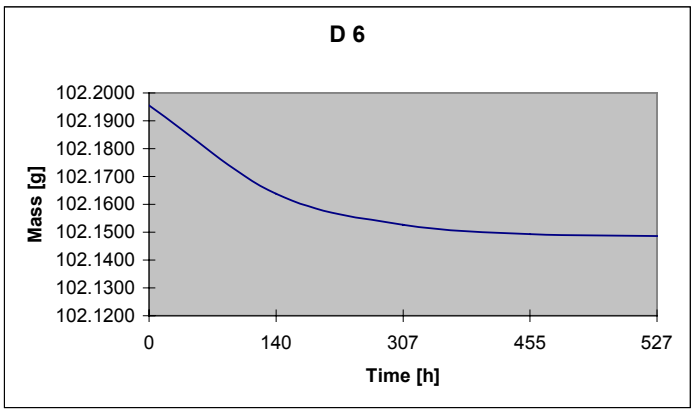


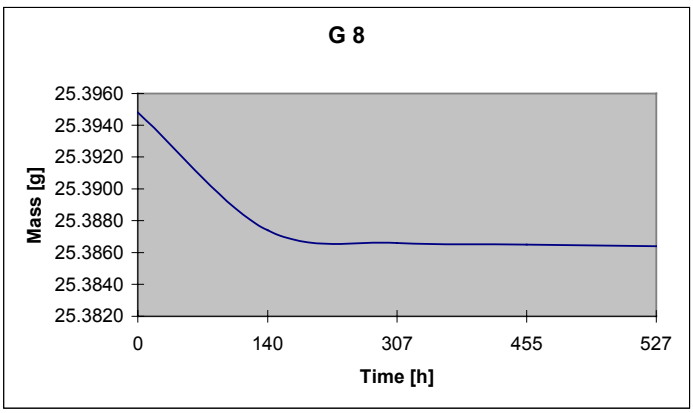


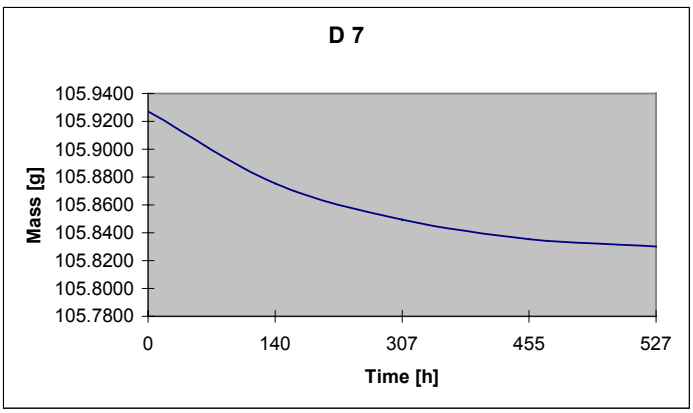

APPENDIX A
Drying curves

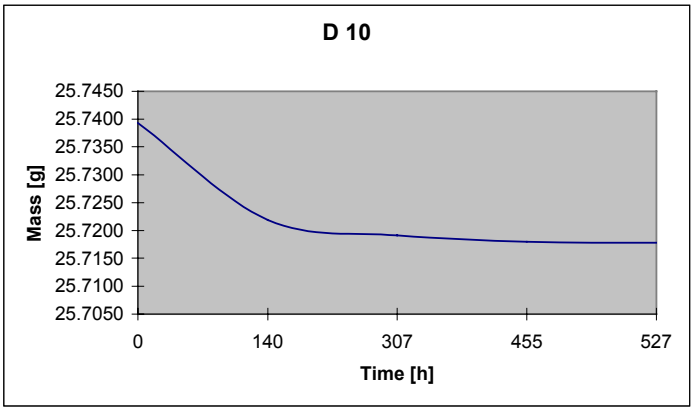


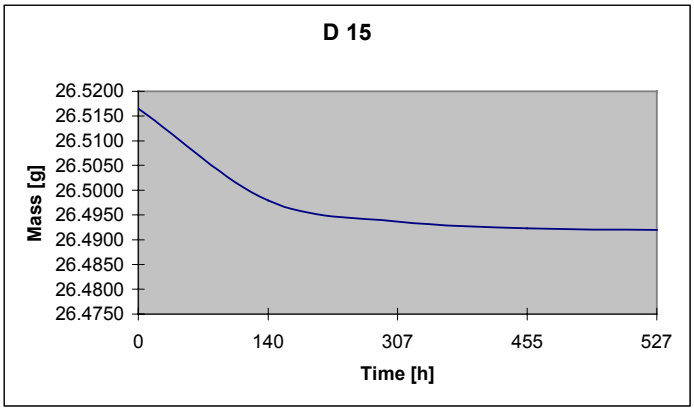


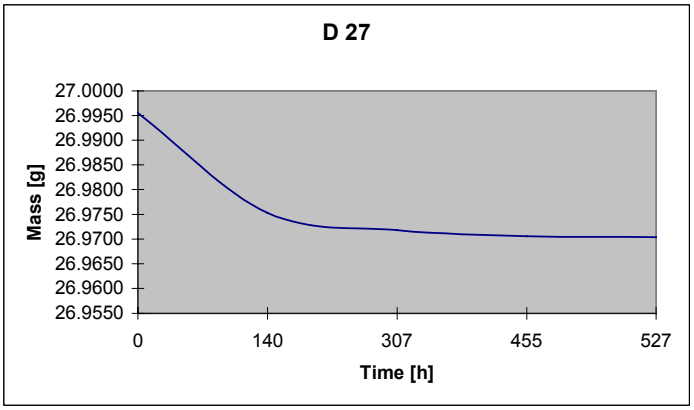


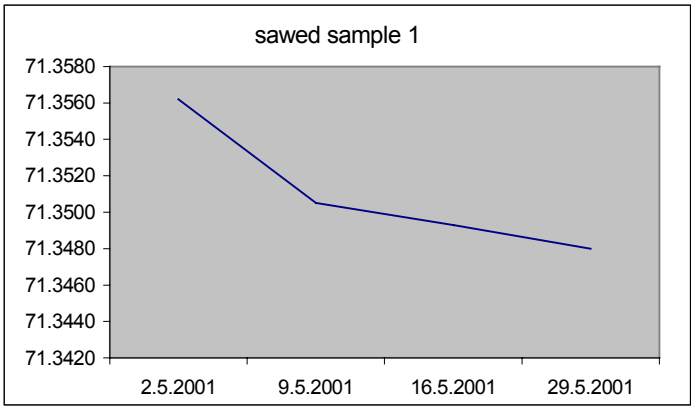


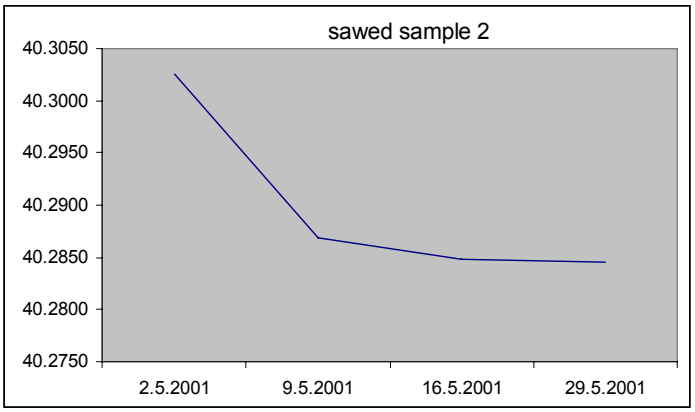


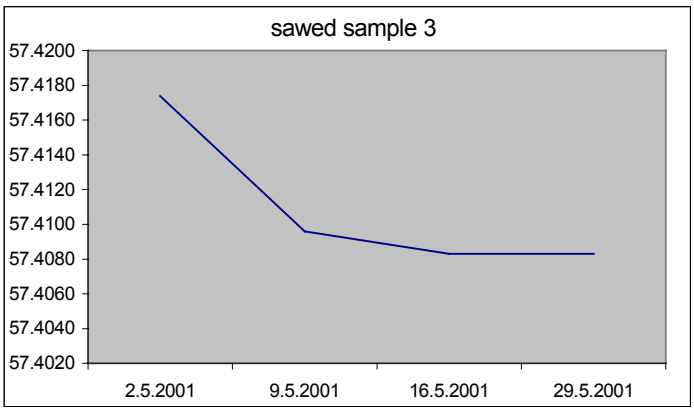


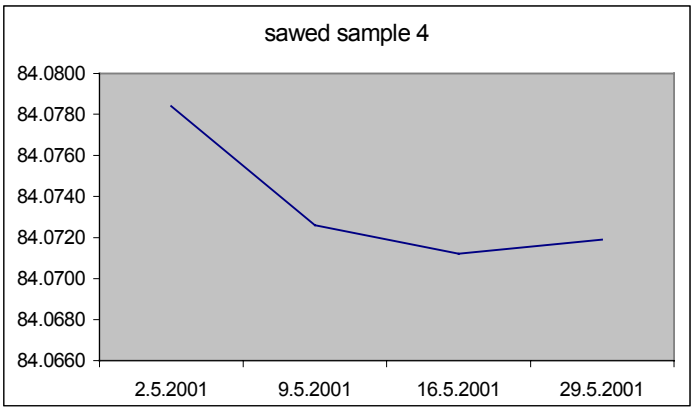


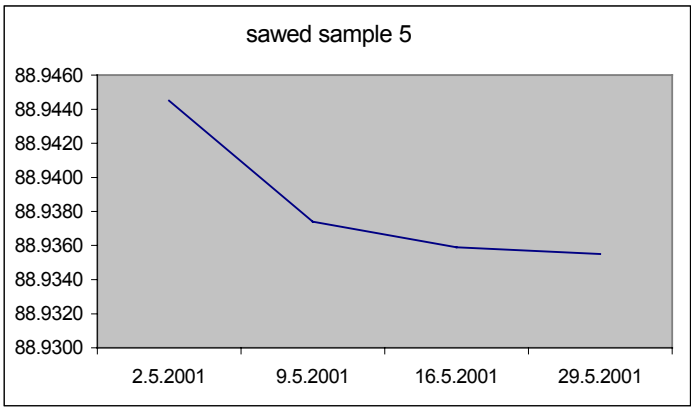

APPENDIX A
Drying curves

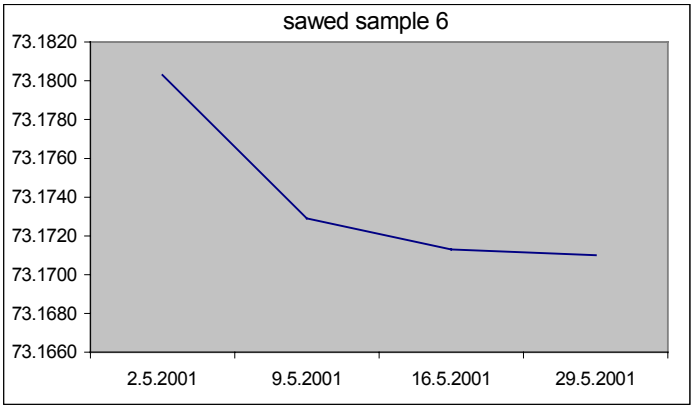


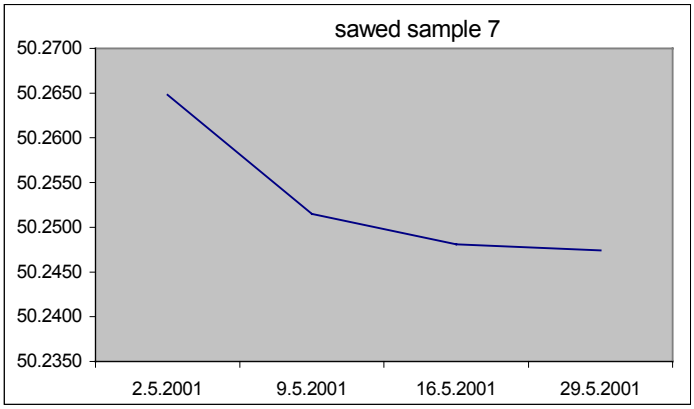


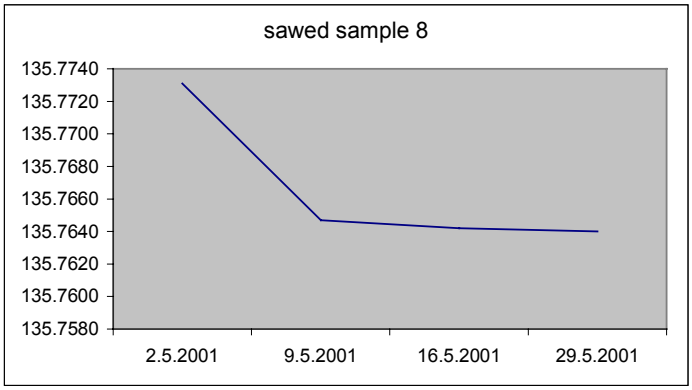

# APPENDIX B

# Diffusion curves for analysed samples

APPENDIX B
Diffusion curves

Diffusion curves of the sample d10

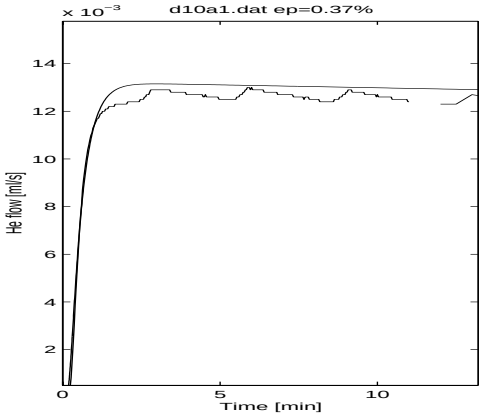


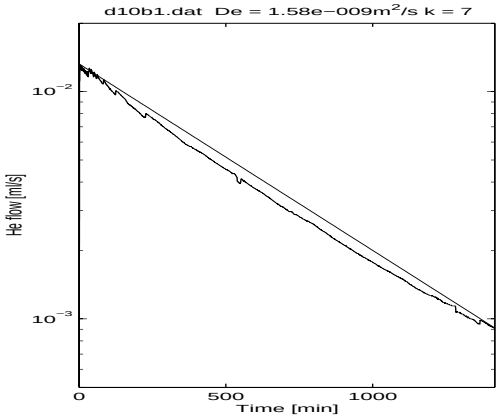


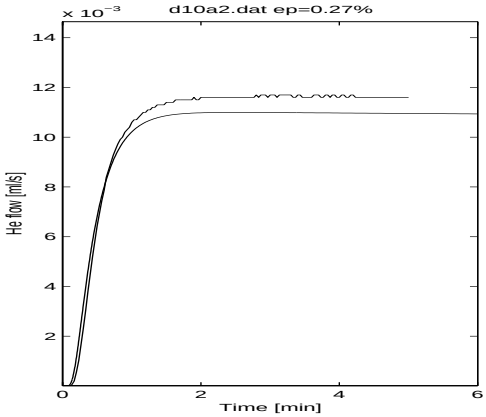


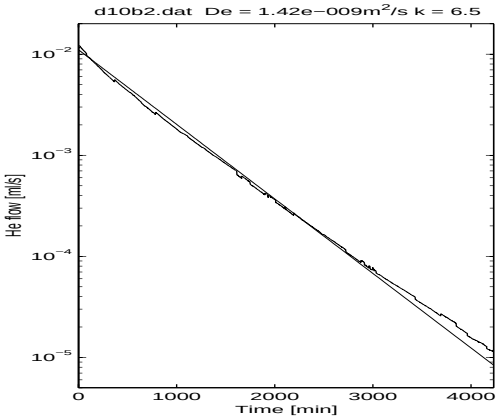


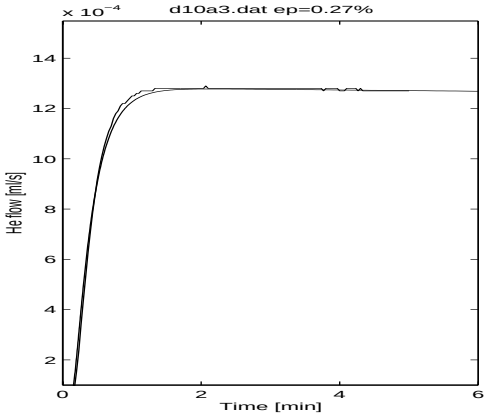


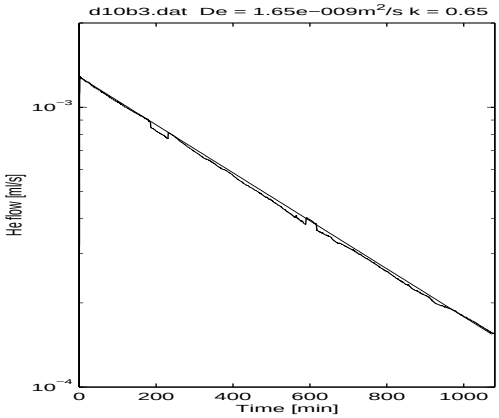

APPENDIX B
Diffusion curves

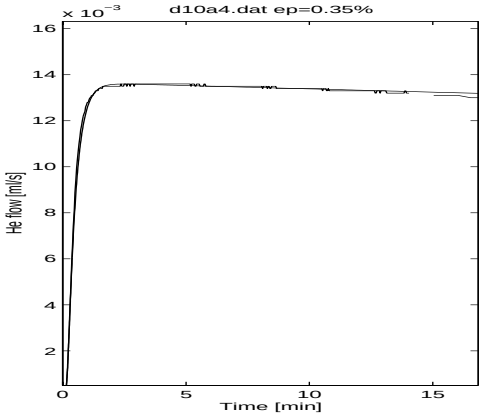


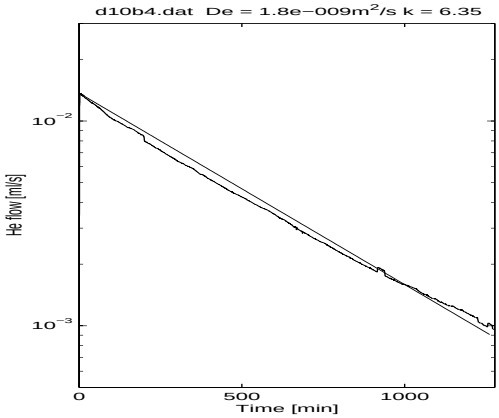


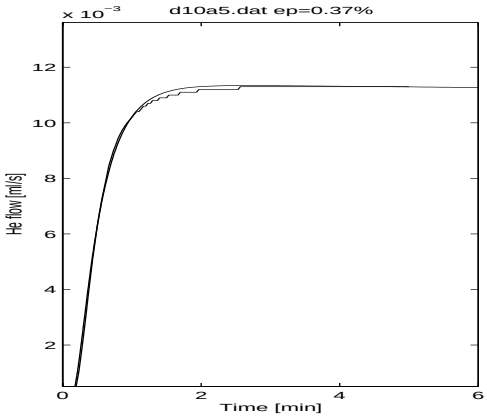


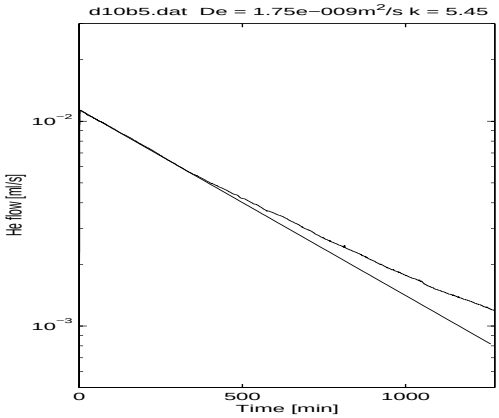


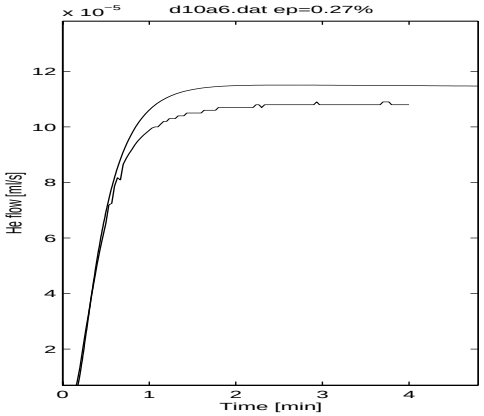


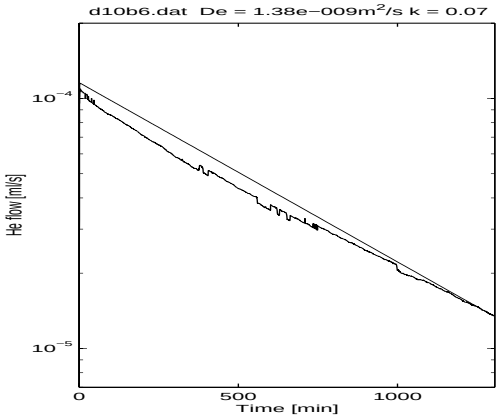

APPENDIX B
Diffusion curves

Diffusion curves of the sample d15

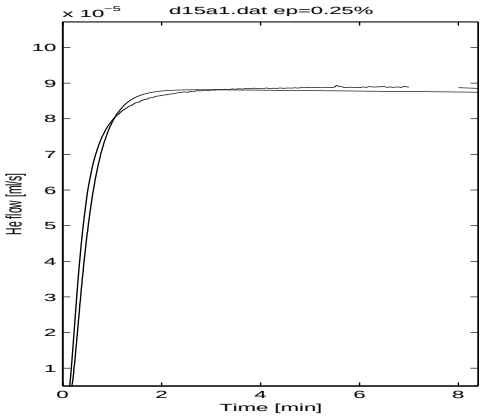


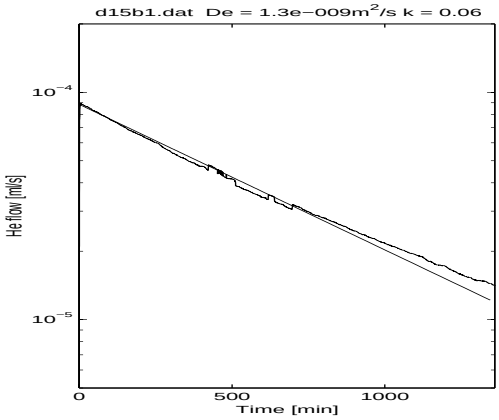


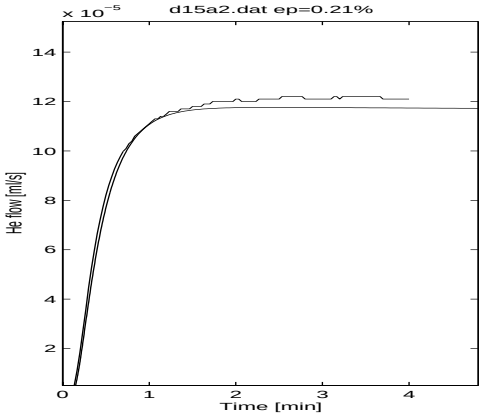


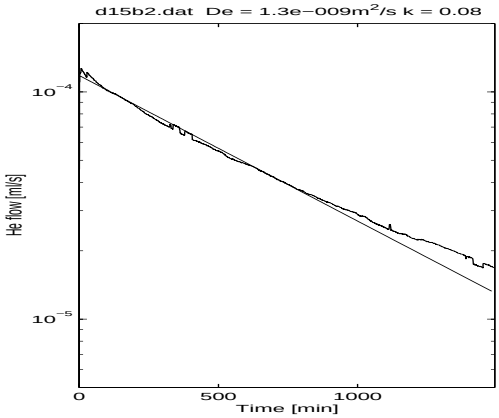


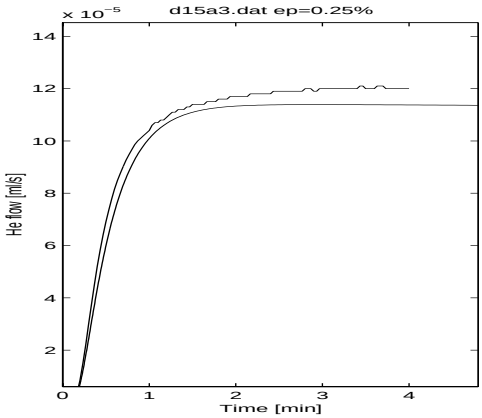


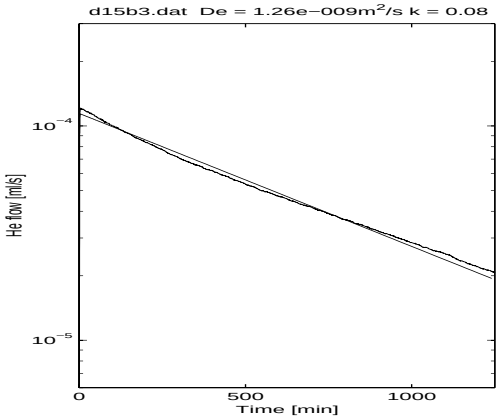

APPENDIX B
Diffusion curves

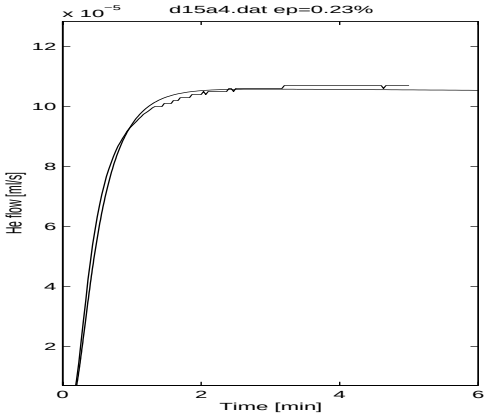


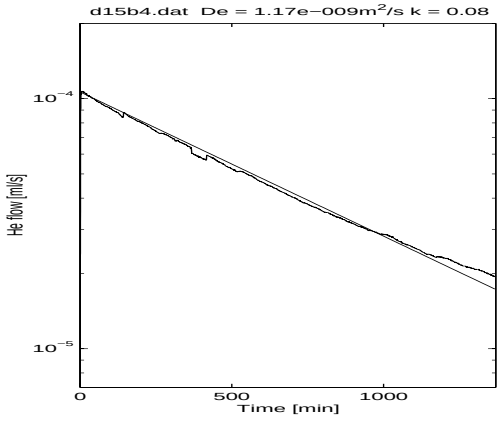


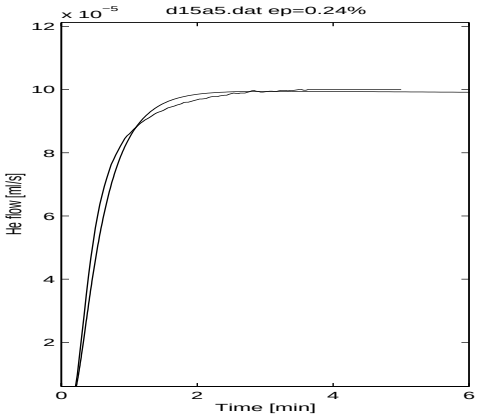


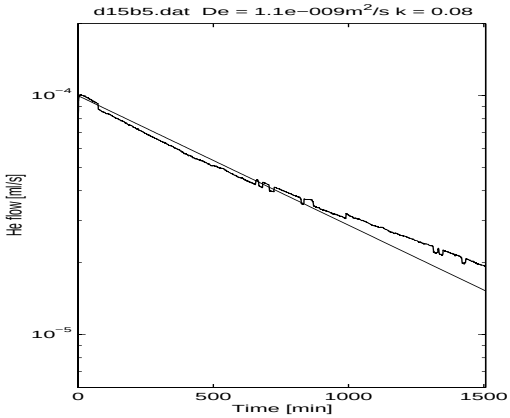

APPENDIX B
Diffusion curves

Diffusion curves of the sample d27

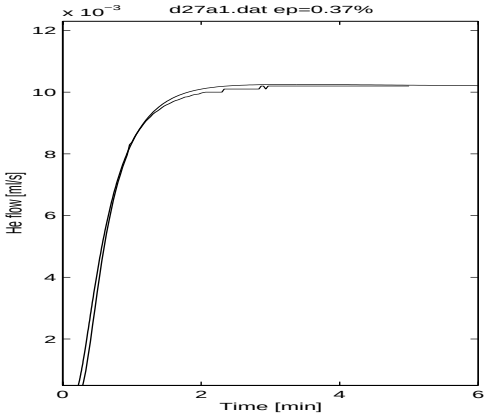


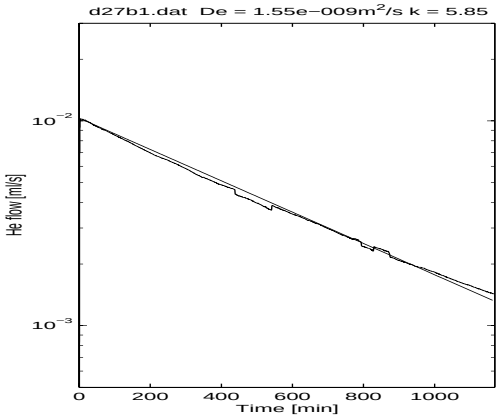


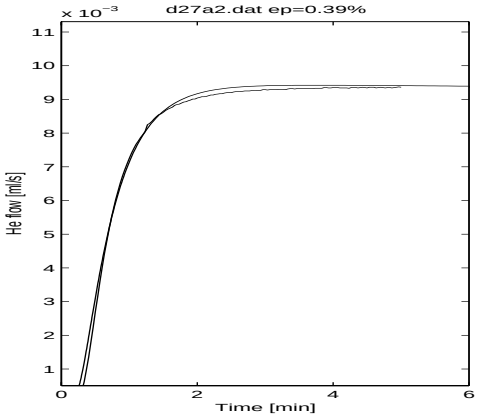


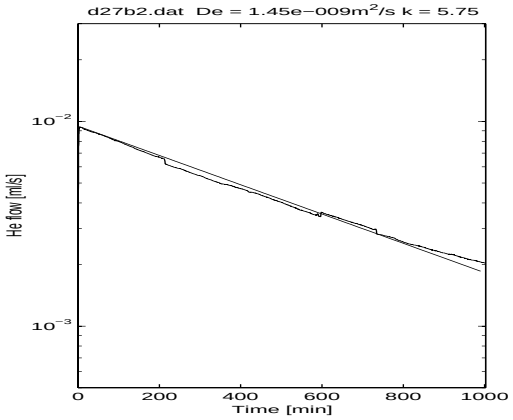


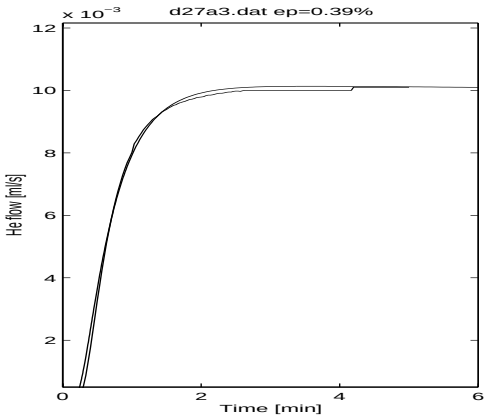


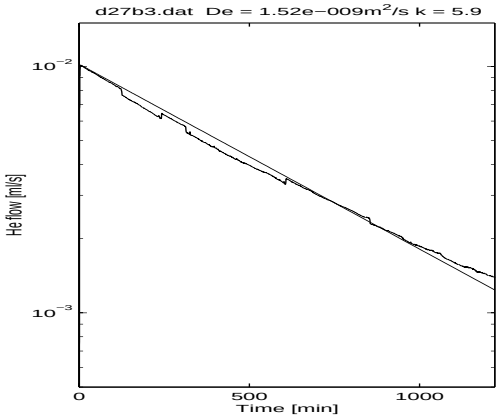

APPENDIX B
Diffusion curves

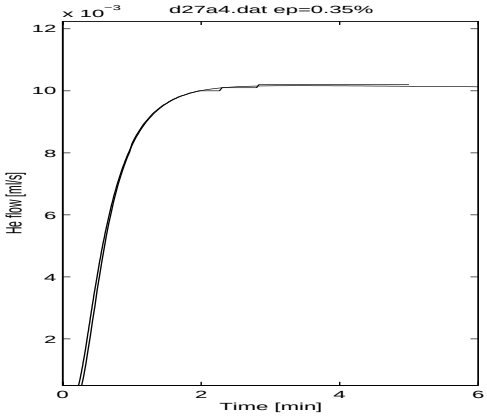


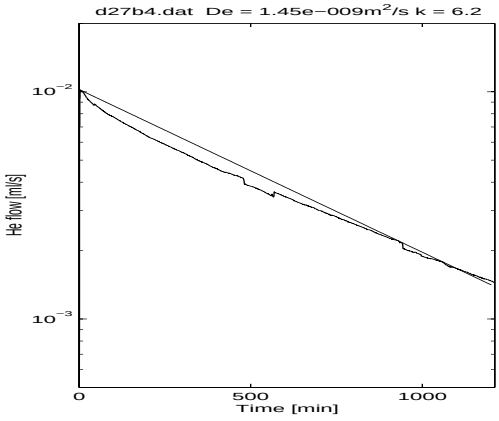


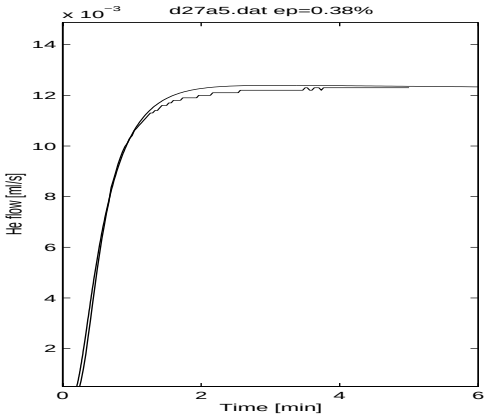


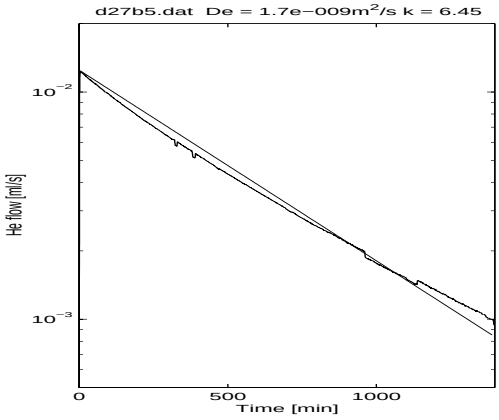


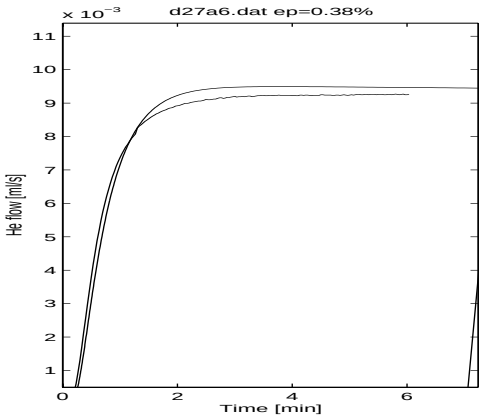


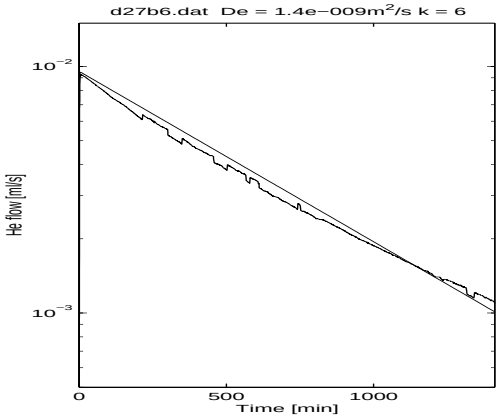

APPENDIX B
Diffusion curves

Diffusion curves of the sample d3

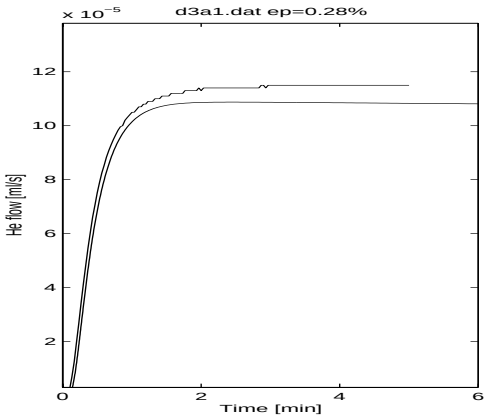


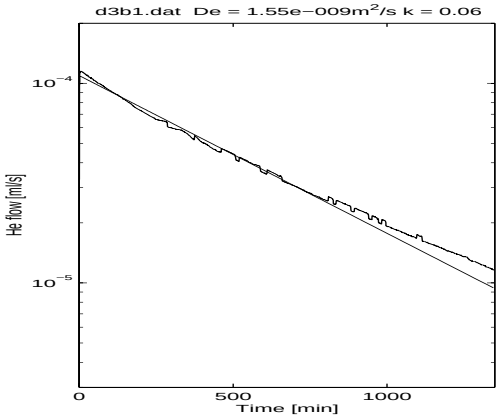


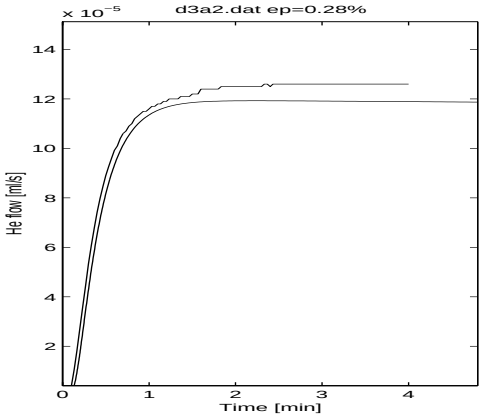


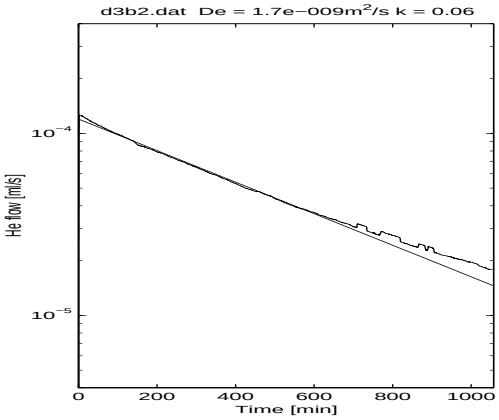


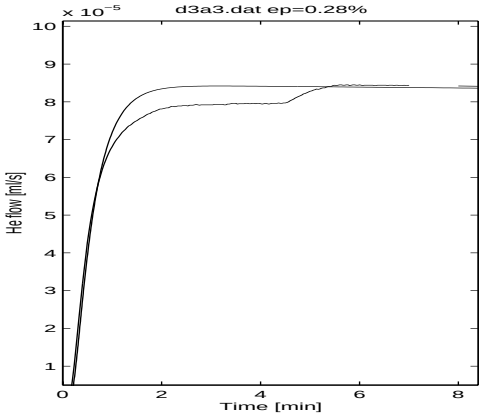


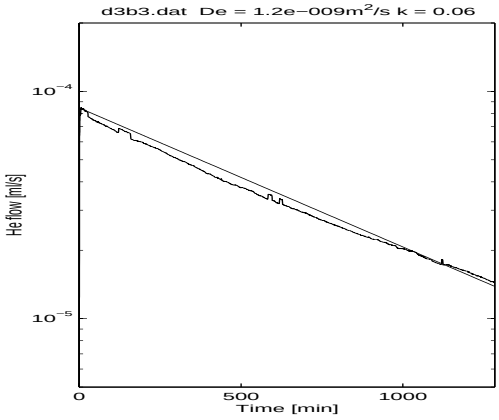

APPENDIX B
Diffusion curves

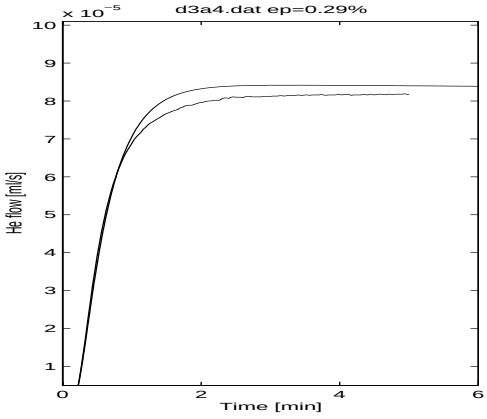


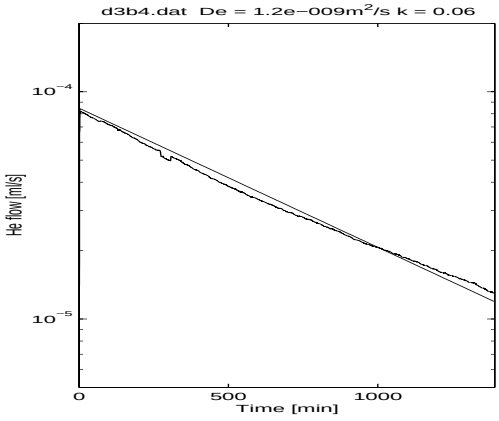


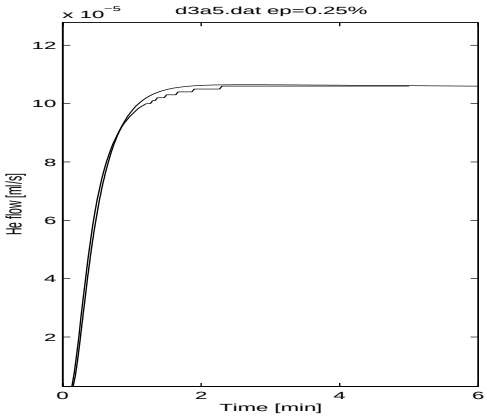


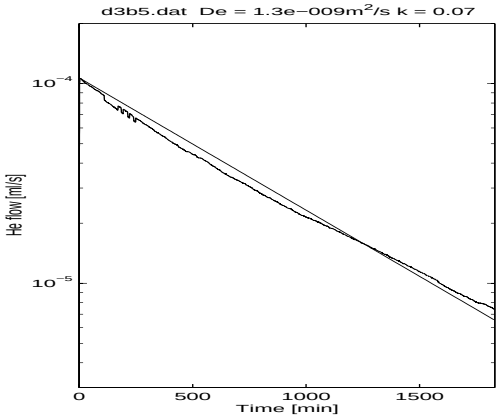

APPENDIX B
Diffusion curves

Diffusion curves of the sample d4

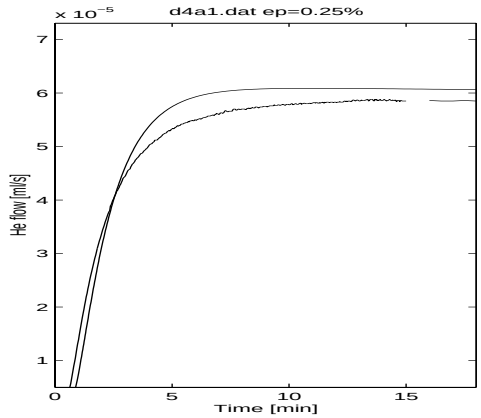


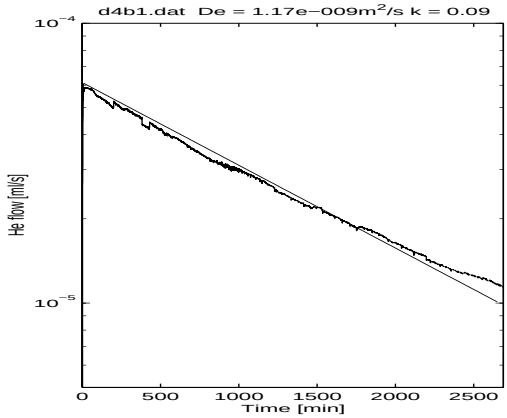


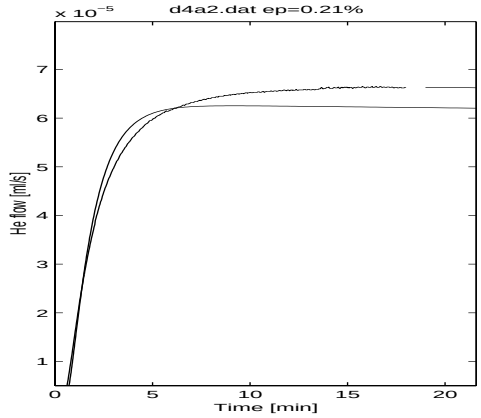


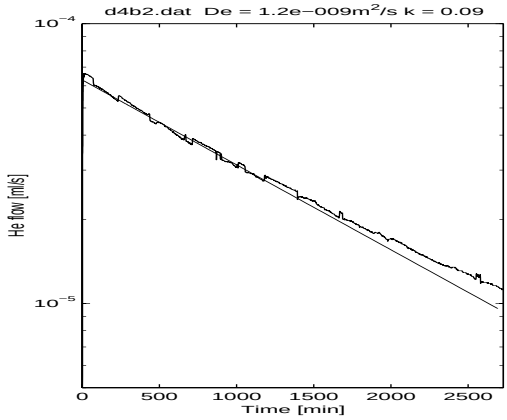


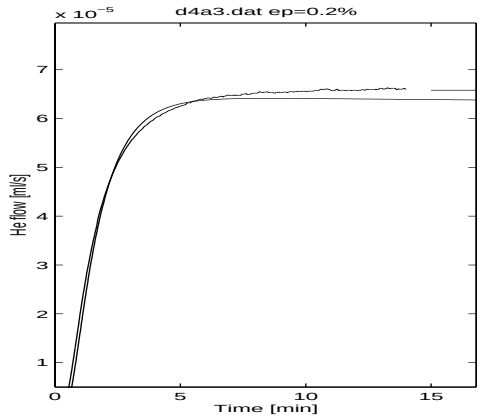


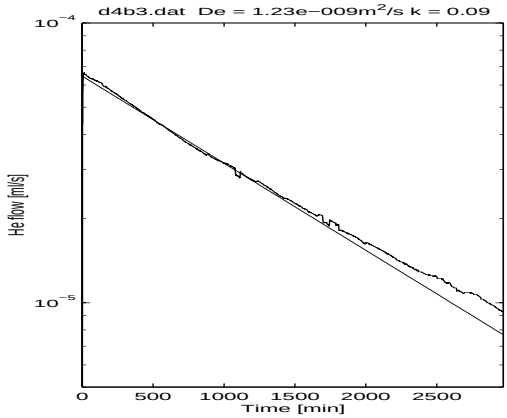

APPENDIX B
Diffusion curves

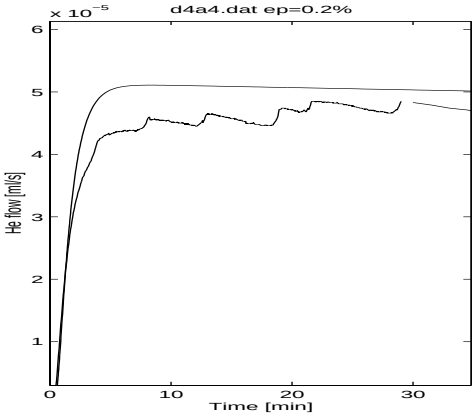


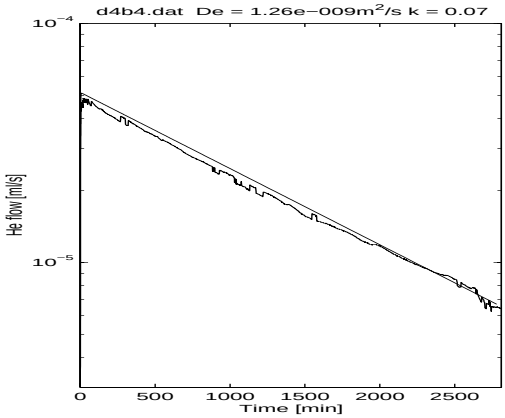


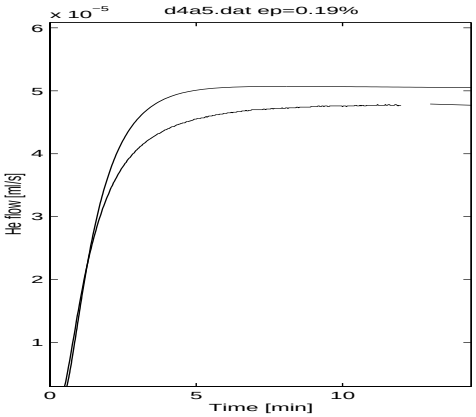


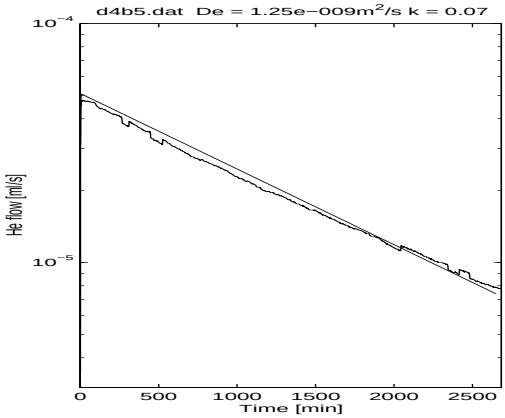

APPENDIX B
Diffusion curves

Diffusion curves of the sample d5

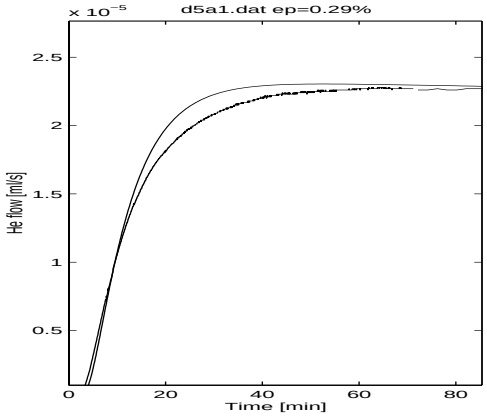


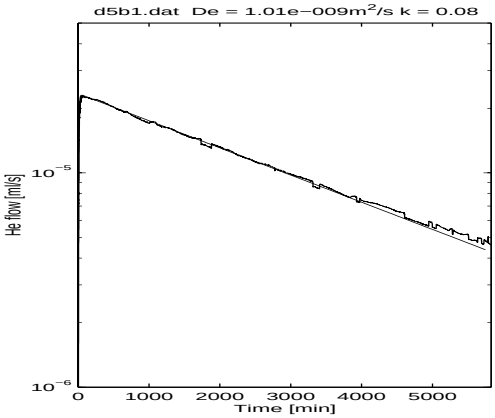


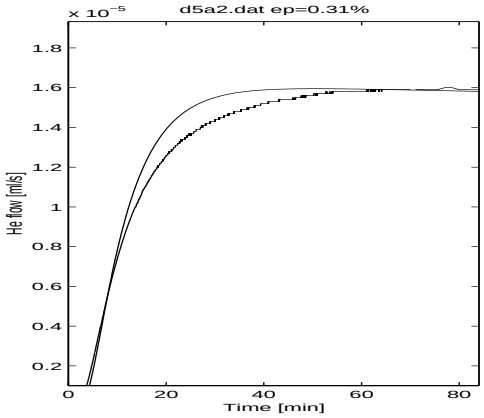


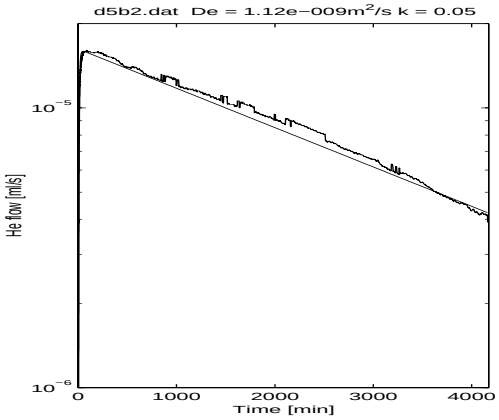


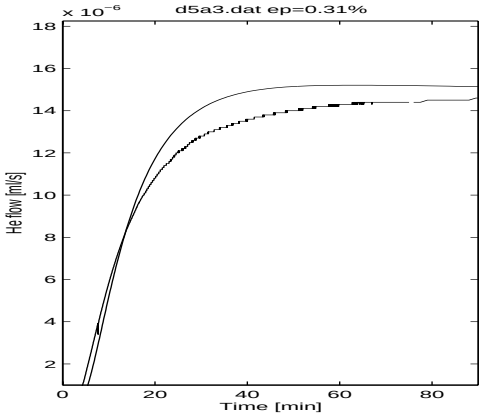


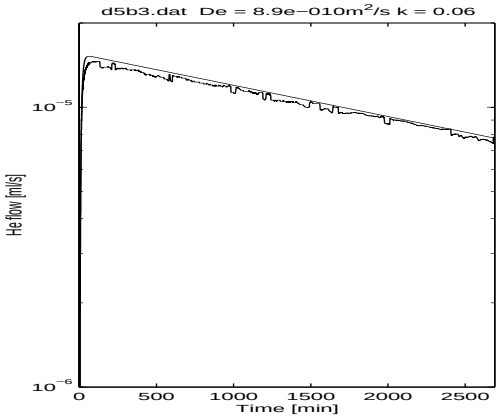

APPENDIX B
Diffusion curves

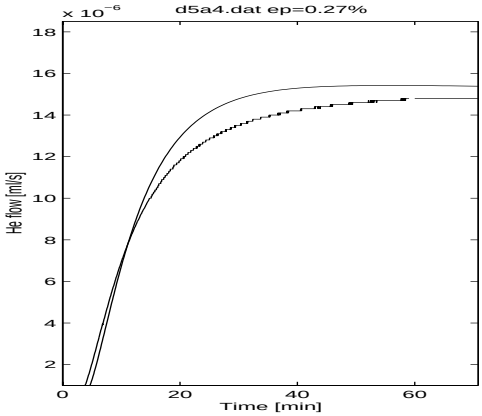


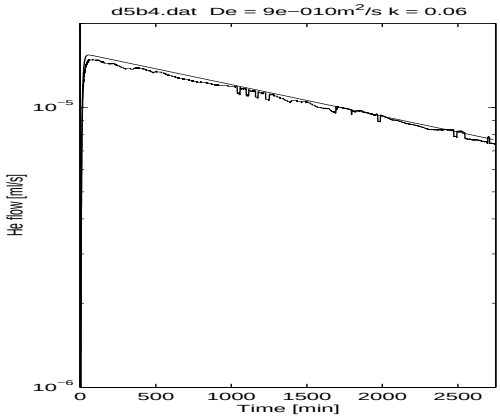


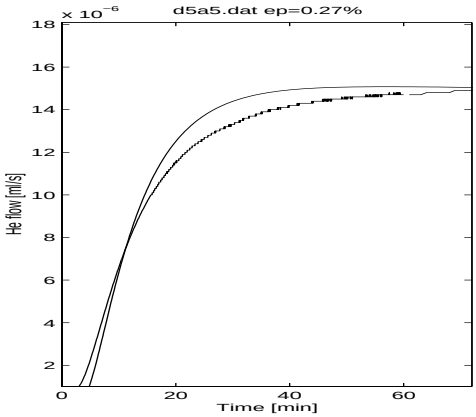


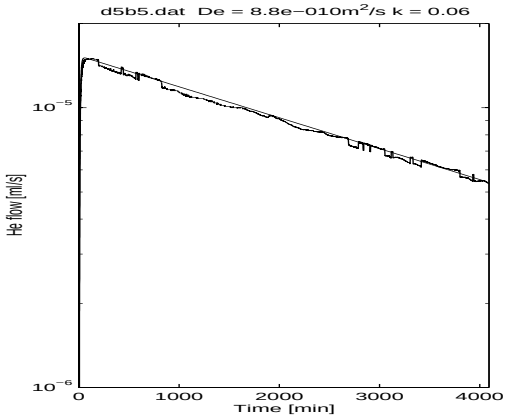

APPENDIX B
Diffusion curves

Diffusion curves of the sample.d7

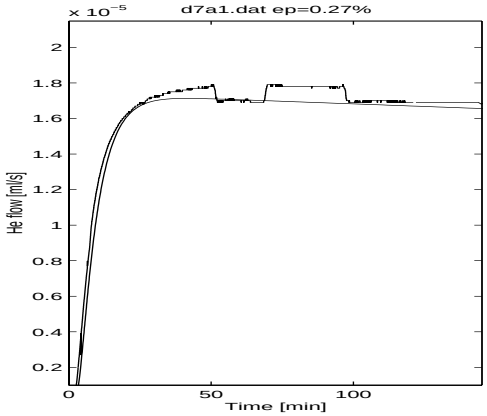


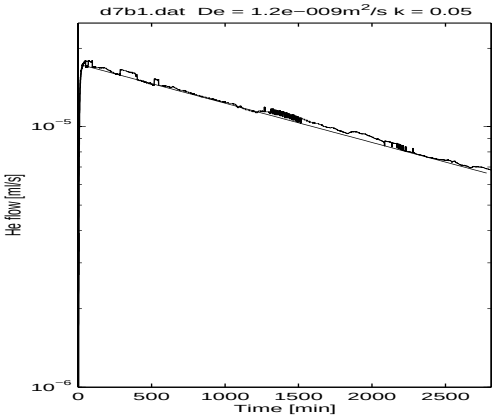


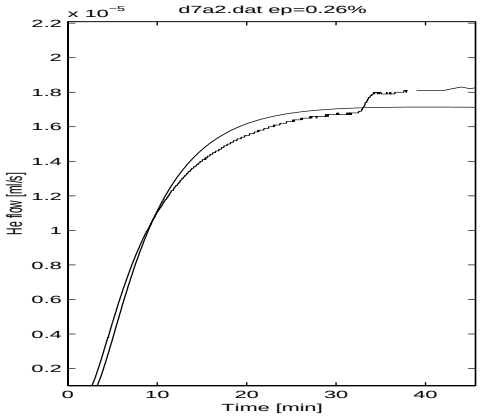


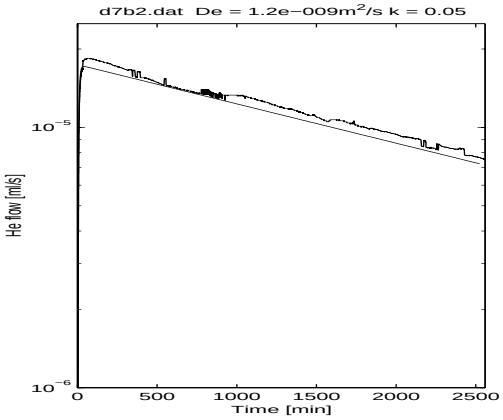


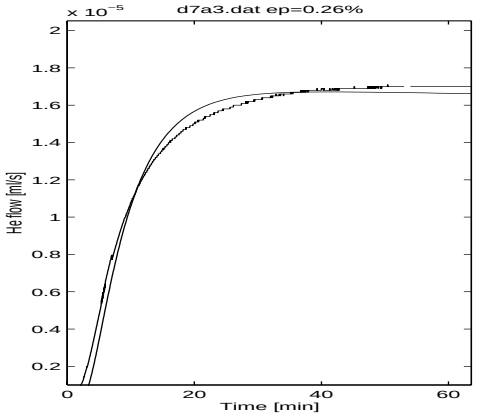


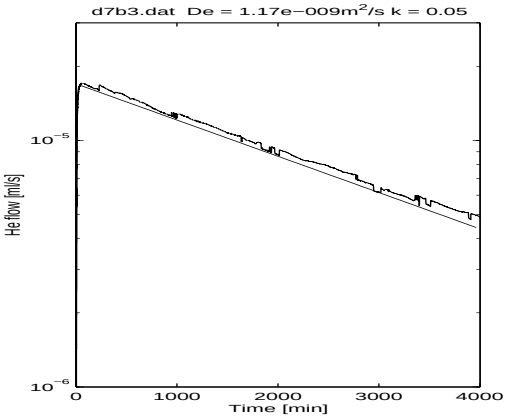

APPENDIX B
Diffusion curves

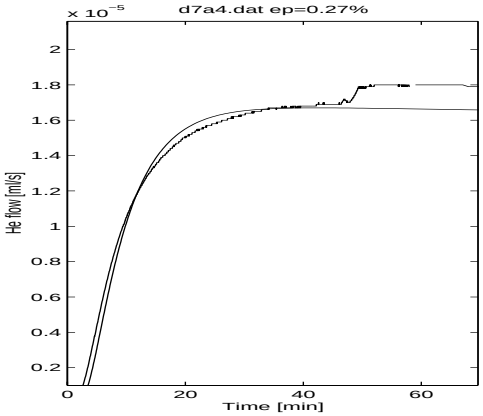


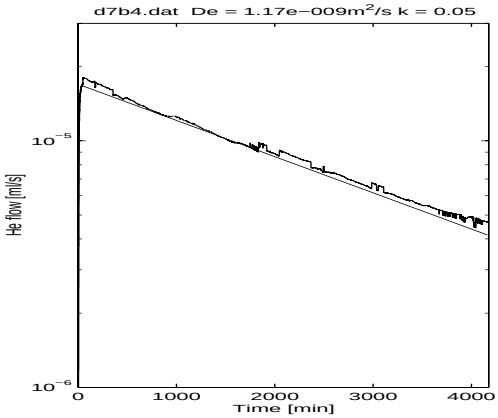


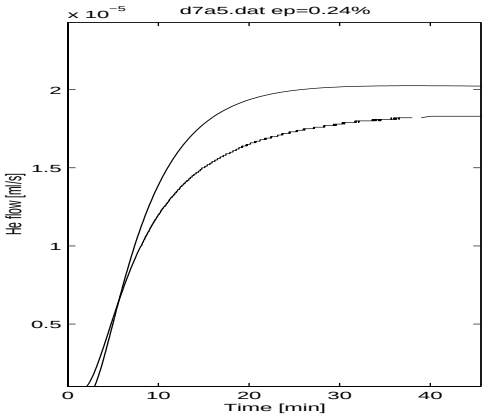


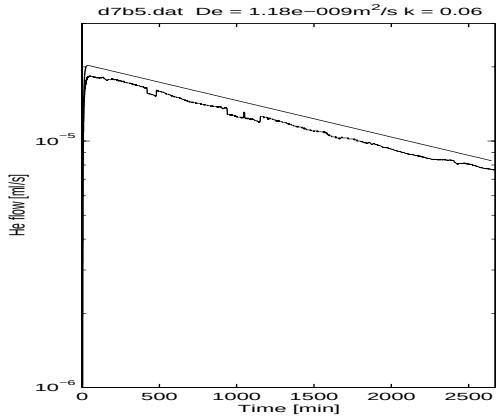

APPENDIX B
Diffusion curves

Diffusion curves of the sample g1

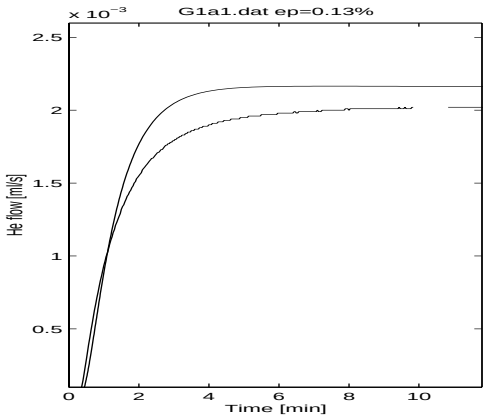


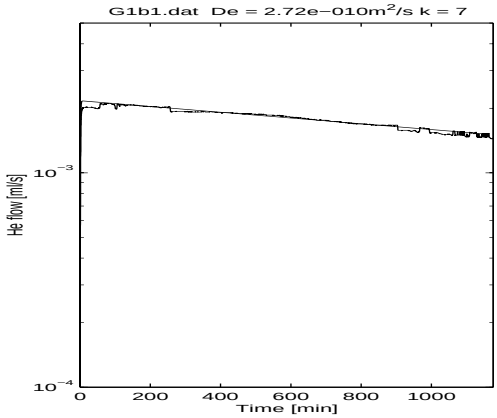


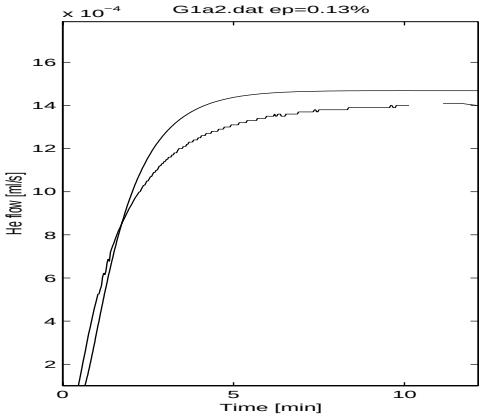


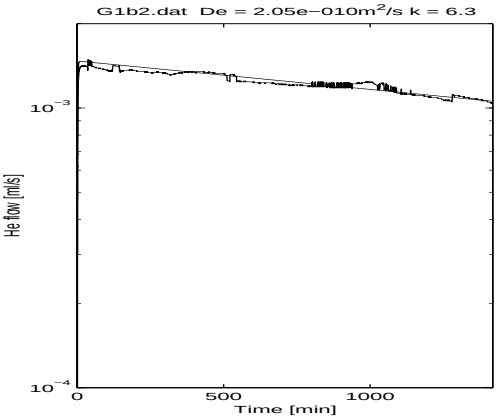

APPENDIX B
Diffusion curves

Diffusion curves of the sample g14

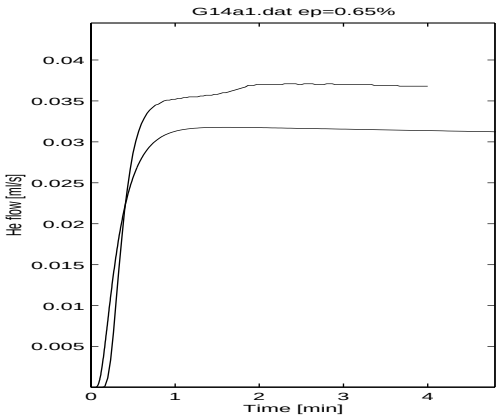


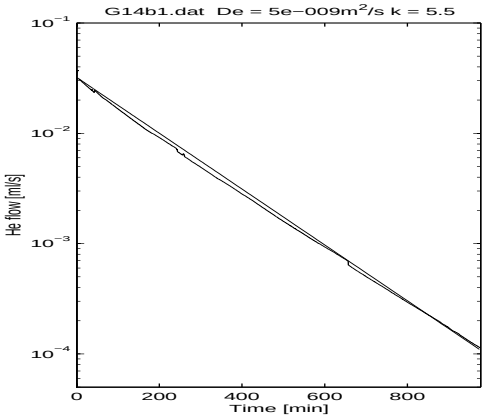


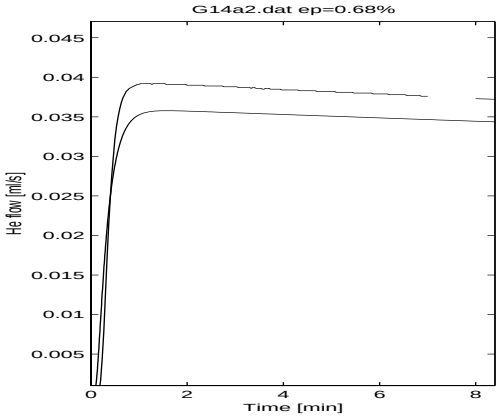


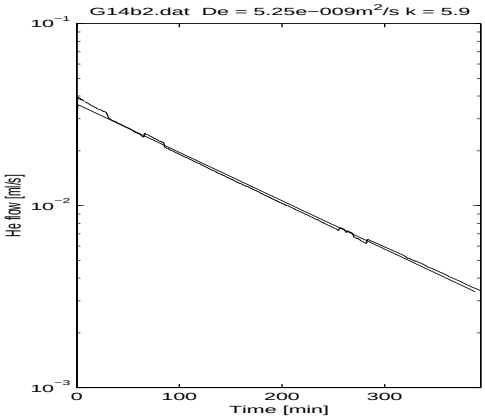


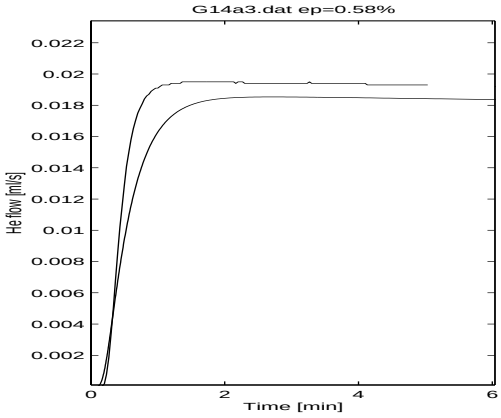


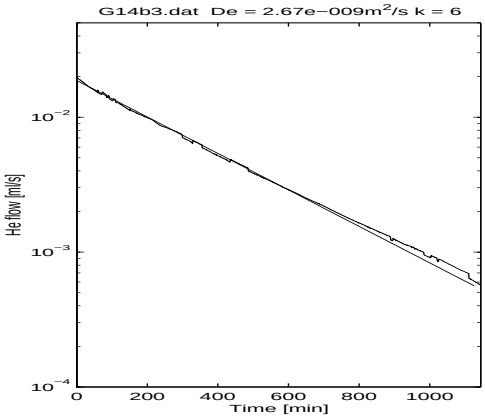

APPENDIX B
Diffusion curves

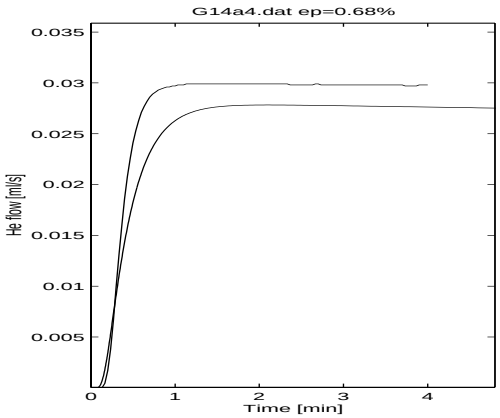


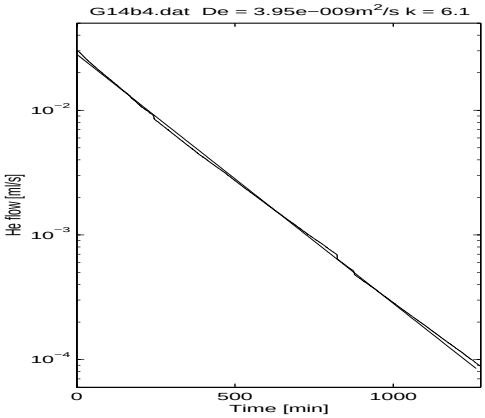


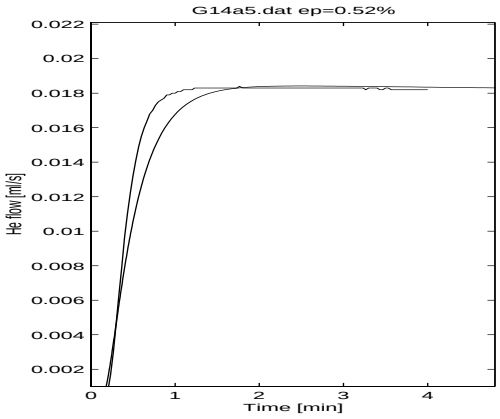


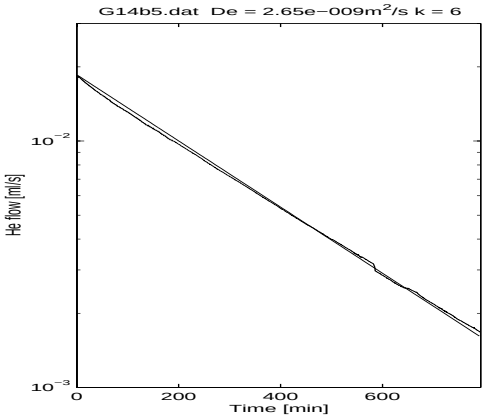


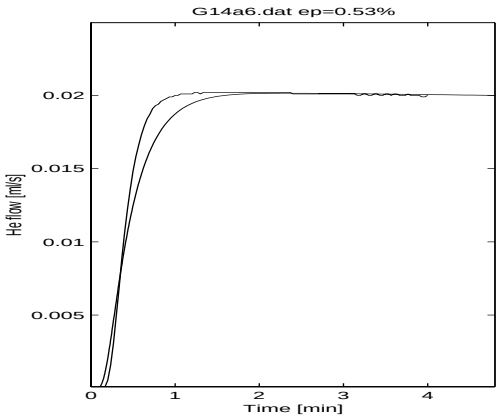


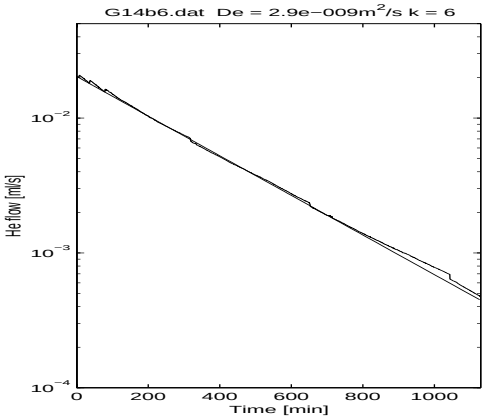

APPENDIX B
Diffusion curves

Diffusion curves of the sample g2

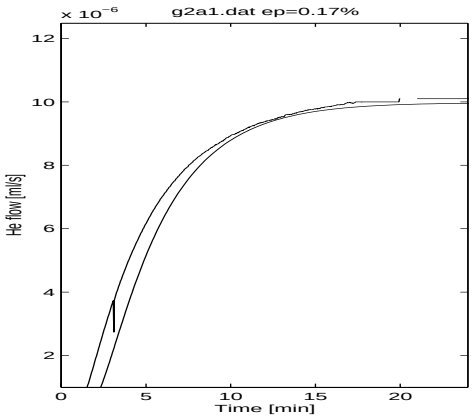


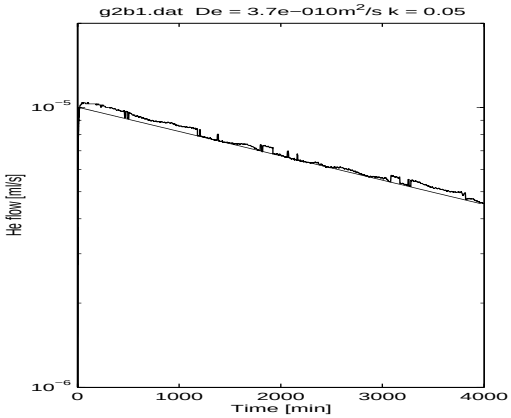


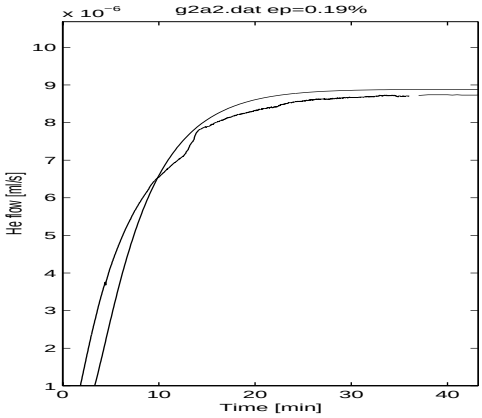


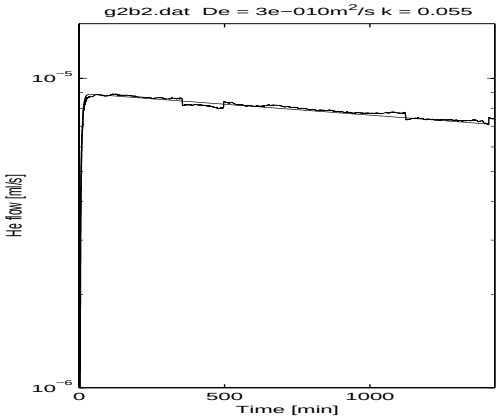


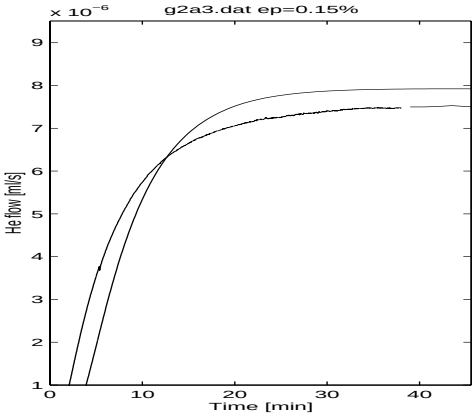


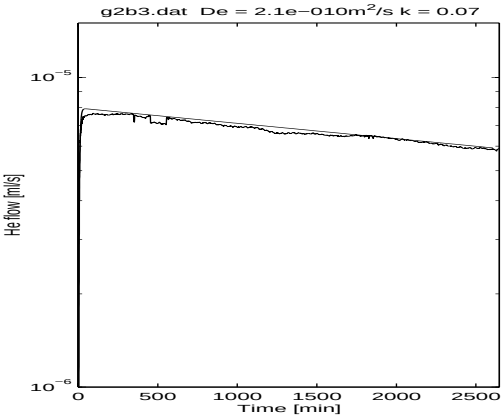

APPENDIX B
Diffusion curves

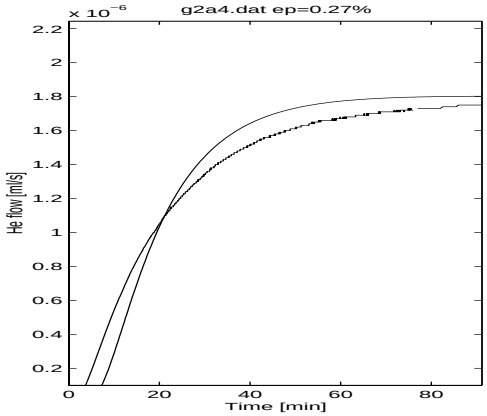


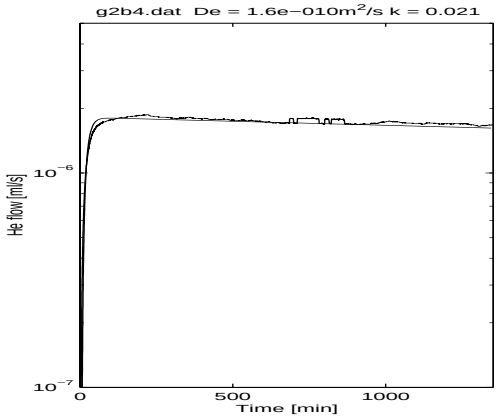


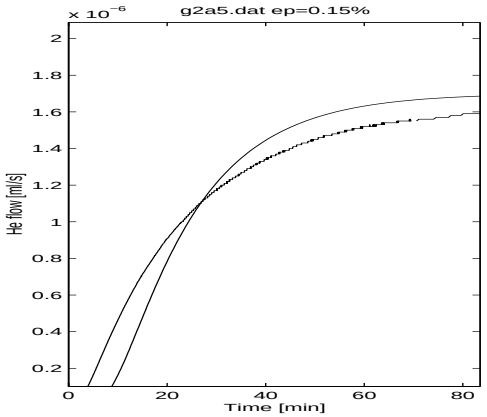


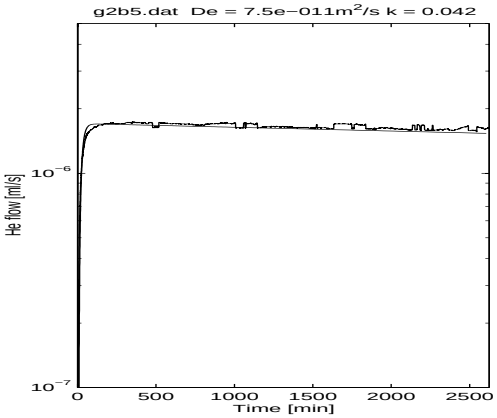


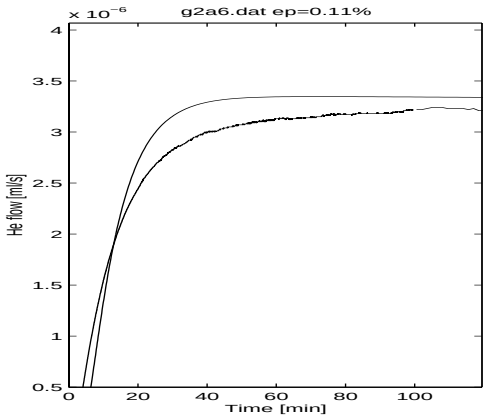


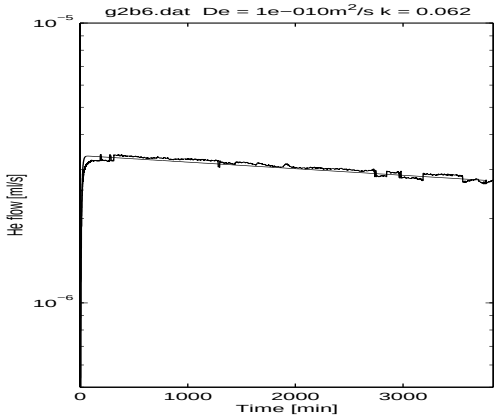

APPENDIX B
Diffusion curves

Diffusion curves of the sample g26

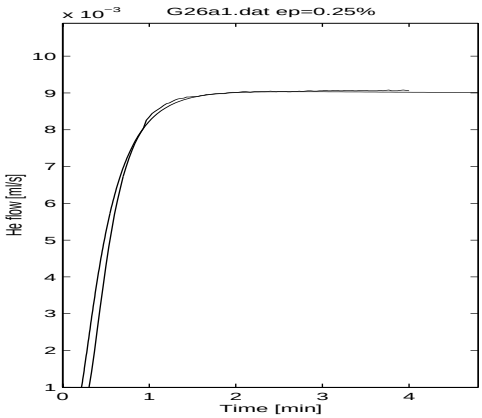


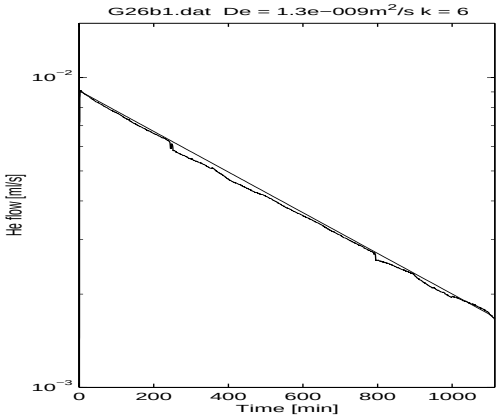


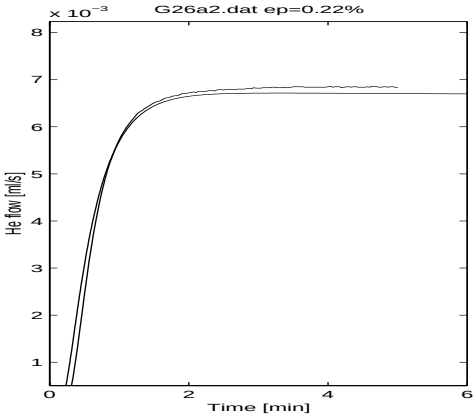


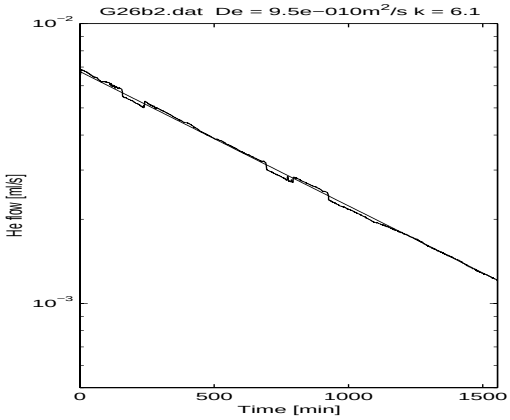


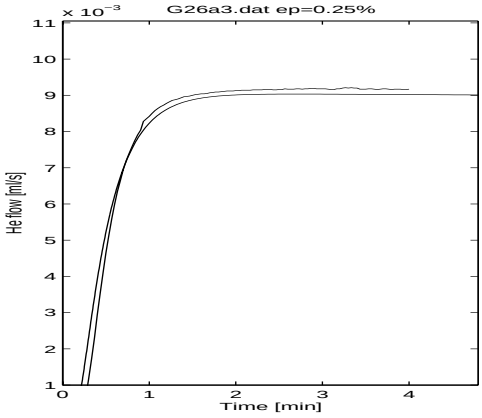


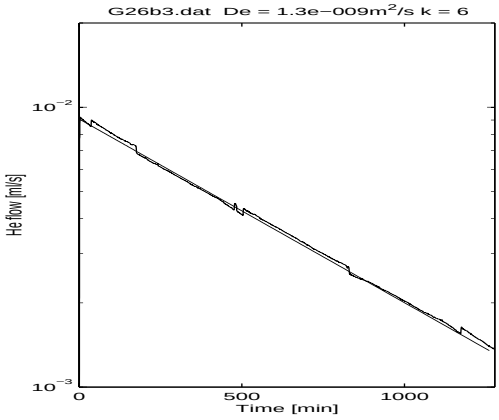

APPENDIX B
Diffusion curves

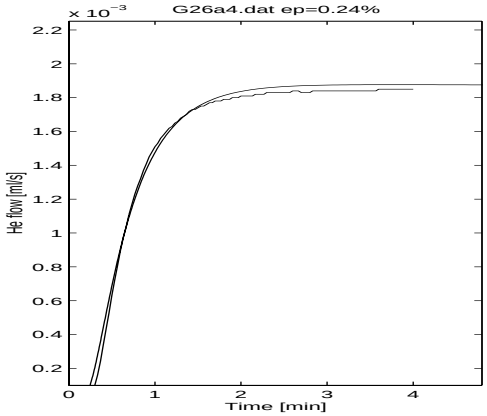


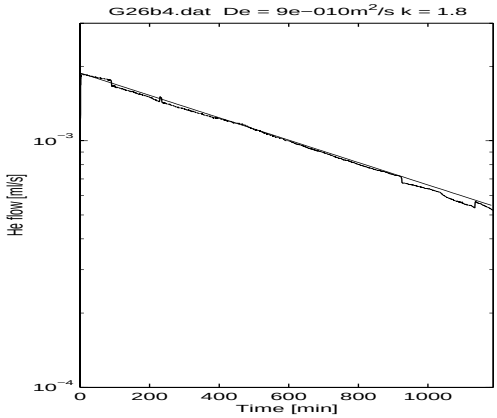


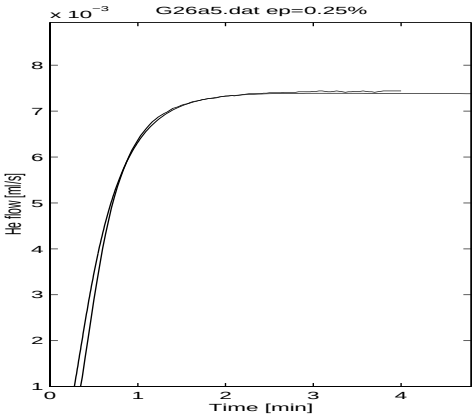


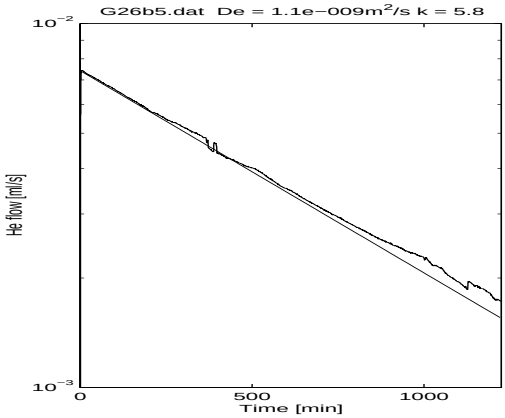

APPENDIX B
Diffusion curves

Diffusion curves of the sample g6

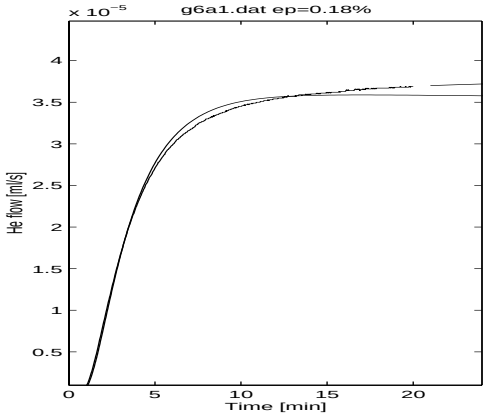


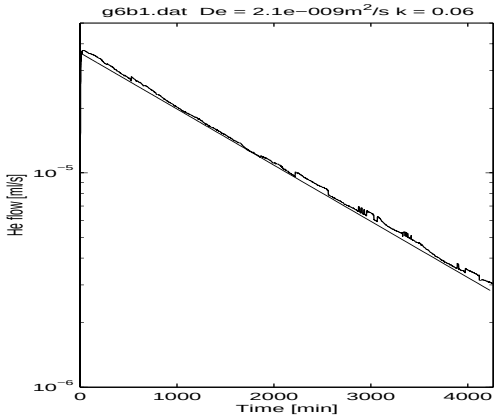


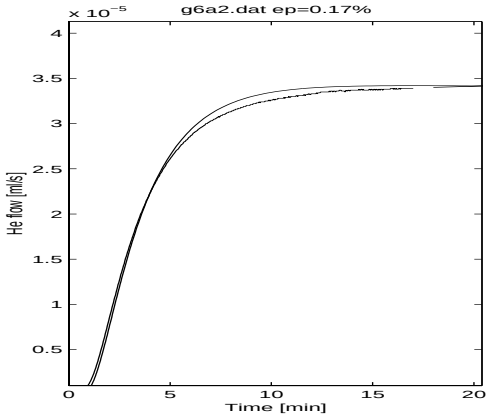


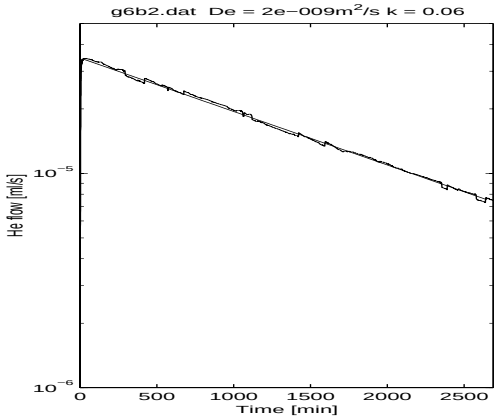


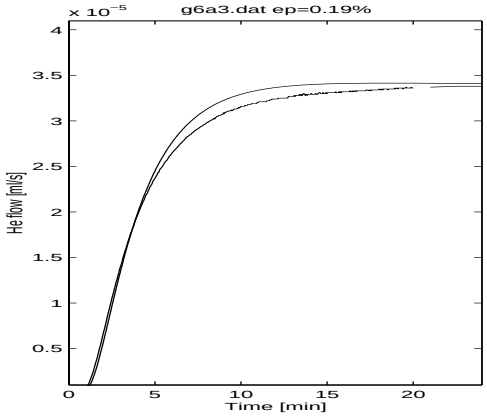


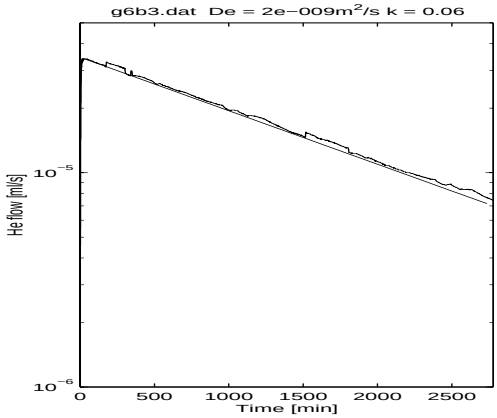

APPENDIX B
Diffusion curves

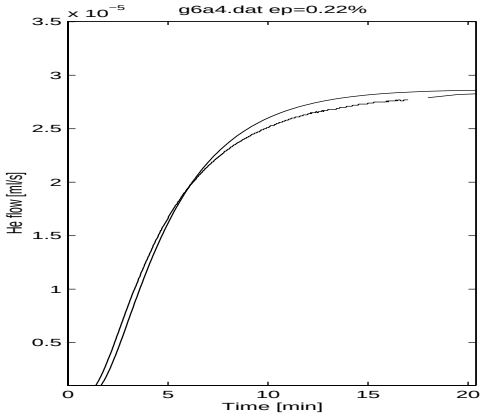


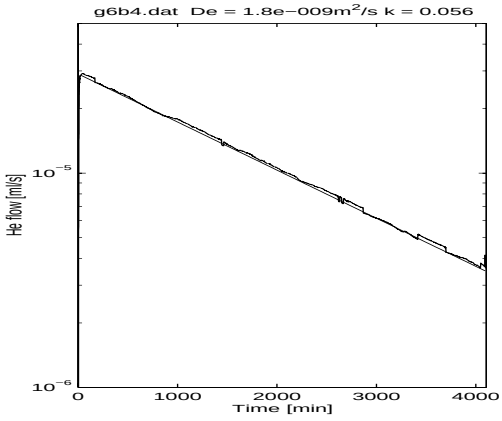


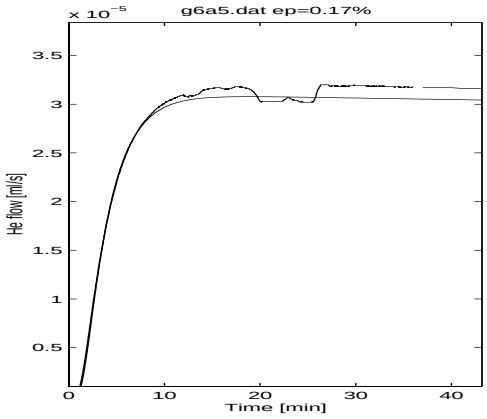


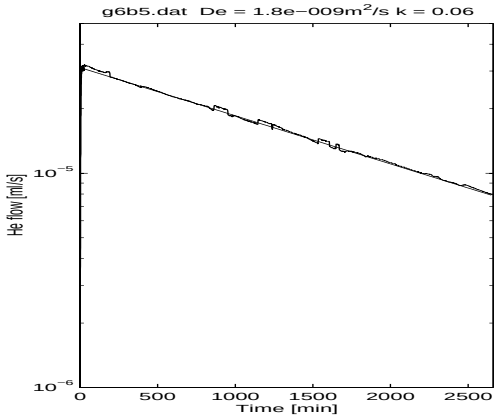


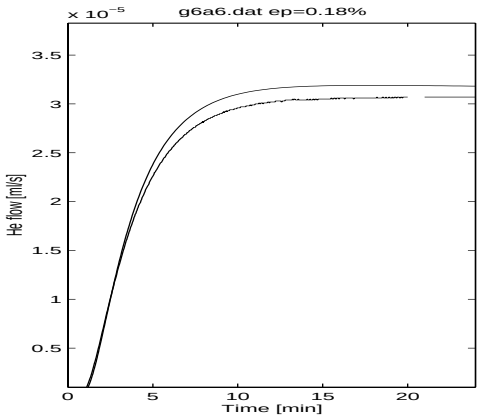


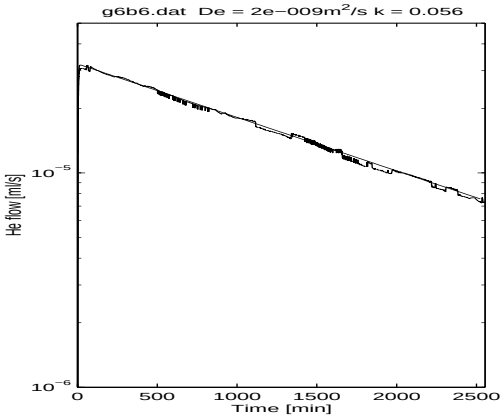

APPENDIX B
Diffusion curves

Diffusion curves of the sample g8

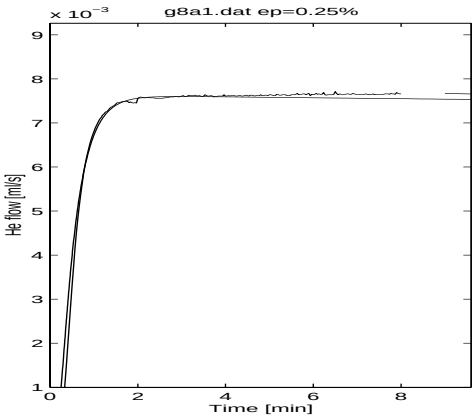


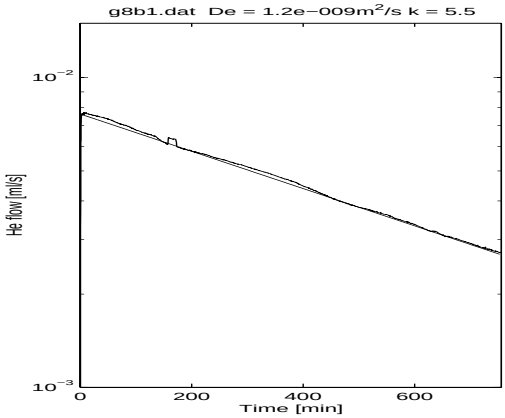


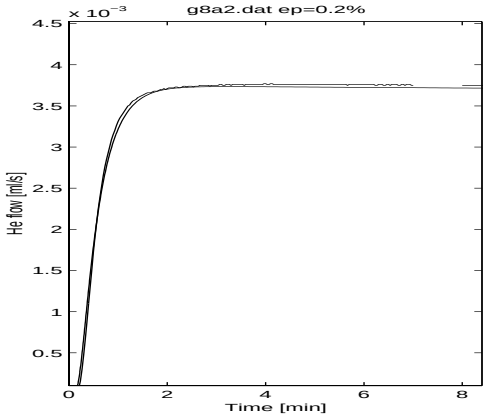


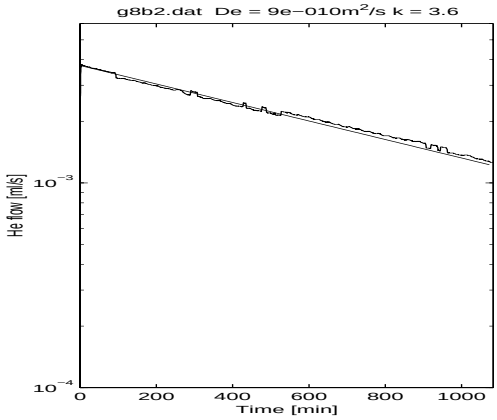


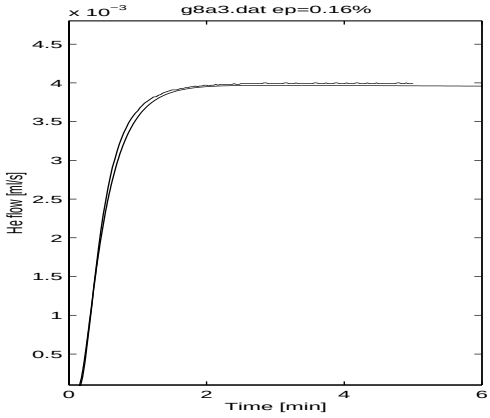


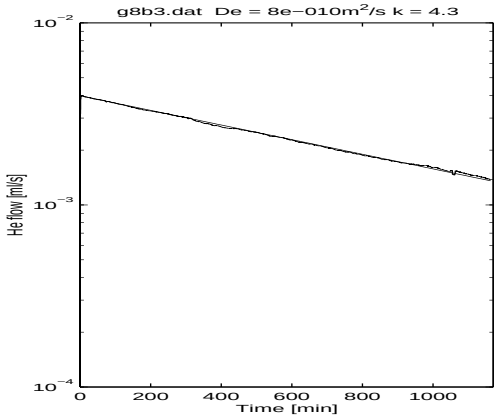

APPENDIX B
Diffusion curves

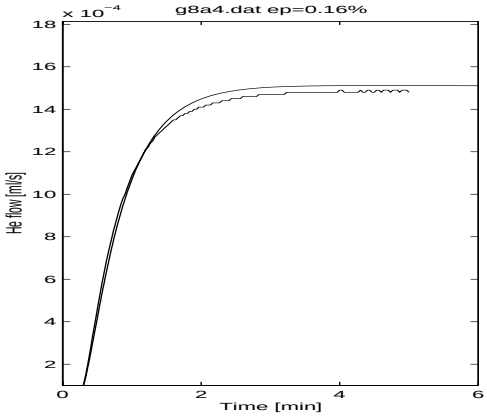


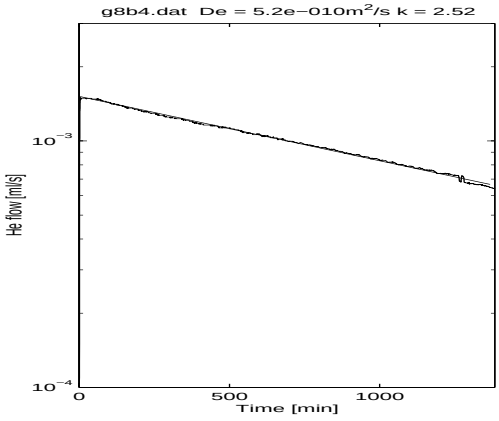


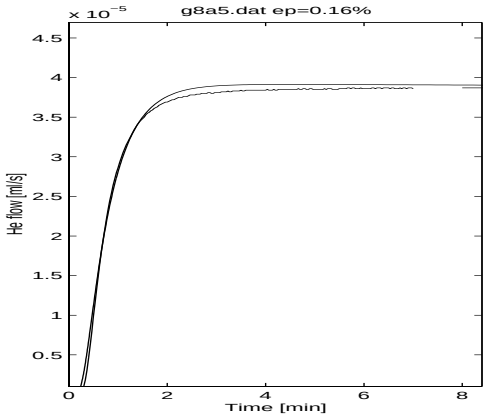


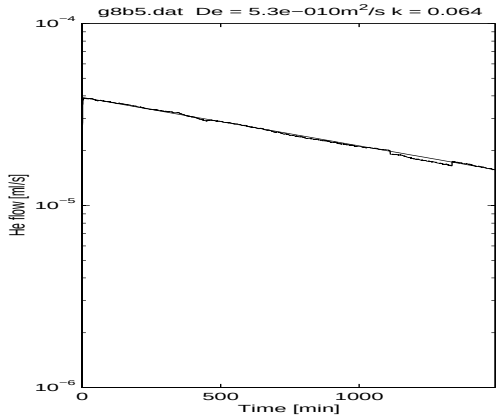


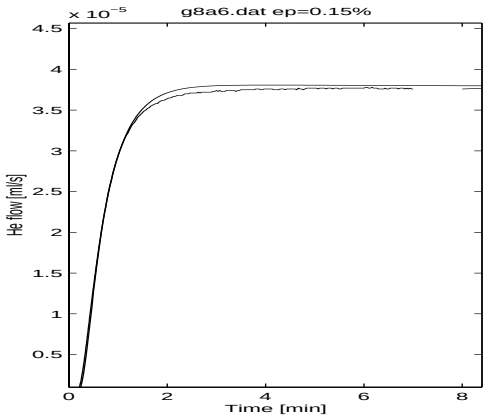


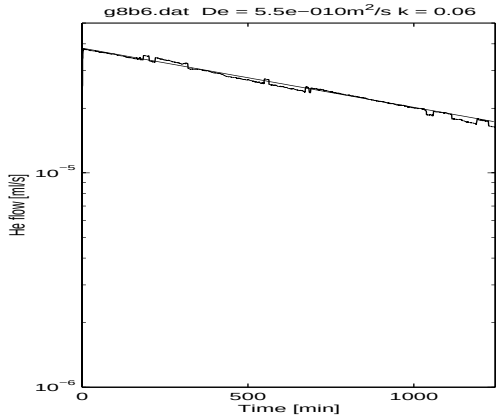

APPENDIX B
Diffusion curves

Diffusion curves for sample 1

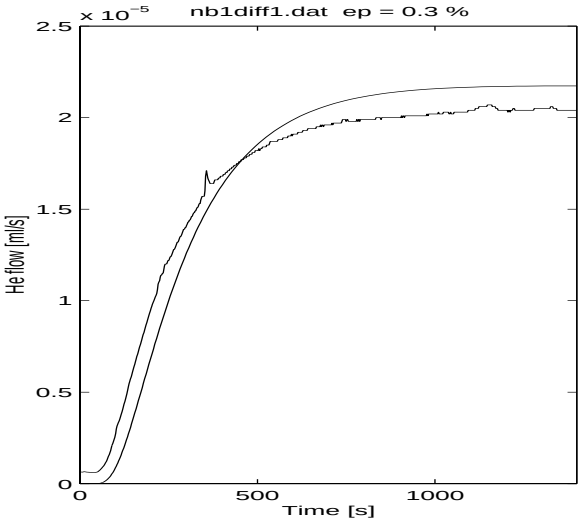


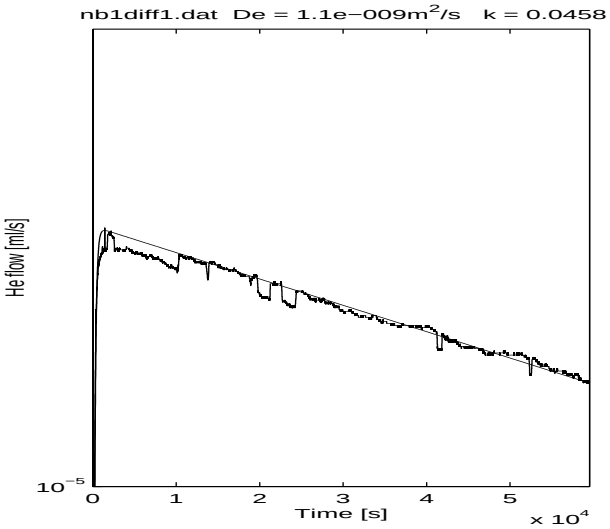


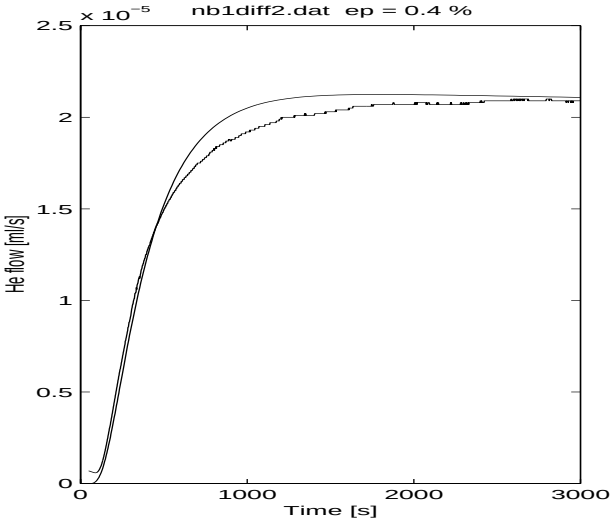


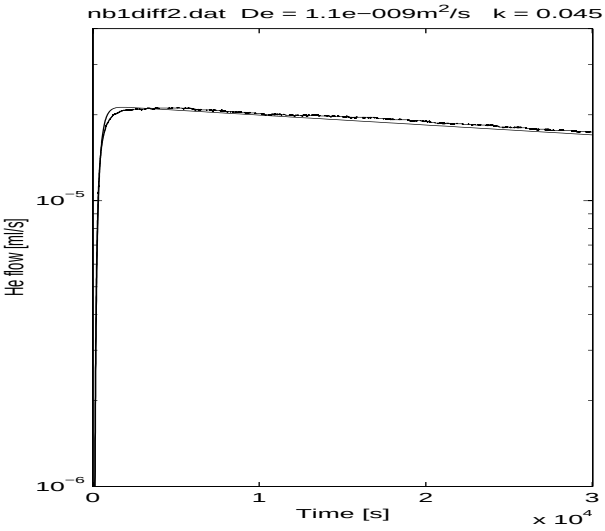

APPENDIX B
Diffusion curves

Diffusion curves for sample 3

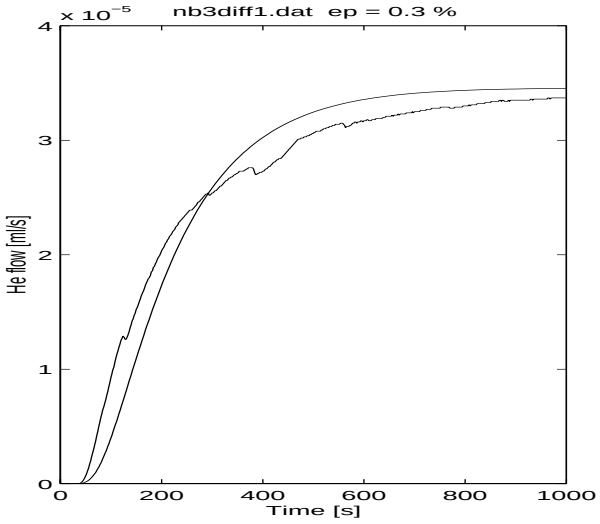


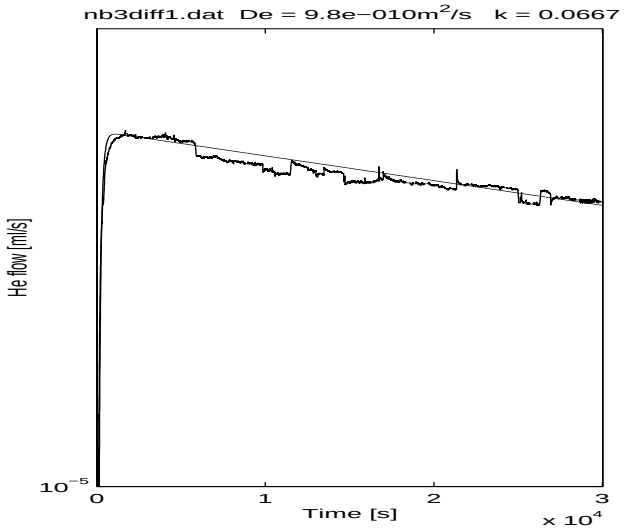


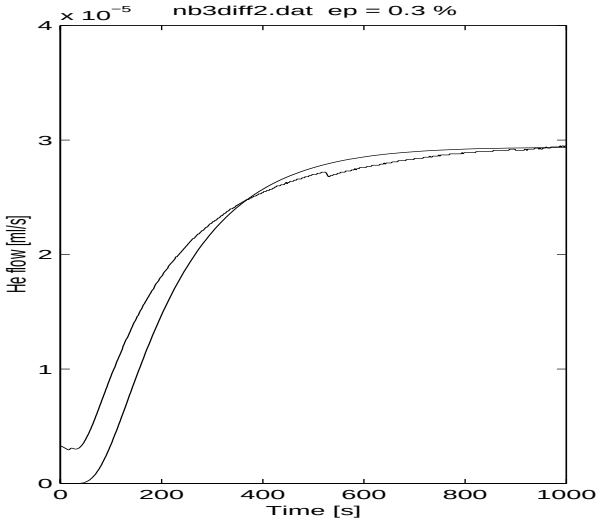


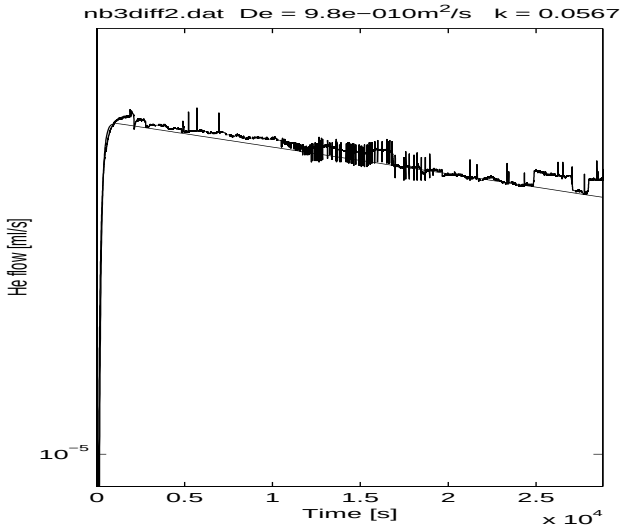

APPENDIX B
Diffusion curves

Diffusion curves for sample 4

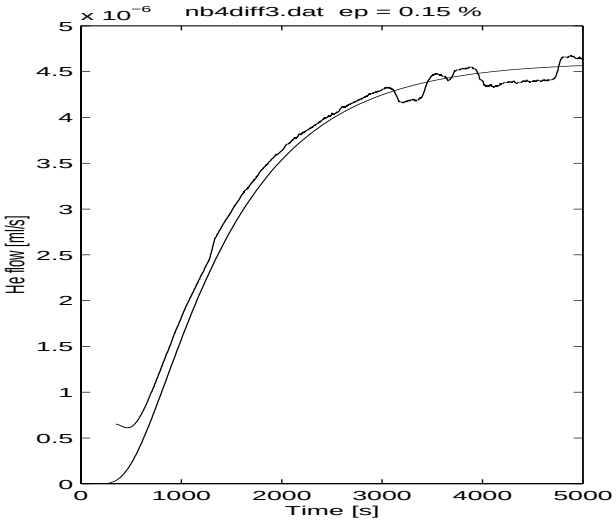


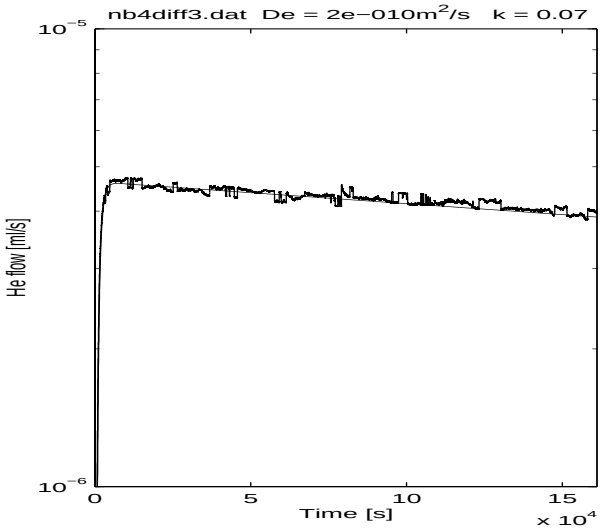


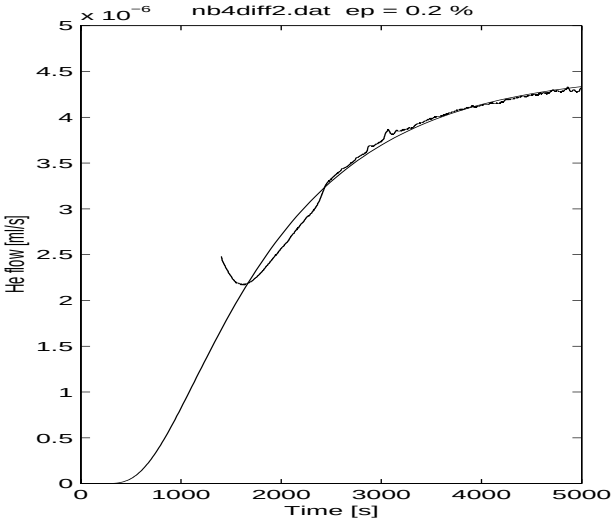


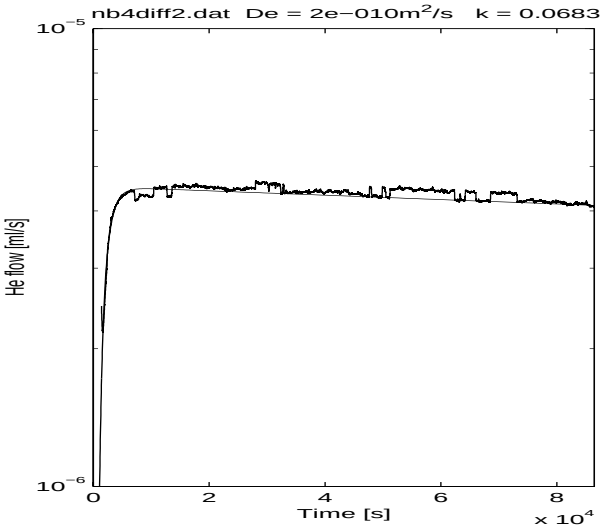

APPENDIX B
Diffusion curves

Diffusion curves for sample 5

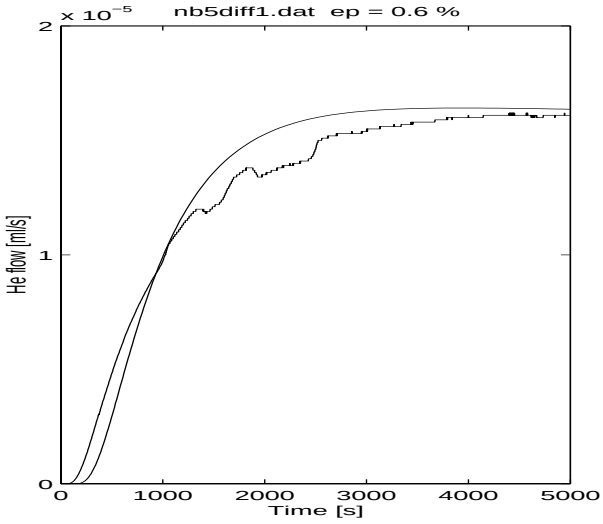


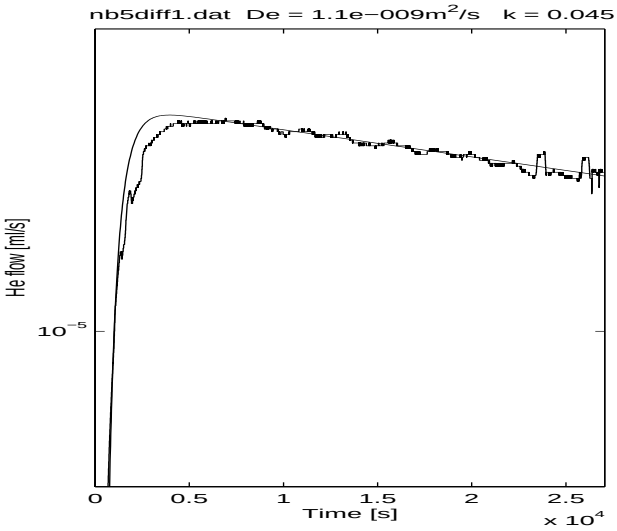


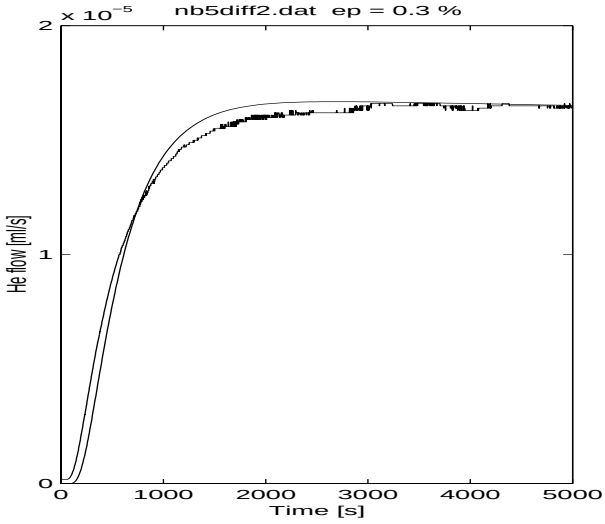


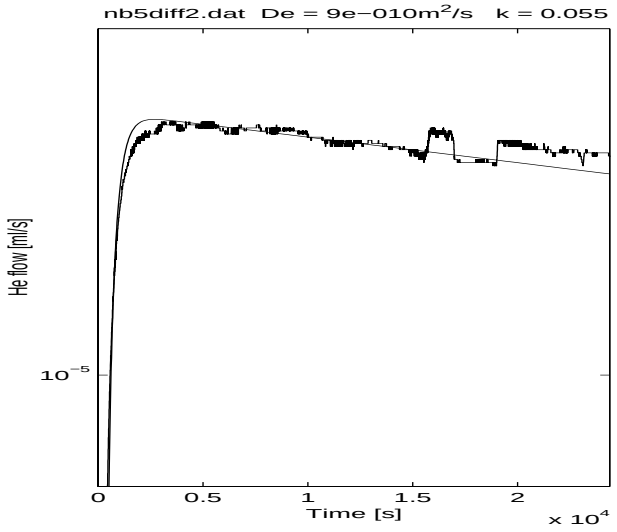

APPENDIX B
Diffusion curves

Diffusion curves for sample 6

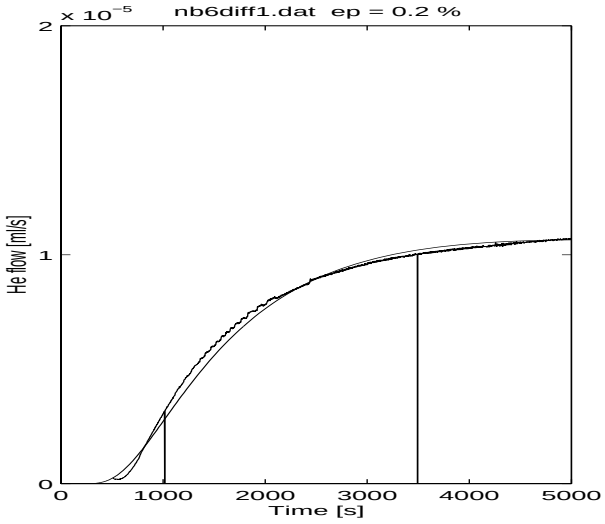


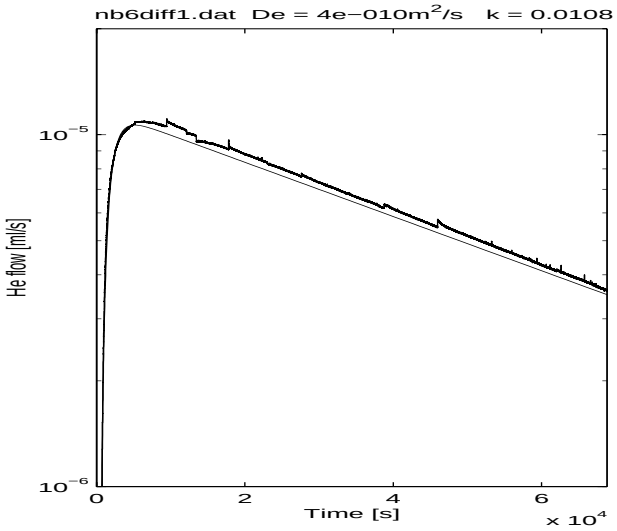


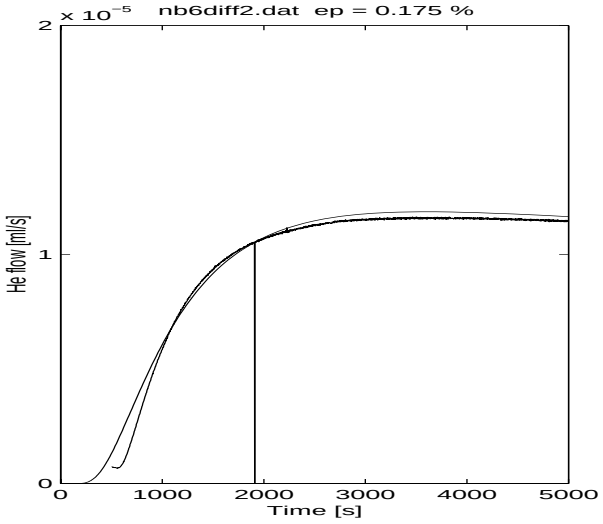


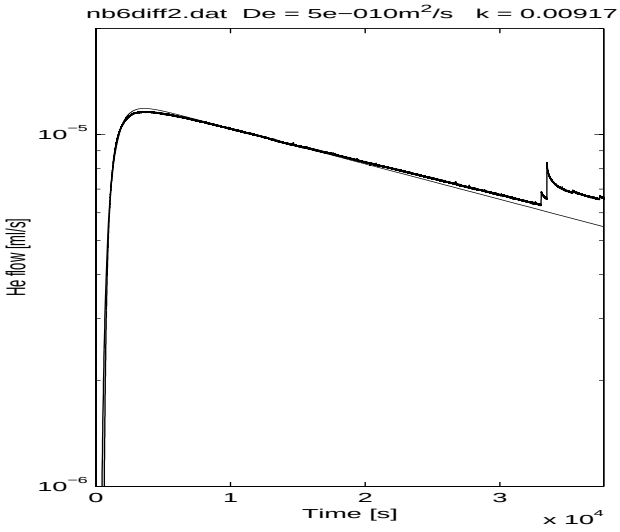

APPENDIX B
Diffusion curves

Diffusion curves for sample 8

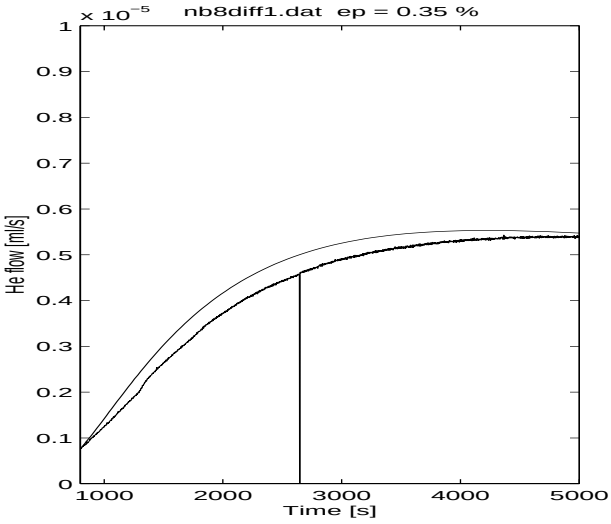


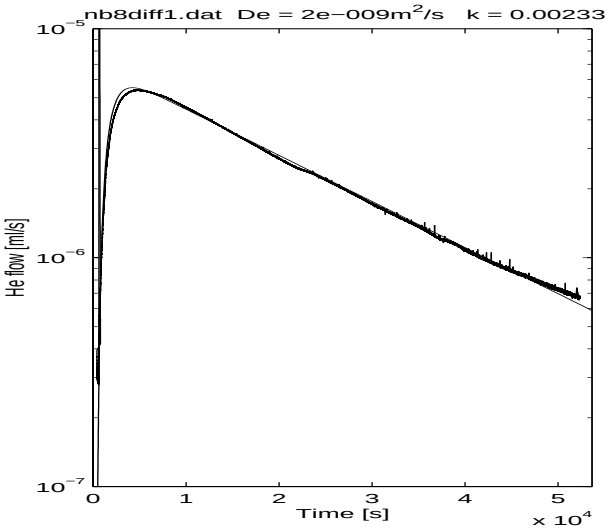


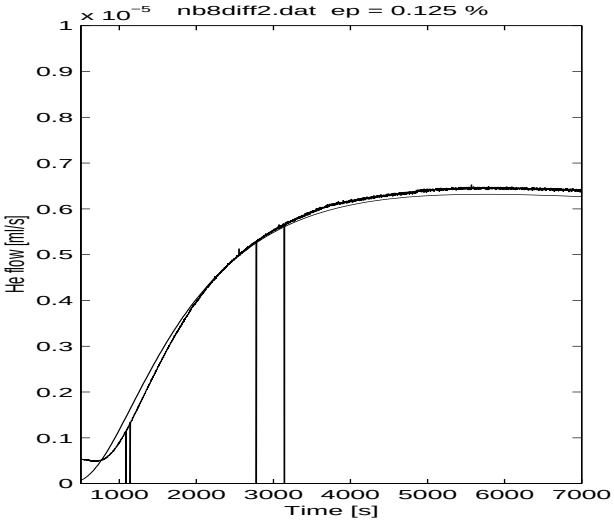


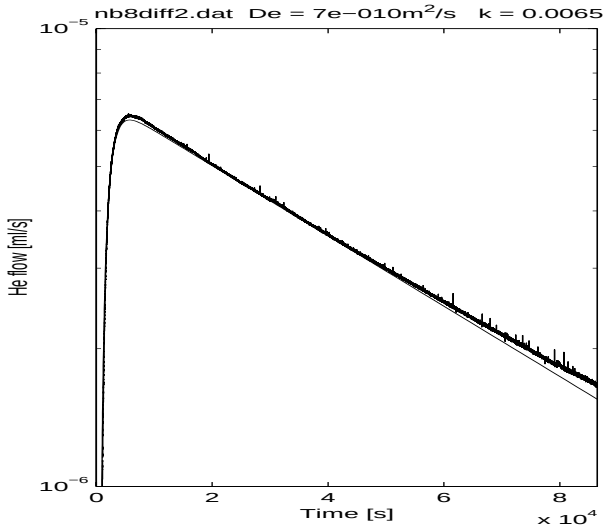

# APPENDIX C

# Permeabity curves for analysed samples

# Permeability curves of the sample d10

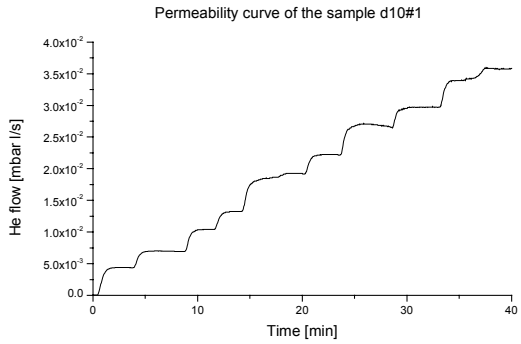


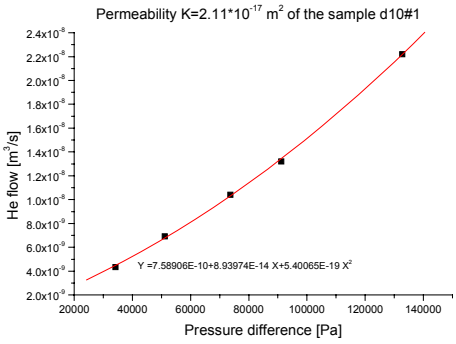


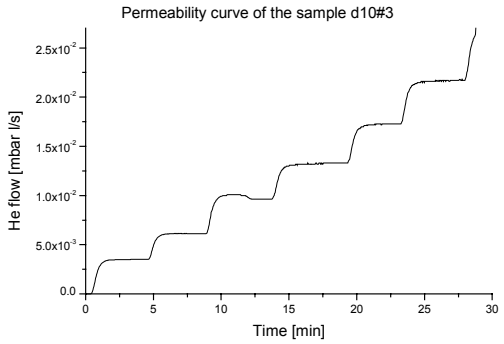


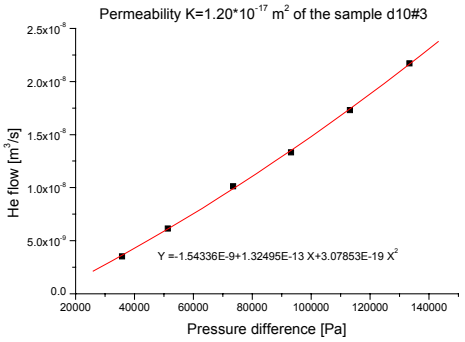


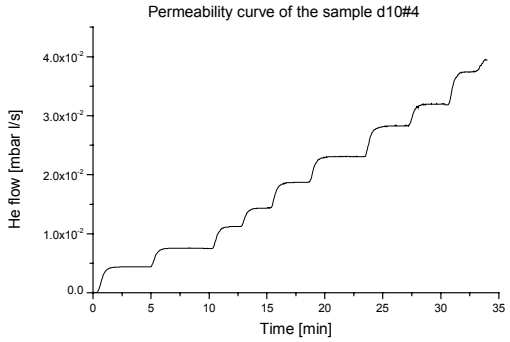


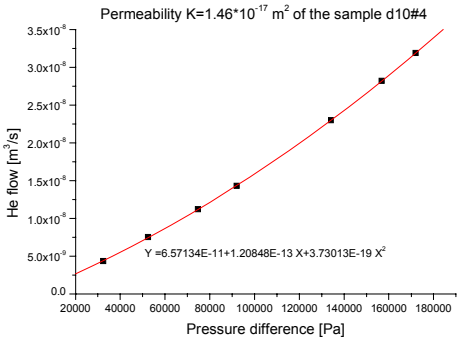

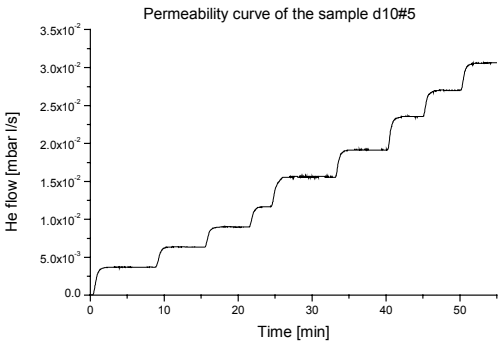
Permeability curve of the sample d10#5
He flow [mbar l/s]
3.5x10-2
3.0x10-2
2.5x10-2
2.0x10-2
1.5x10-2
1.0x10-2
5.0x10-3
0.0
0
10
20
30
40
50
Time [min]

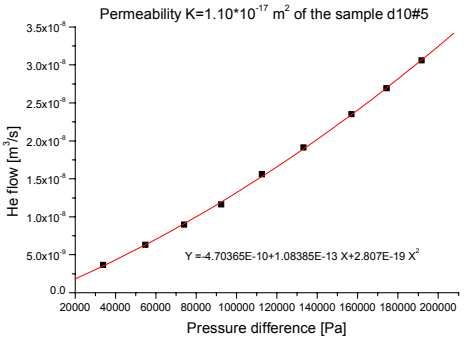
Permeability K=1.10*10-17 m2 of the sample d10#5
He flow [m3/s]
3.5x10-8
3.0x10-8
2.5x10-8
2.0x10-8
1.5x10-8
1.0x10-8
5.0x10-9
0.0
Y =-4.70365E-10+1.08385E-13 X+2.807E-19 X2
20000
40000
60000
80000
100000
120000
140000
160000
180000
200000
Pressure difference [Pa]

# Permeability curves of the sample d15

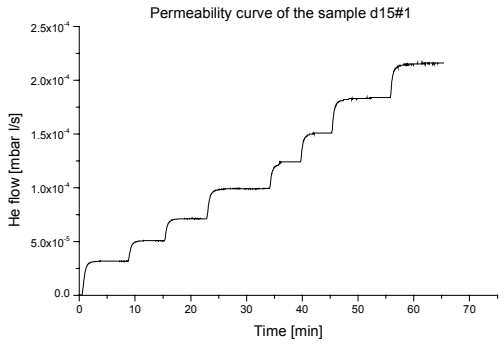


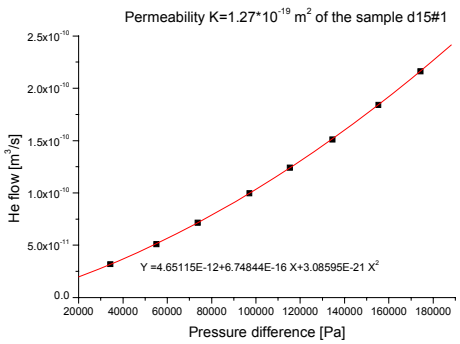


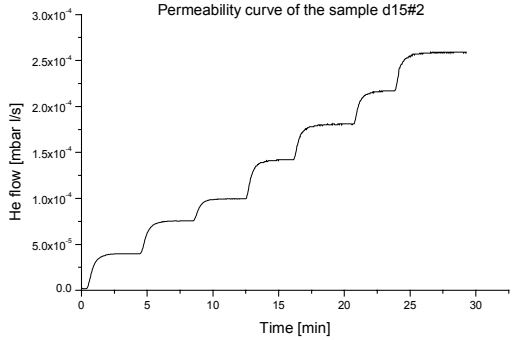


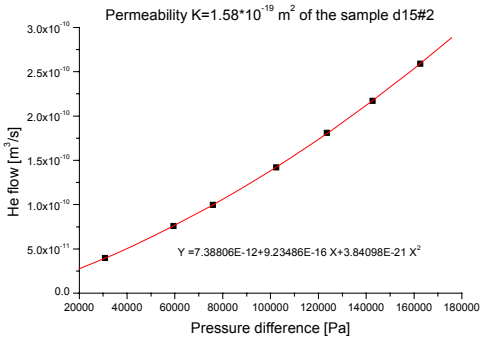


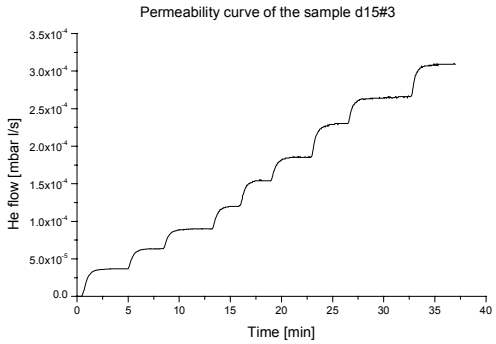


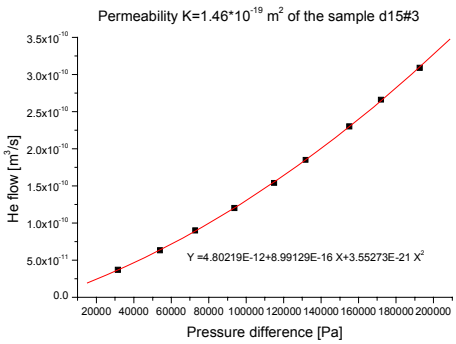

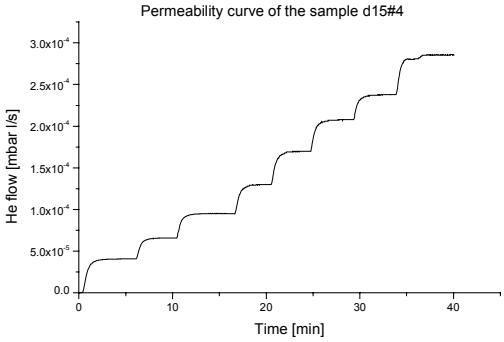
Permeability curve of the sample d15#4
He flow [mbar l/s]
Time [min]

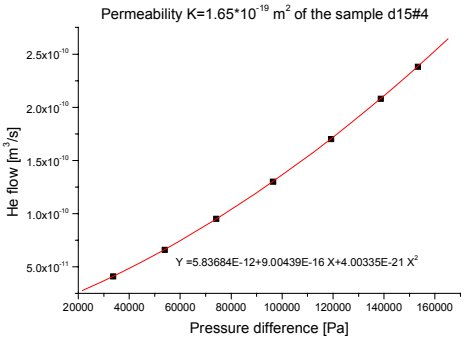
Permeability K=1.65*10-19 m2 of the sample d15#4
He flow [m3/s]
Y =5.83684E-12+9.00439E-16 X+4.00335E-21 X2
Pressure difference [Pa]

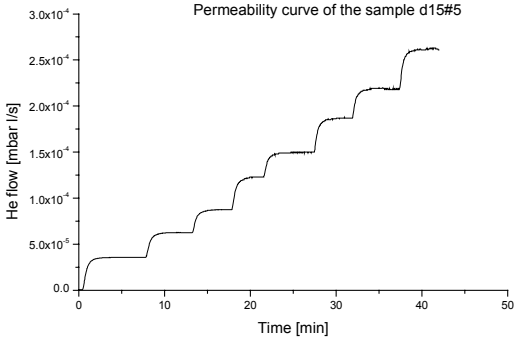
Permeability curve of the sample d15#5
He flow [mbar l/s]
Time [min]

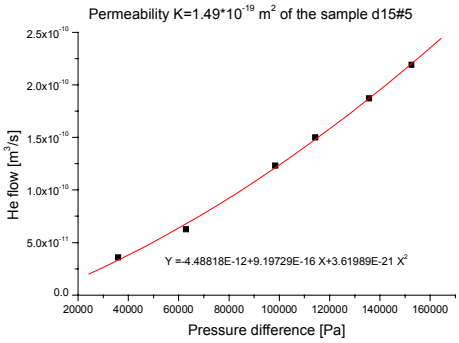
Permeability K=1.49*10-19 m2 of the sample d15#5
He flow [m3/s]
Y =-4.48818E-12+9.19729E-16 X+3.61989E-21 X2
Pressure difference [Pa]

# Permeability curves of the sample d27

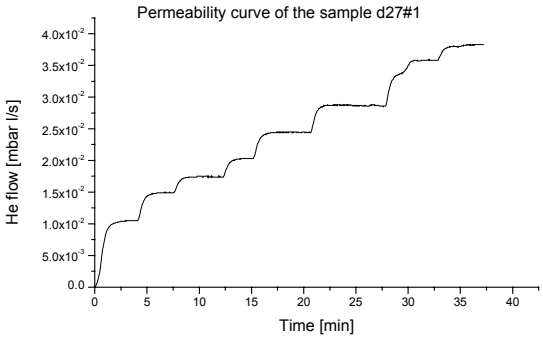


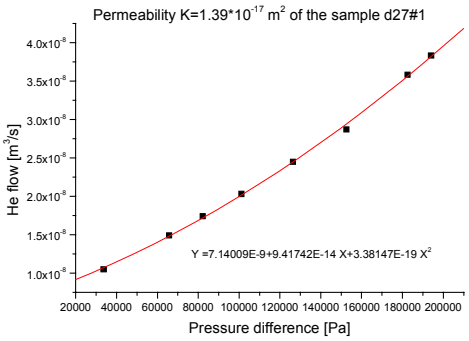


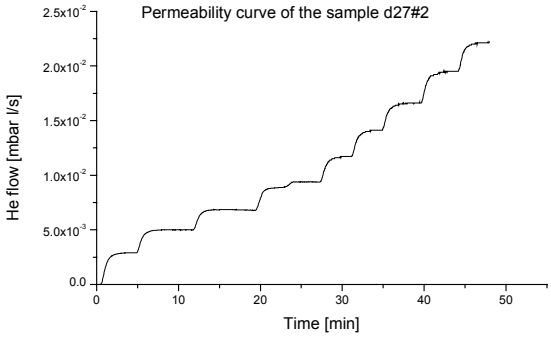


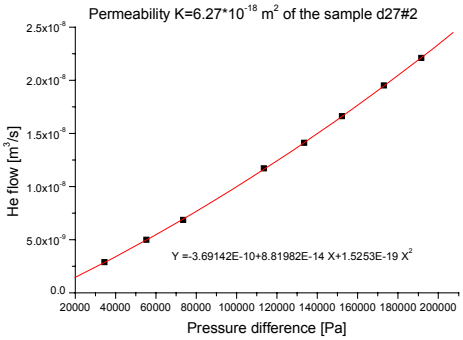


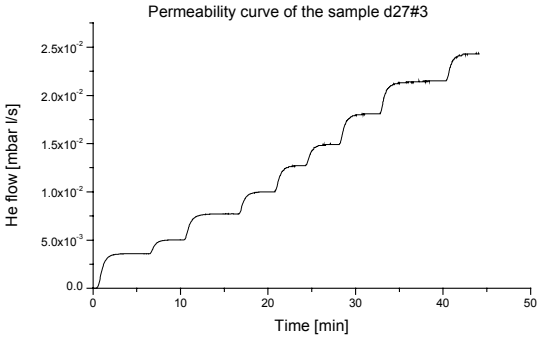


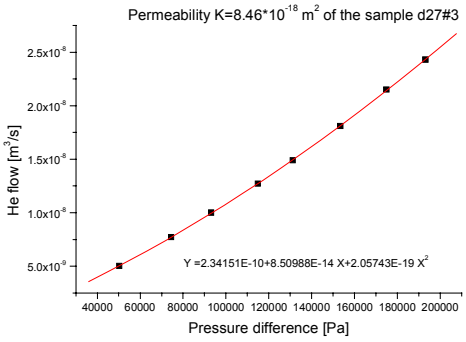

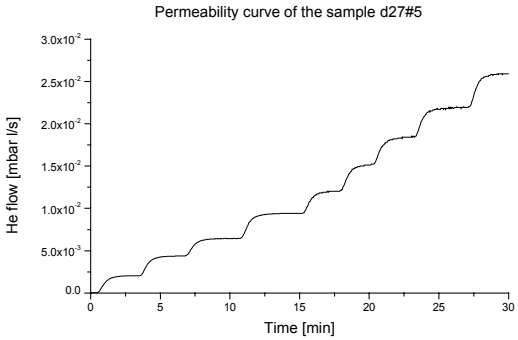
Permeability curve of the sample d27#5
He flow [mbar l/s]
Time [min]

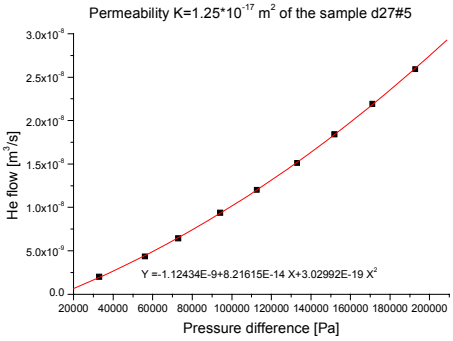
Permeability K=1.25*10-17 m2 of the sample d27#5
He flow [m3/s]
Y =-1.12434E-9+8.21615E-14 X+3.02992E-19 X2
Pressure difference [Pa]

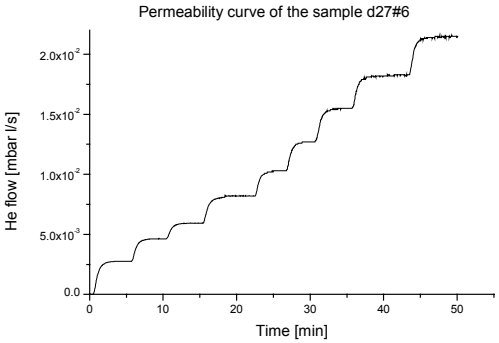
Permeability curve of the sample d27#6
He flow [mbar l/s]
Time [min]

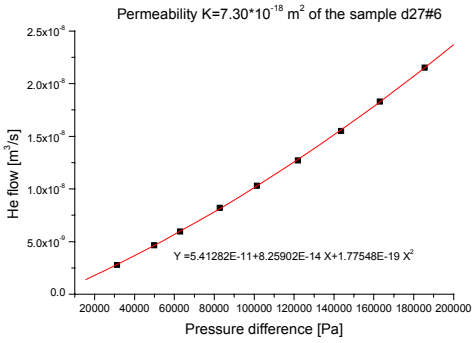
Permeability K=7.30*10-18 m2 of the sample d27#6
He flow [m3/s]
Y =5.41282E-11+8.25902E-14 X+1.77548E-19 X2
Pressure difference [Pa]

# Permeability curves of the sample d3

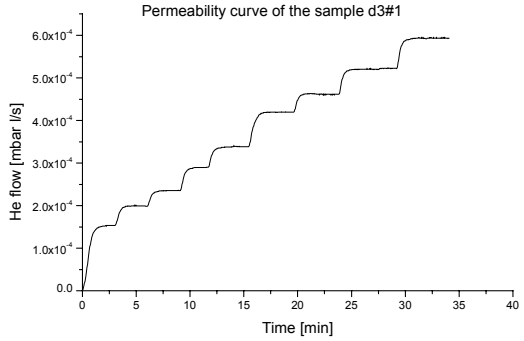


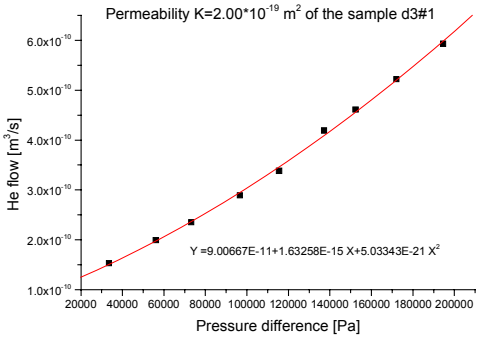


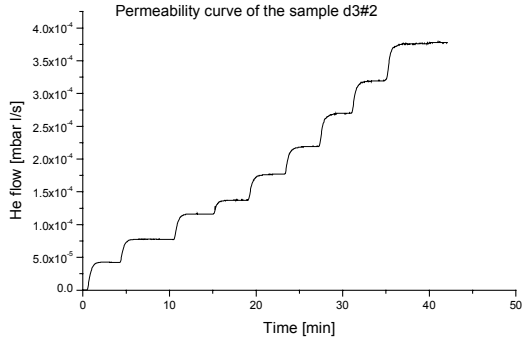


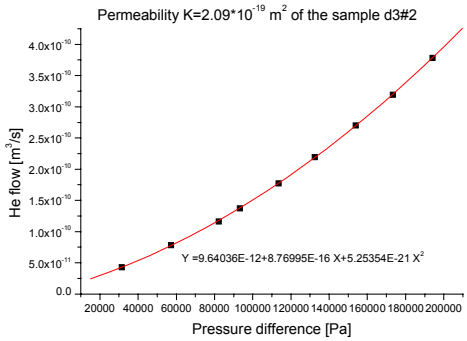


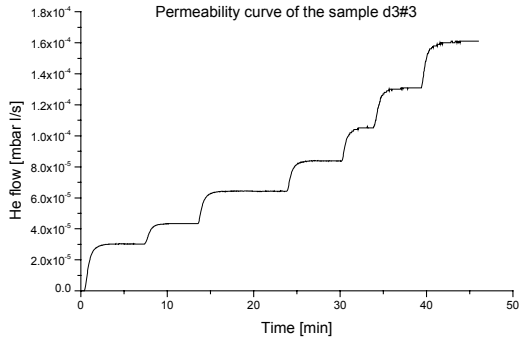


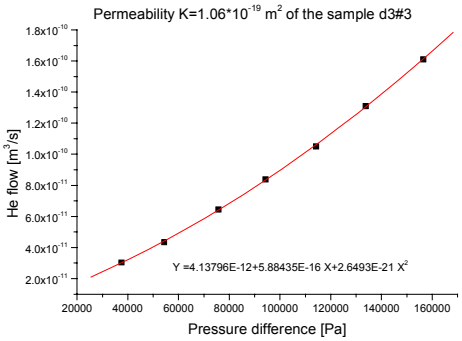

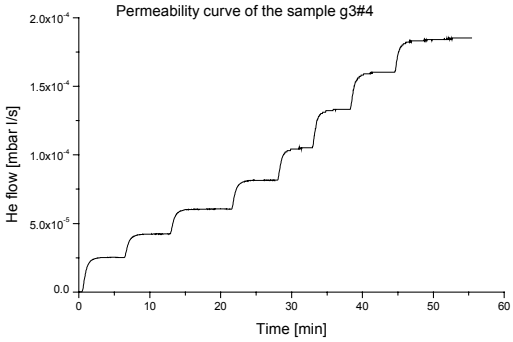
Permeability curve of the sample g3#4
He flow [mbar l/s]
2.0x10-4
1.5x10-4
1.0x10-4
5.0x10-5
0.0
0
10
20
30
40
50
60
Time [min]

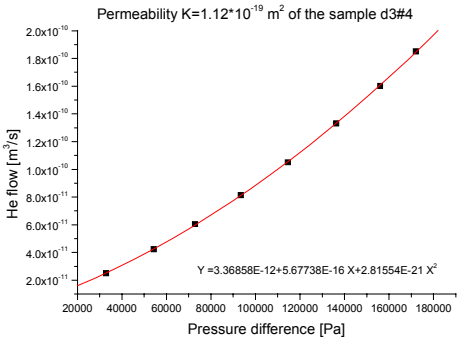
Permeability K=1.12*10-19 m2 of the sample d3#4
He flow [m3/s]
2.0x10-10
1.8x10-10
1.6x10-10
1.4x10-10
1.2x10-10
1.0x10-10
8.0x10-11
6.0x10-11
4.0x10-11
2.0x10-11
Y =3.36858E-12+5.67738E-16 X+2.81554E-21 X2
20000
40000
60000
80000
100000
120000
140000
160000
180000
Pressure difference [Pa]

# Permeability curves of the sample d4

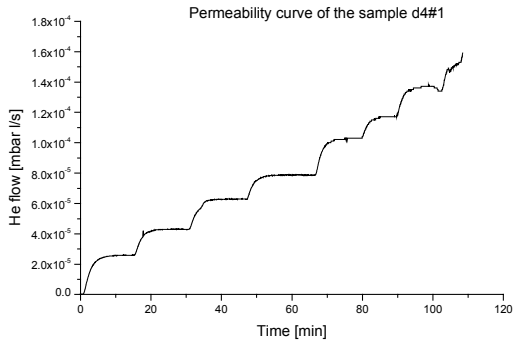


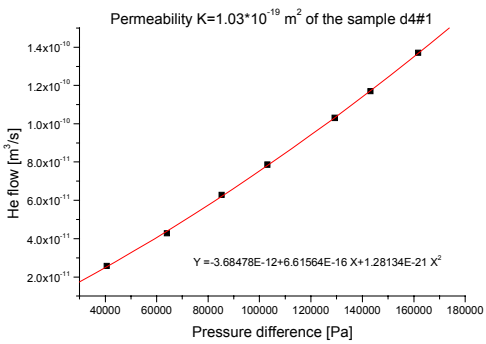


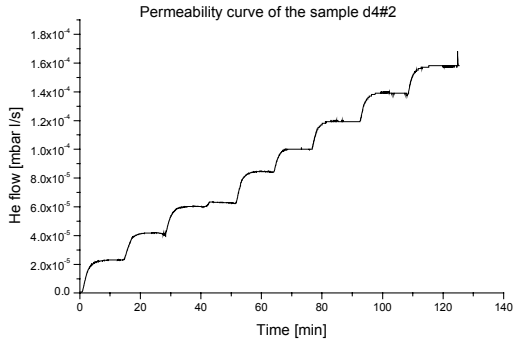


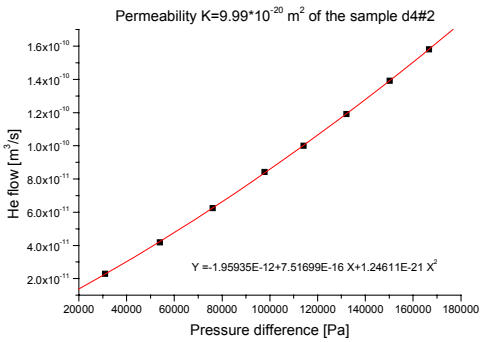


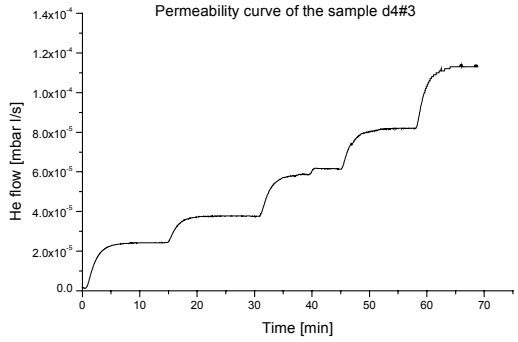


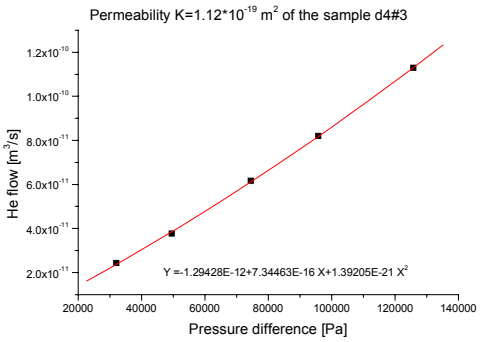

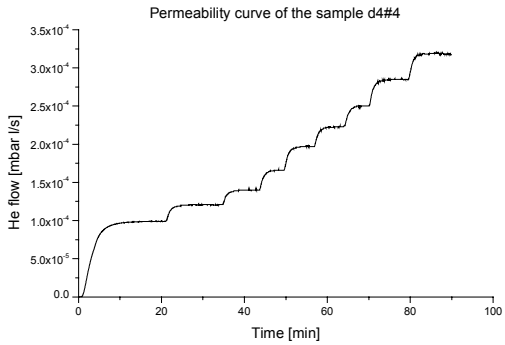
Permeability curve of the sample d4#4
He flow [mbar l/s]
Time [min]

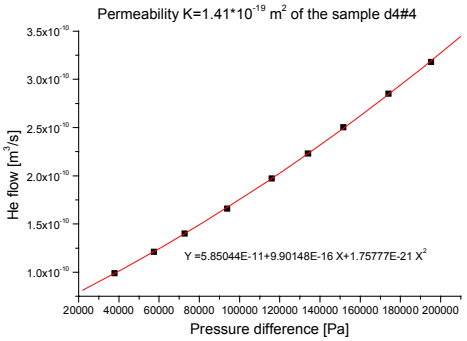
Permeability K=1.41*10-19 m2 of the sample d4#4
He flow [m3/s]
Y =5.85044E-11+9.90148E-16 X+1.75777E-21 X2
Pressure difference [Pa]

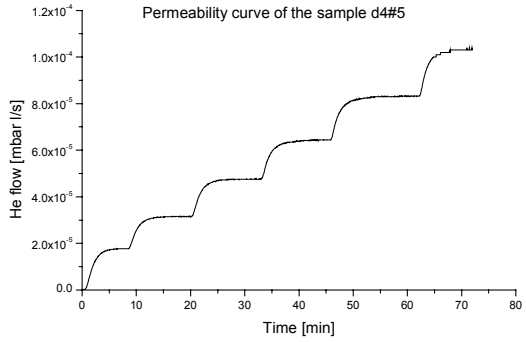
Permeability curve of the sample d4#5
He flow [mbar l/s]
Time [min]

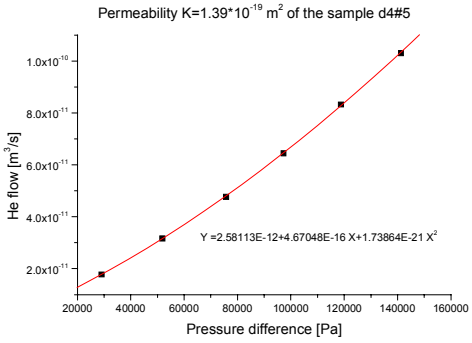
Permeability K=1.39*10-19 m2 of the sample d4#5
He flow [m3/s]
Y =2.58113E-12+4.67048E-16 X+1.73864E-21 X2
Pressure difference [Pa]

# Permeability curves of the sample d5

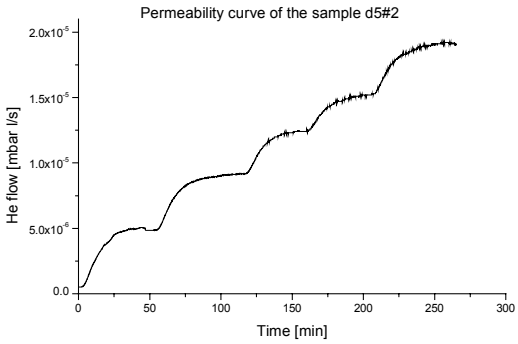


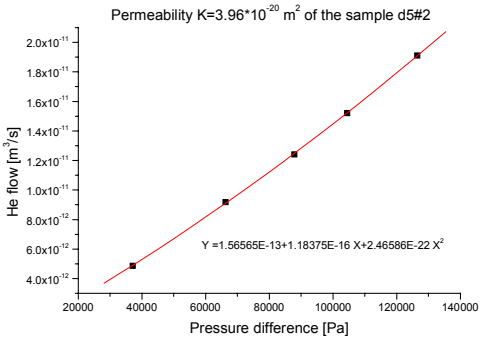


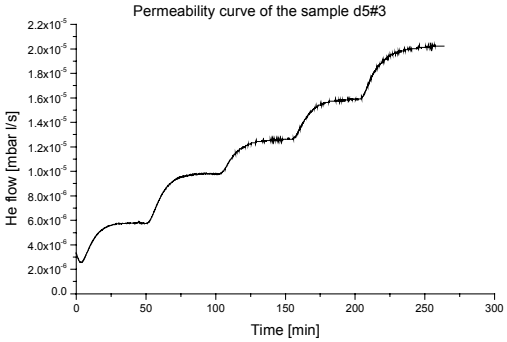


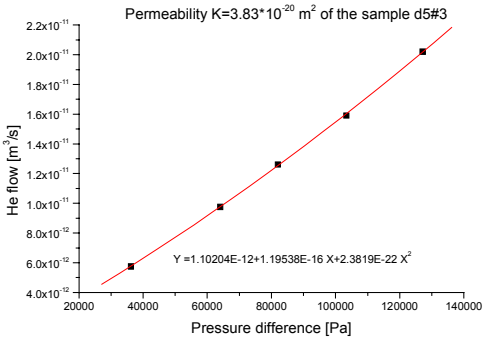


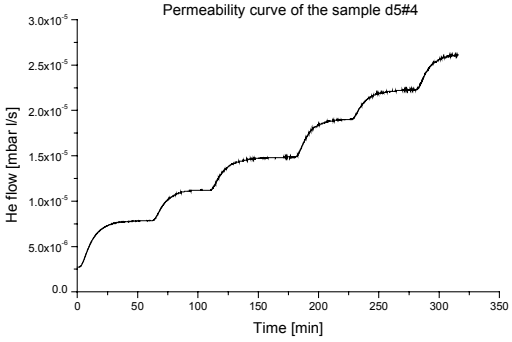


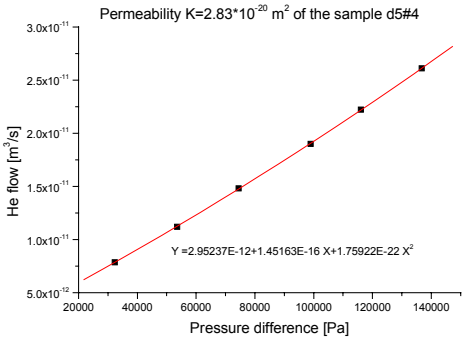

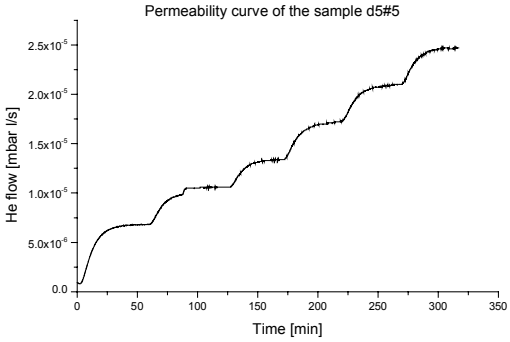
Permeability curve of the sample d5#5
He flow [mbar l/s]
Time [min]

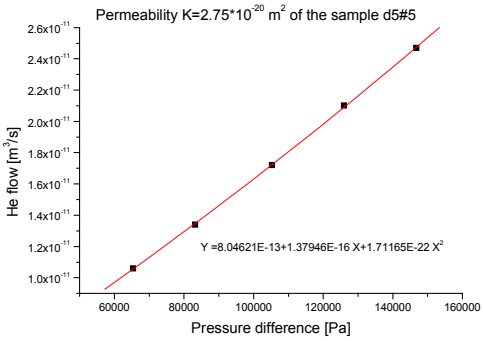
Permeability K=2.75*10^-20 m^2 of the sample d5#5
He flow [m^3/s]
Y =8.04621E-13+1.37946E-16 X+1.71165E-22 X^2
Pressure difference [Pa]

# Permeability curves of the sample d7

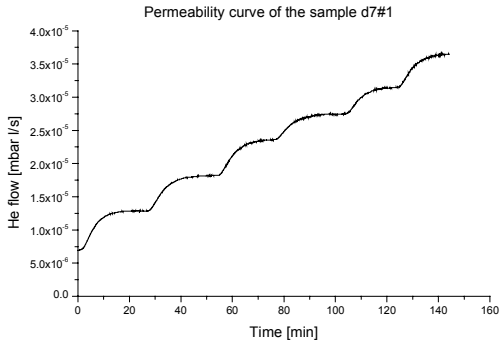


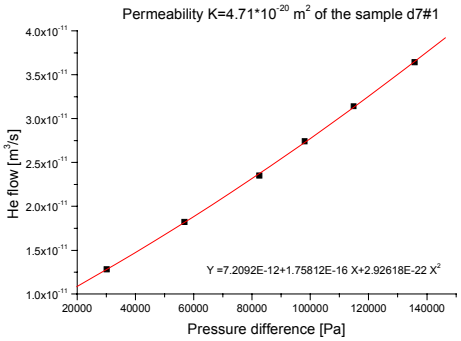


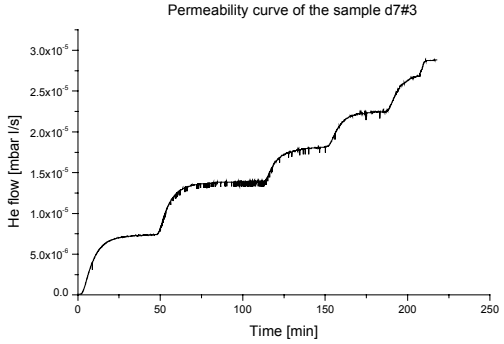


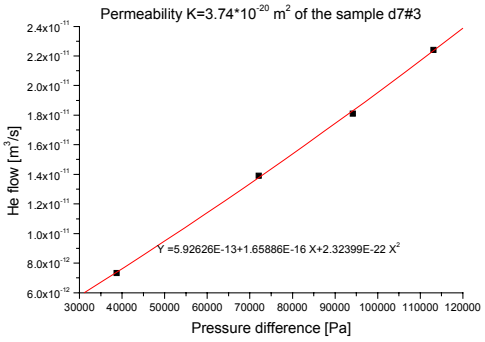


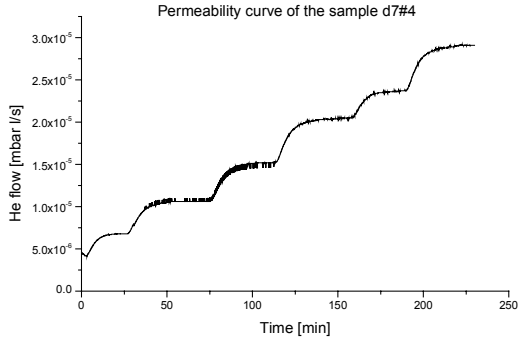


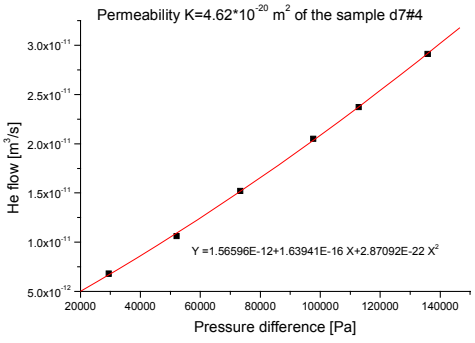

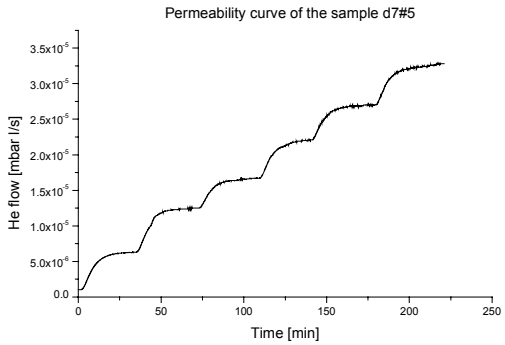
Permeability curve of the sample d7#5
He flow [mbar l/s]
Time [min]

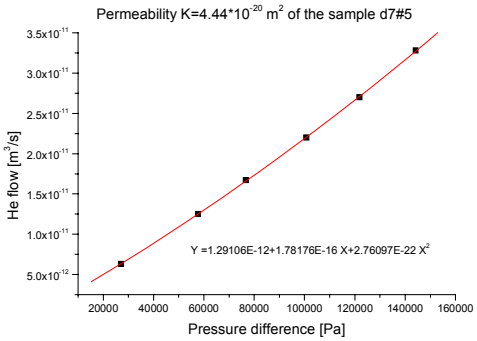
Permeability K=4.44*10-20 m2 of the sample d7#5
He flow [m3/s]
Y =1.29106E-12+1.78176E-16 X+2.76097E-22 X2
Pressure difference [Pa]

# Permeability curves of the sample g1

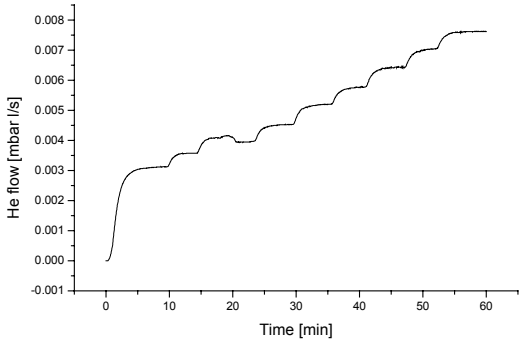


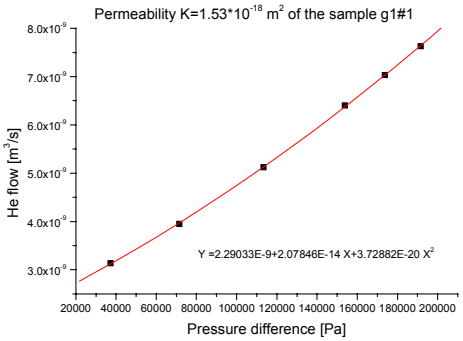


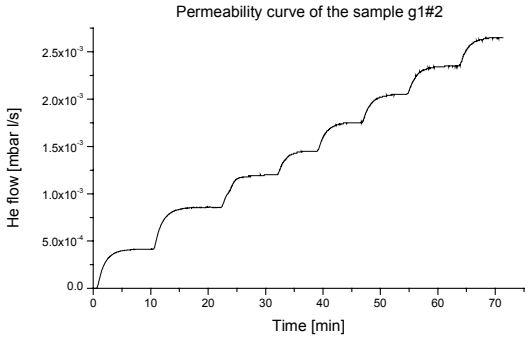


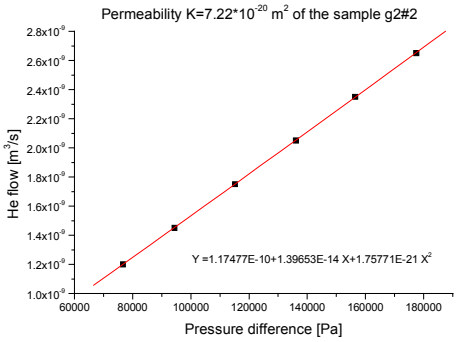

# Permeability curves of the sample g14

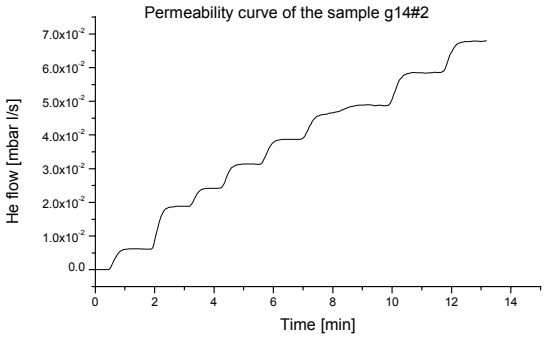


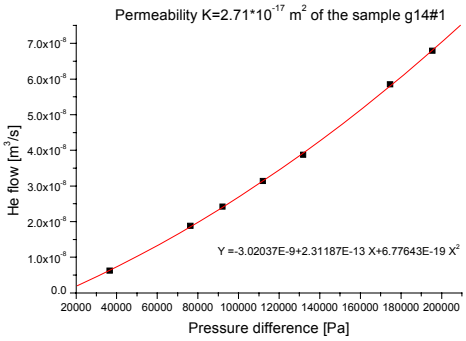


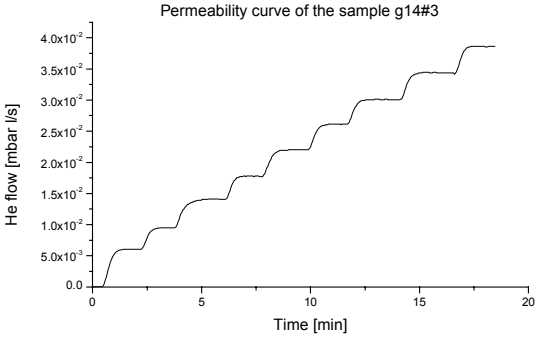


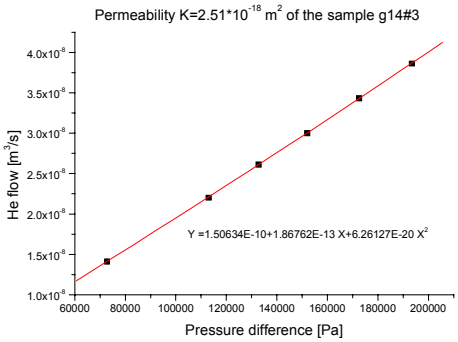


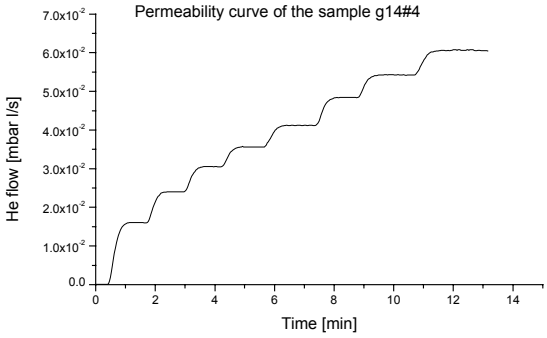


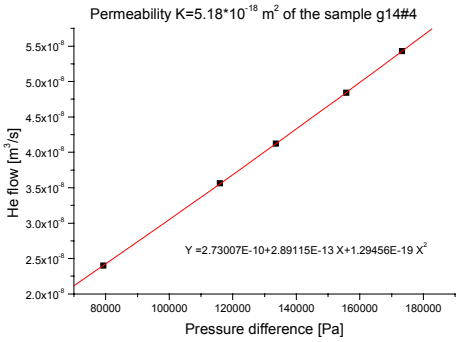

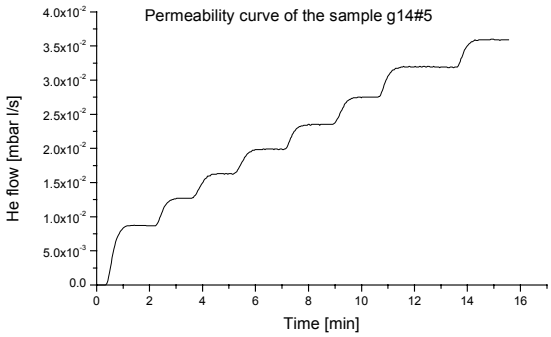
Permeability curve of the sample g14#5
He flow [mbar l/s]
Time [min]

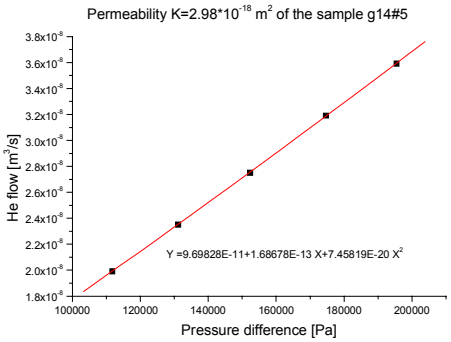
Permeability K=2.98*10-18 m2 of the sample g14#5
He flow [m3/s]
Y =9.69828E-11+1.68678E-13 X+7.45819E-20 X2
Pressure difference [Pa]

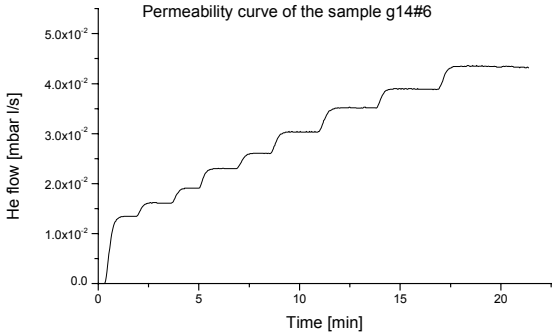
Permeability curve of the sample g14#6
He flow [mbar l/s]
Time [min]

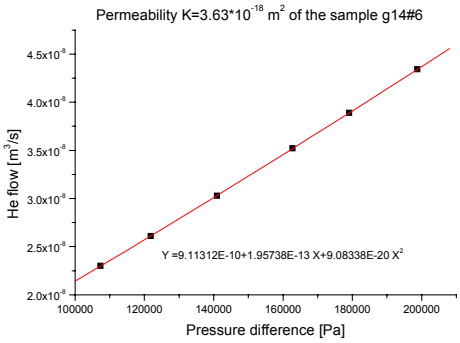
Permeability K=3.63*10-18 m2 of the sample g14#6
He flow [m3/s]
Y =9.11312E-10+1.95738E-13 X+9.08338E-20 X2
Pressure difference [Pa]

# Permeability curves of the sample g2

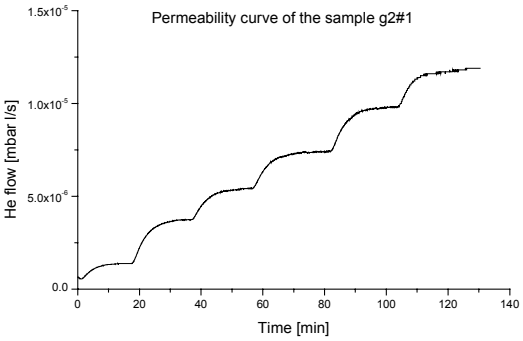


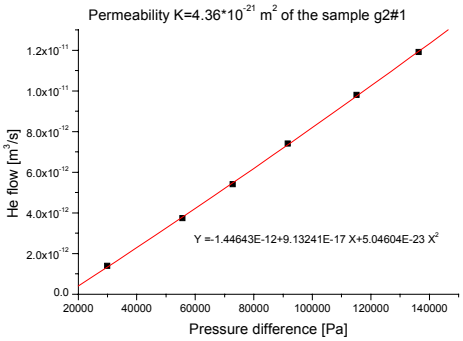


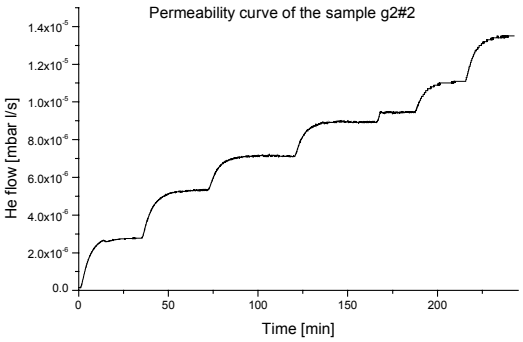


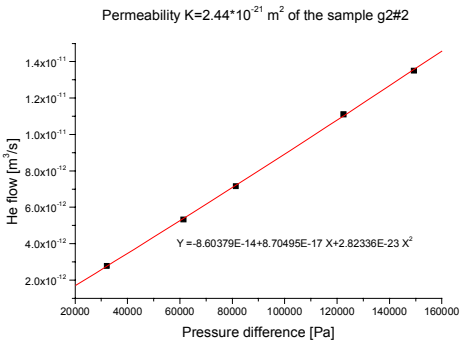


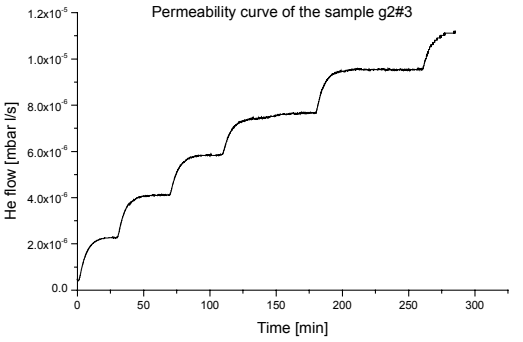


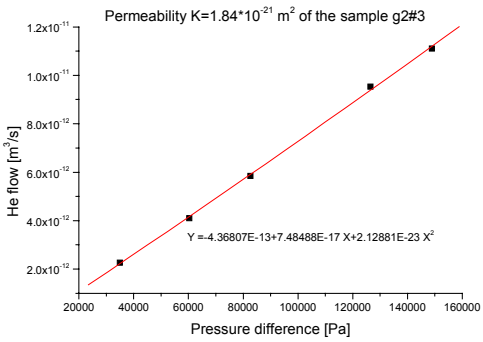

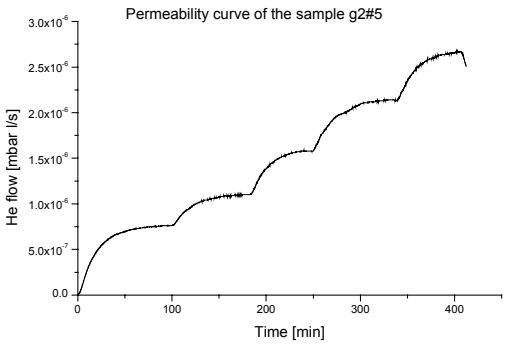
Permeability curve of the sample g2#5
He flow [mbar l/s]
Time [min]
3.0x10-6
2.5x10-6
2.0x10-6
1.5x10-6
1.0x10-6
5.0x10-7
0.0
0
100
200
300
400

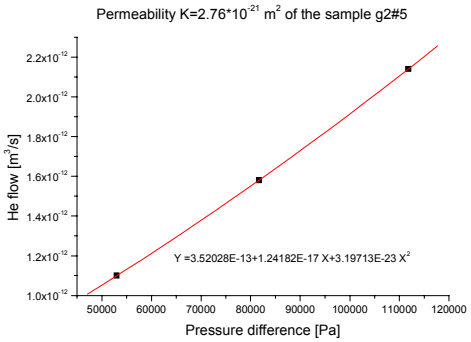
Permeability K=2.76*10-21 m2 of the sample g2#5
He flow [m3/s]
Pressure difference [Pa]
Y =3.52028E-13+1.24182E-17 X+3.19713E-23 X2
2.2x10-12
2.0x10-12
1.8x10-12
1.6x10-12
1.4x10-12
1.2x10-12
1.0x10-12
50000
60000
70000
80000
90000
100000
110000
120000

# Permeability curves of the sample g26

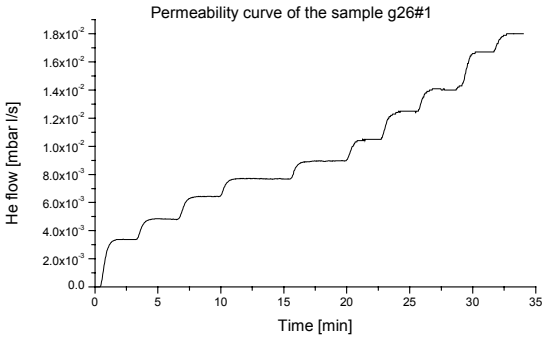


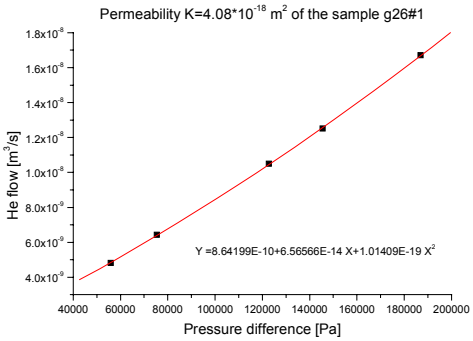


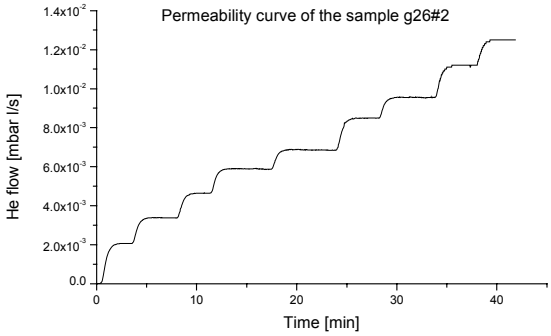


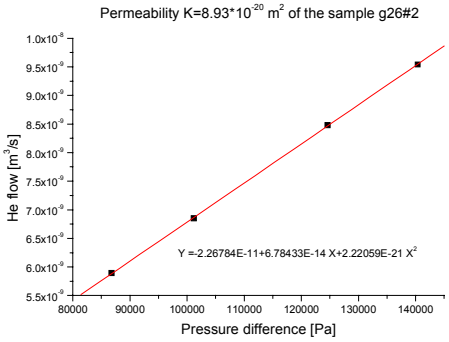


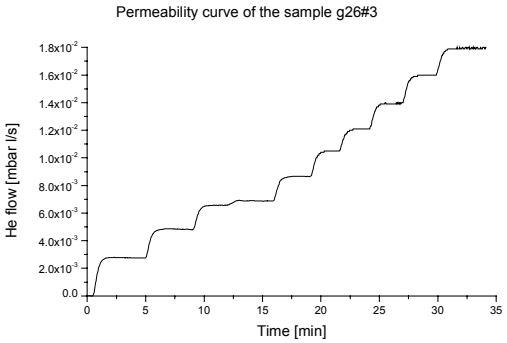


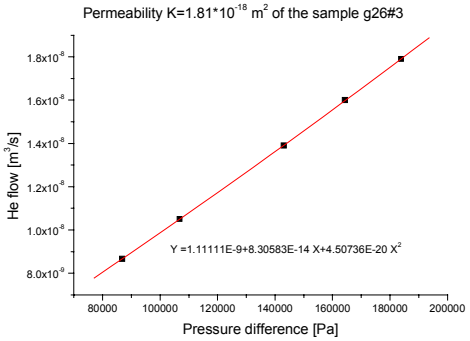

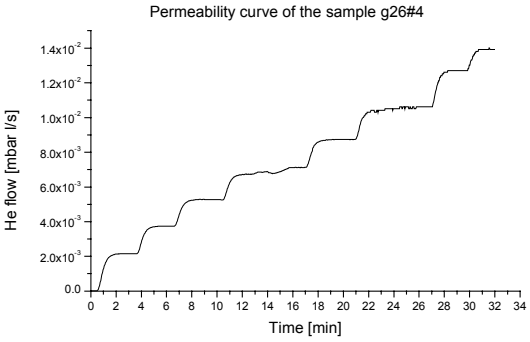
Permeability curve of the sample g26#4
He flow [mbar l/s]
Time [min]

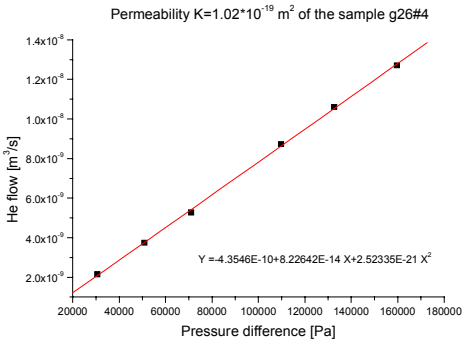
Permeability K=1.02*10-19 m2 of the sample g26#4
He flow [m3/s]
Y =-4.3546E-10+8.22642E-14 X+2.52335E-21 X2
Pressure difference [Pa]

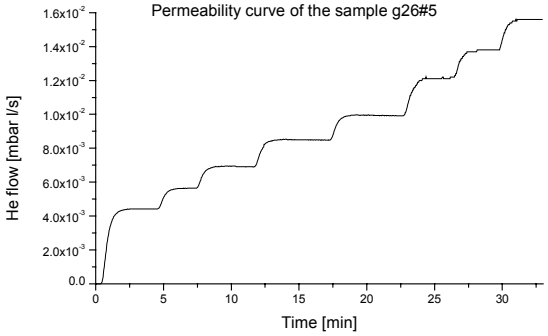
Permeability curve of the sample g26#5
He flow [mbar l/s]
Time [min]

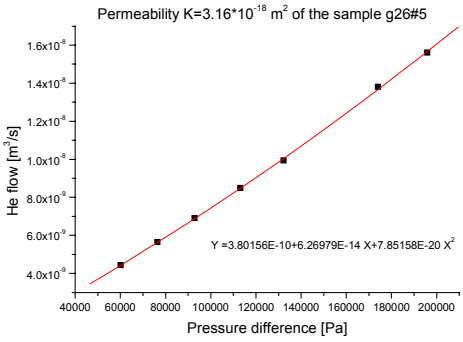
Permeability K=3.16*10-18 m2 of the sample g26#5
He flow [m3/s]
Y =3.80156E-10+6.26979E-14 X+7.85158E-20 X2
Pressure difference [Pa]

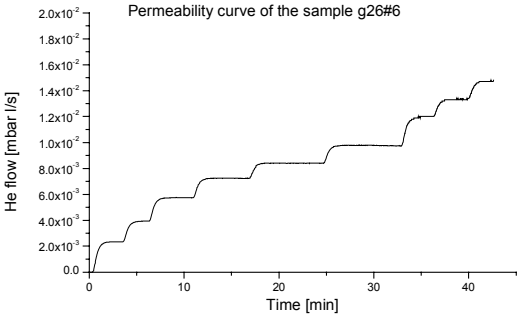
Permeability curve of the sample g26#6
He flow [mbar l/s]
Time [min]

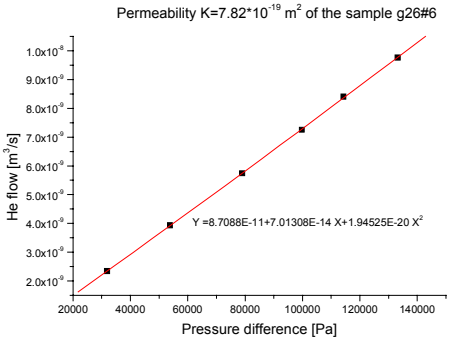
Permeability K=7.82*10-19 m2 of the sample g26#6
He flow [m3/s]
Y =8.7088E-11+7.01308E-14 X+1.94525E-20 X2
Pressure difference [Pa]

# Permeability curves of the sample g6

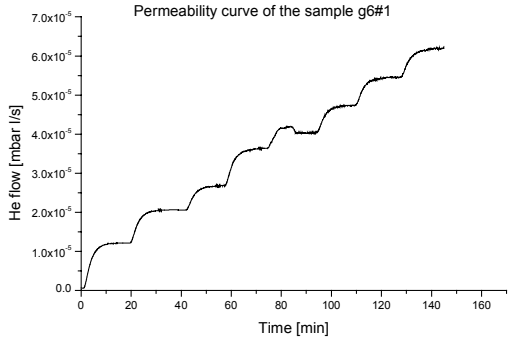


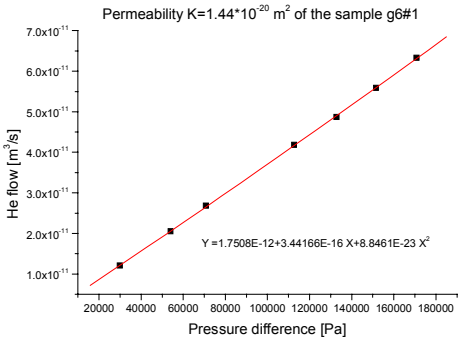


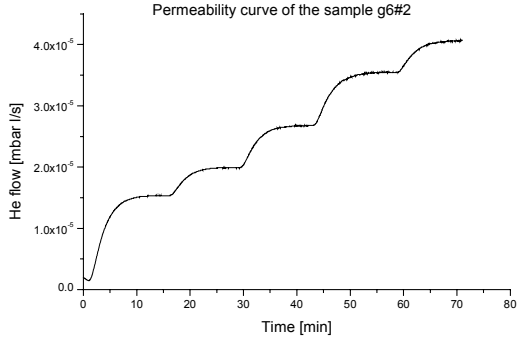


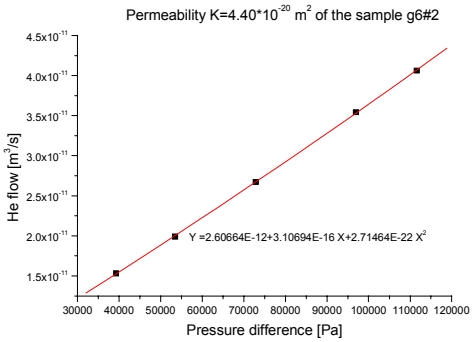


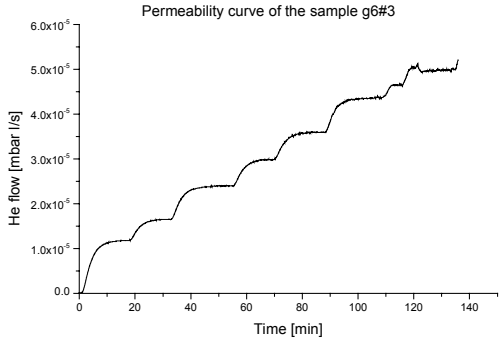


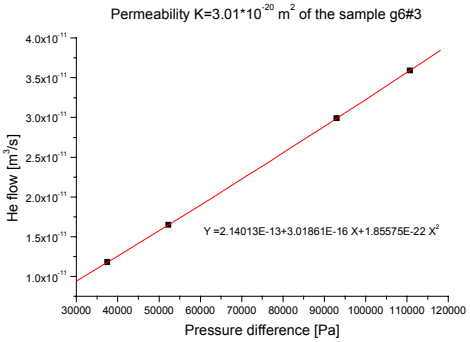

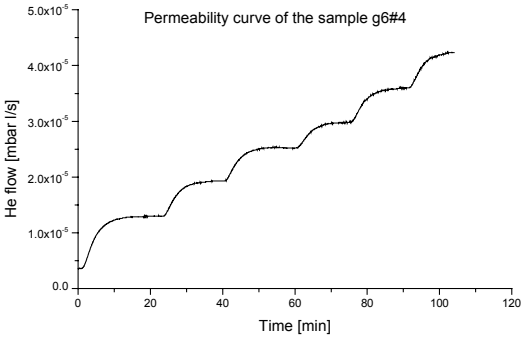
Permeability curve of the sample g6#4
He flow [mbar l/s]
Time [min]

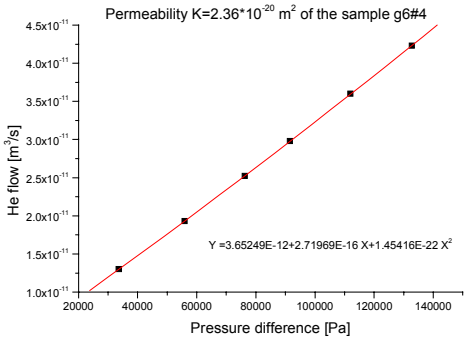
Permeability K=2.36*10-20 m2 of the sample g6#4
He flow [m3/s]
Y =3.65249E-12+2.71969E-16 X+1.45416E-22 X2
Pressure difference [Pa]

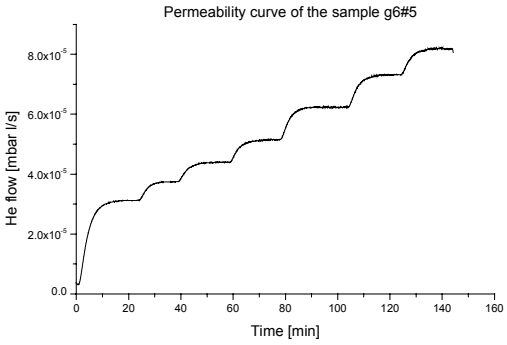
Permeability curve of the sample g6#5
He flow [mbar l/s]
Time [min]

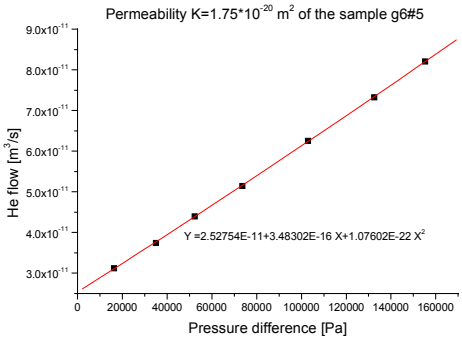
Permeability K=1.75*10-20 m2 of the sample g6#5
He flow [m3/s]
Y =2.52754E-11+3.48302E-16 X+1.07602E-22 X2
Pressure difference [Pa]

# Permeability curves of the sample g8

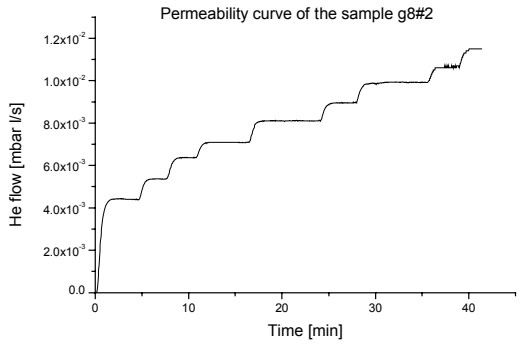


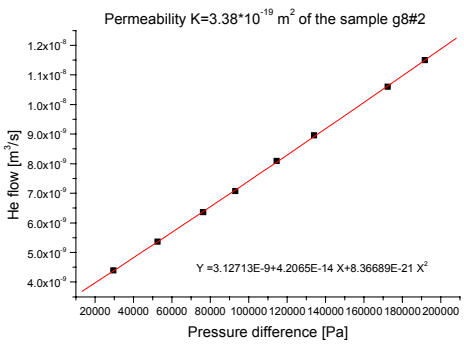


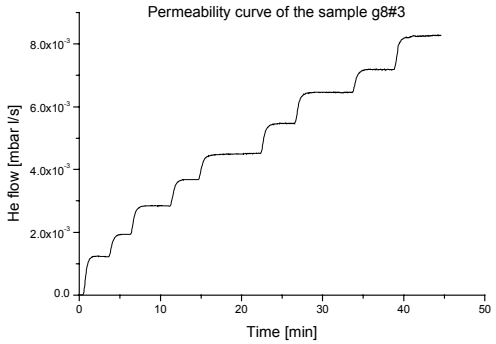


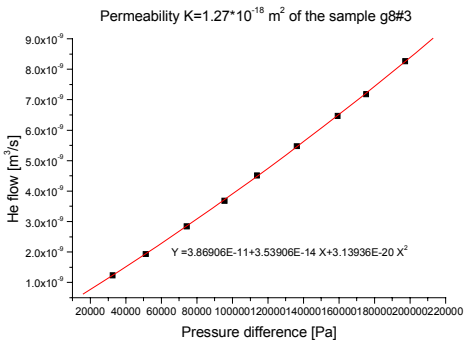


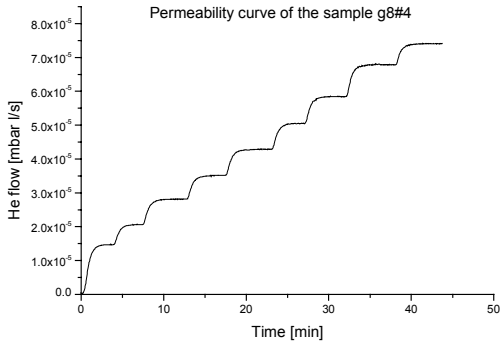


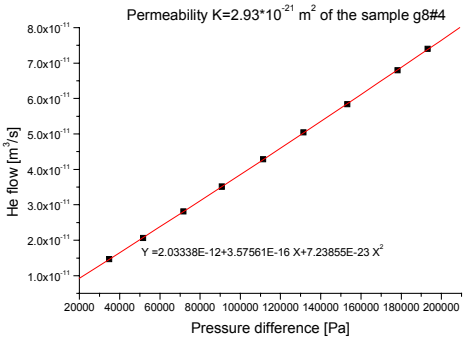

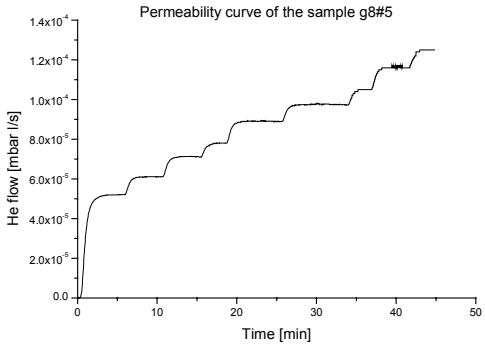
Permeability curve of the sample g8#5
He flow [mbar l/s]
1.4x10-4
1.2x10-4
1.0x10-4
8.0x10-5
6.0x10-5
4.0x10-5
2.0x10-5
0.0
0
10
20
30
40
50
Time [min]

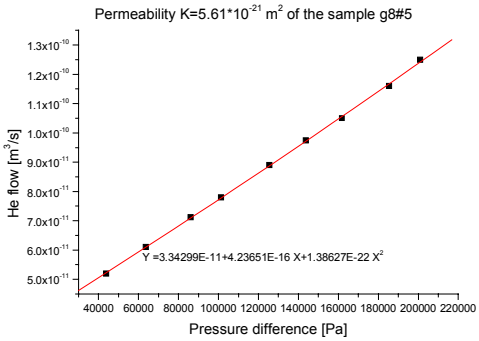
Permeability K=5.61*10-21 m2 of the sample g8#5
He flow [m3/s]
1.3x10-10
1.2x10-10
1.1x10-10
1.0x10-10
9.0x10-11
8.0x10-11
7.0x10-11
6.0x10-11
5.0x10-11
Y =3.34299E-11+4.23651E-16 X+1.38627E-22 X2
40000
60000
80000
100000
120000
140000
160000
180000
200000
220000
Pressure difference [Pa]

## Permeability curves for sample 1

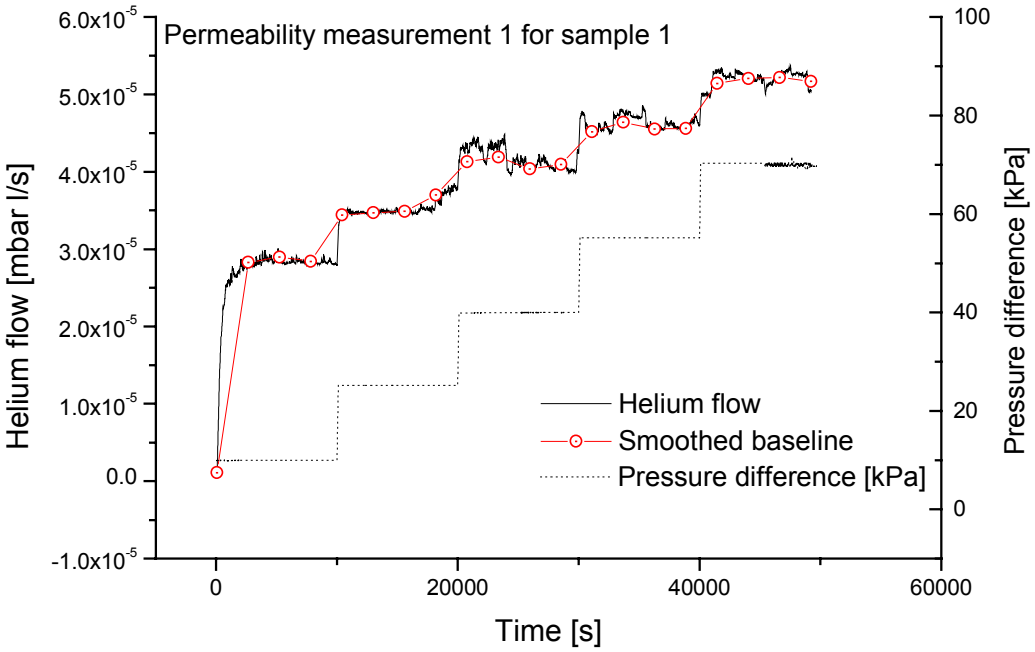


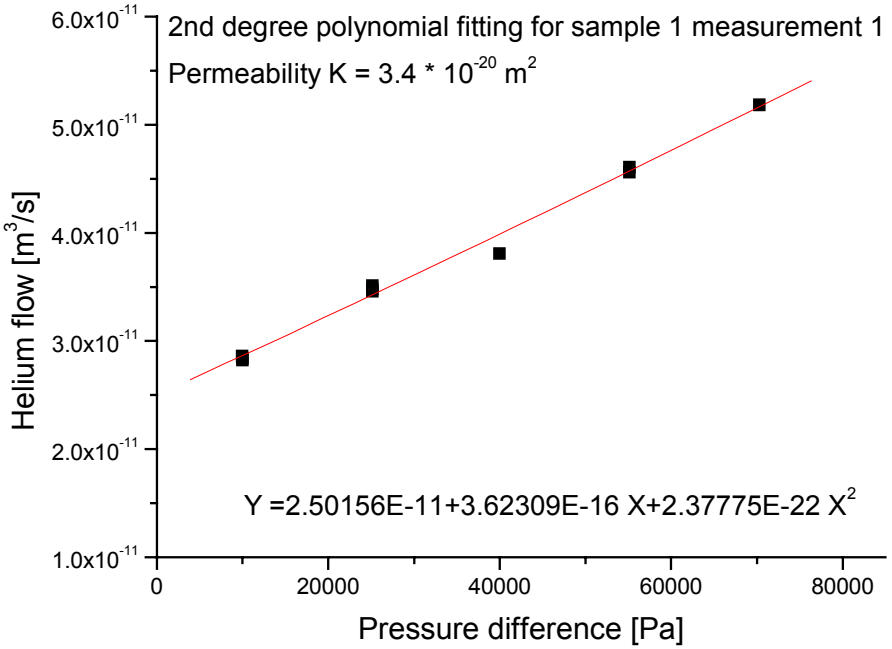

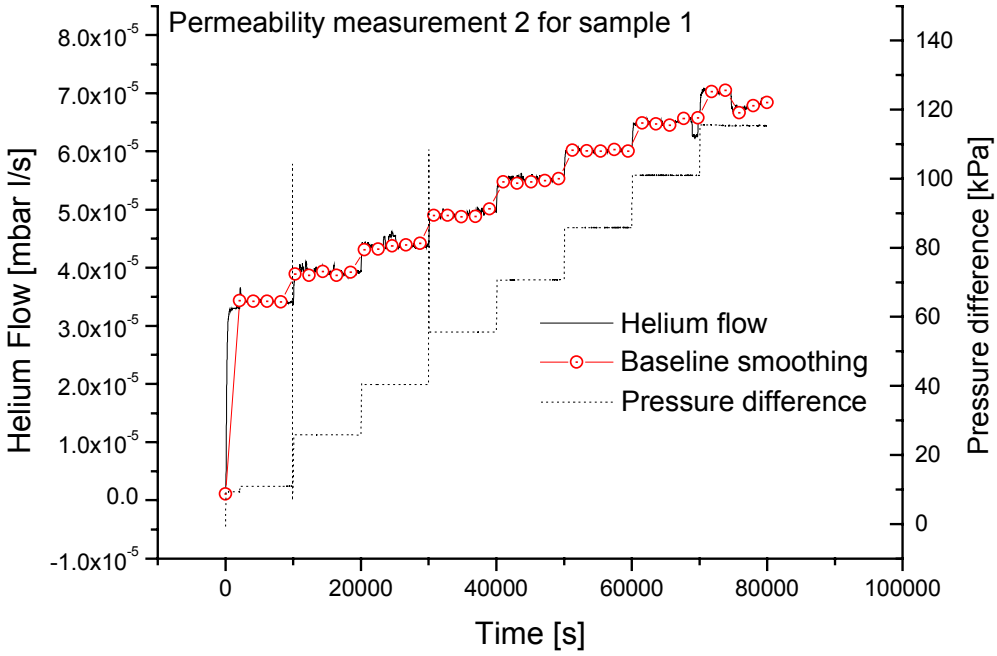
Permeability measurement 2 for sample 1
Helium Flow [mbar l/s]
Pressure difference [kPa]
Time [s]
Helium flow
Baseline smoothing
Pressure difference
8.0x10-5
7.0x10-5
6.0x10-5
5.0x10-5
4.0x10-5
3.0x10-5
2.0x10-5
1.0x10-5
0.0
-1.0x10-5
140
120
100
80
60
40
20
0
0
20000
40000
60000
80000
100000

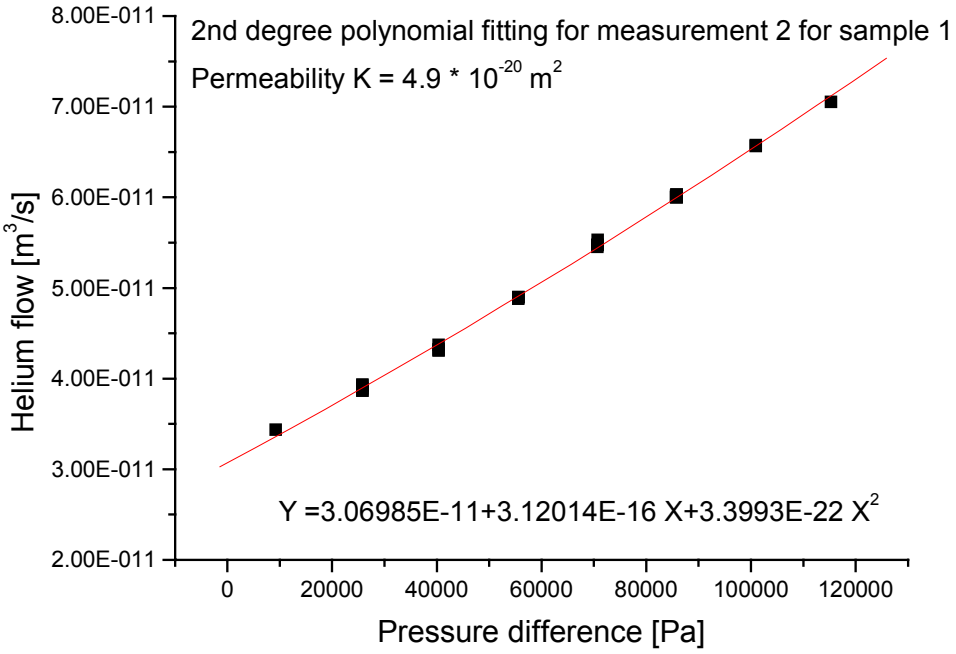
2nd degree polynomial fitting for measurement 2 for sample 1
Permeability K = 4.9 * 10-20 m2
Helium flow [m3/s]
Pressure difference [Pa]
Y =3.06985E-11+3.12014E-16 X+3.3993E-22 X2
8.00E-011
7.00E-011
6.00E-011
5.00E-011
4.00E-011
3.00E-011
2.00E-011
0
20000
40000
60000
80000
100000
120000

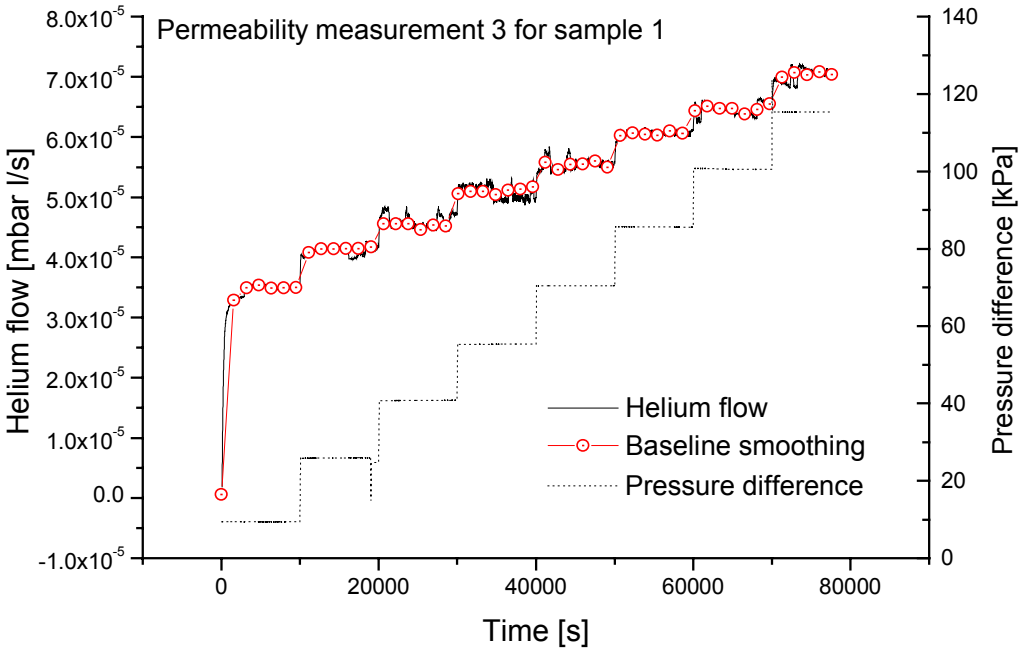
Permeability measurement 3 for sample 1
Helium flow [mbar l/s]
Pressure difference [kPa]
Time [s]
Helium flow
Baseline smoothing
Pressure difference
8.0x10-5
7.0x10-5
6.0x10-5
5.0x10-5
4.0x10-5
3.0x10-5
2.0x10-5
1.0x10-5
0.0
-1.0x10-5
140
120
100
80
60
40
20
0
0
20000
40000
60000
80000

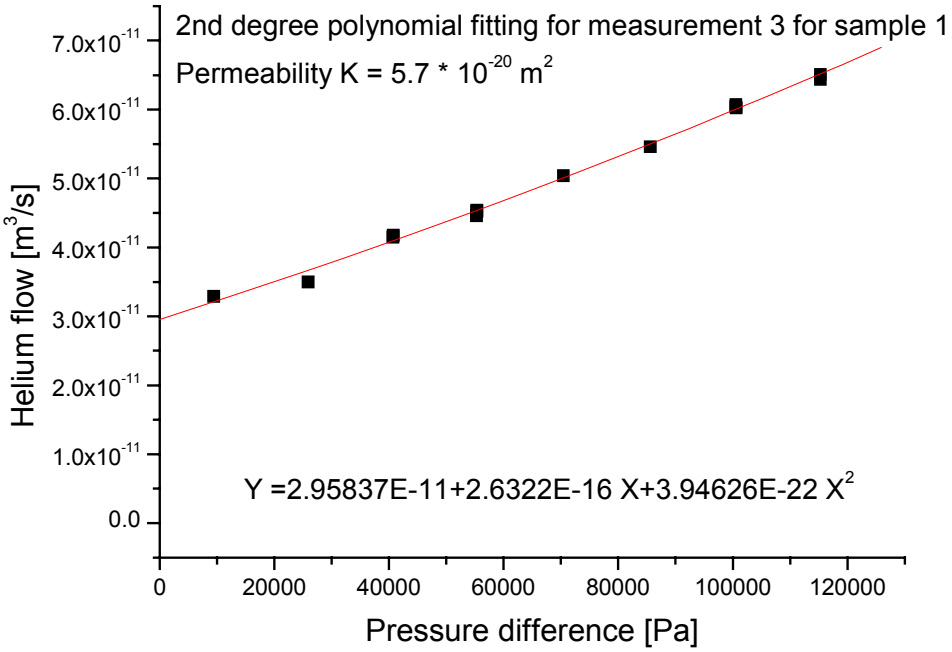
2nd degree polynomial fitting for measurement 3 for sample 1
Permeability K = 5.7 * 10-20 m2
Helium flow [m3/s]
Pressure difference [Pa]
Y =2.95837E-11+2.6322E-16 X+3.94626E-22 X2
7.0x10-11
6.0x10-11
5.0x10-11
4.0x10-11
3.0x10-11
2.0x10-11
1.0x10-11
0.0
0
20000
40000
60000
80000
100000
120000

## Permeability curves for sample 3

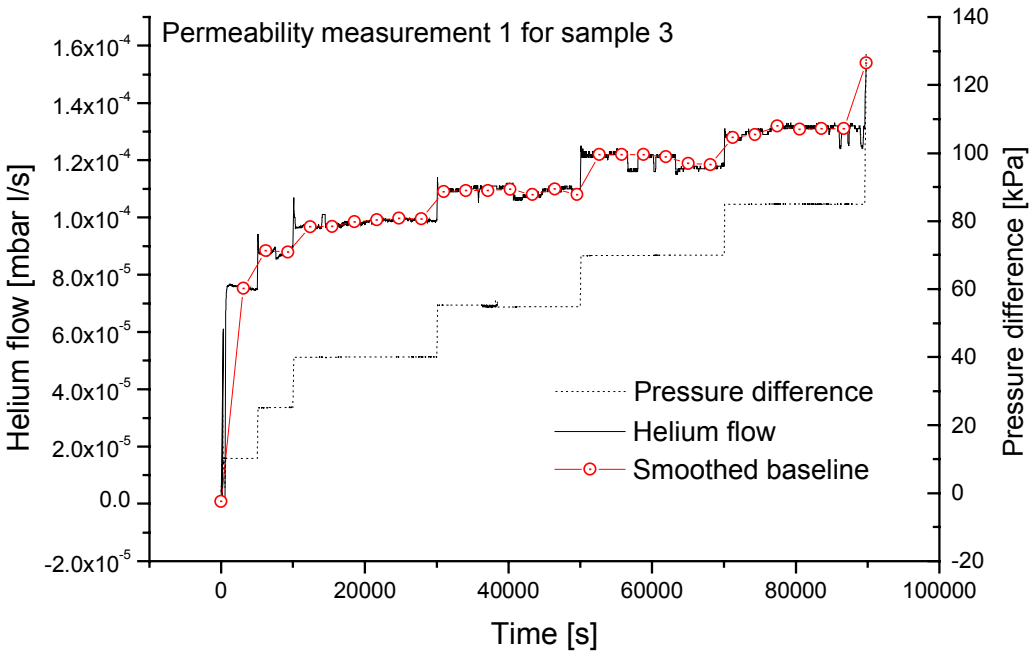


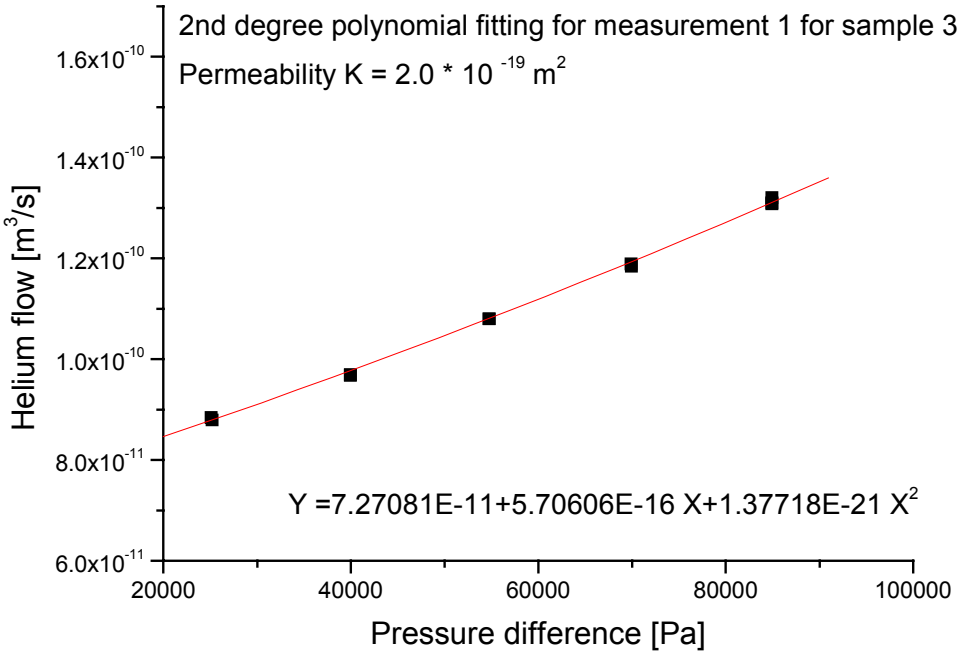

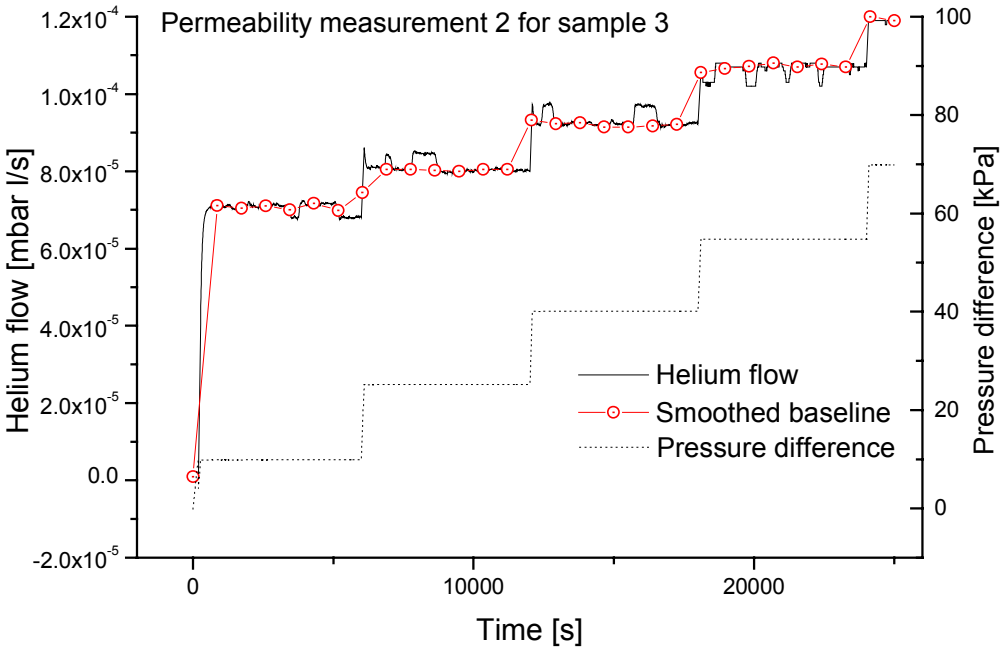
Permeability measurement 2 for sample 3
Helium flow [mbar l/s]
Pressure difference [kPa]
Time [s]
Helium flow
Smoothed baseline
Pressure difference
1.2x10-4
1.0x10-4
8.0x10-5
6.0x10-5
4.0x10-5
2.0x10-5
0.0
-2.0x10-5
100
80
60
40
20
0
0
10000
20000

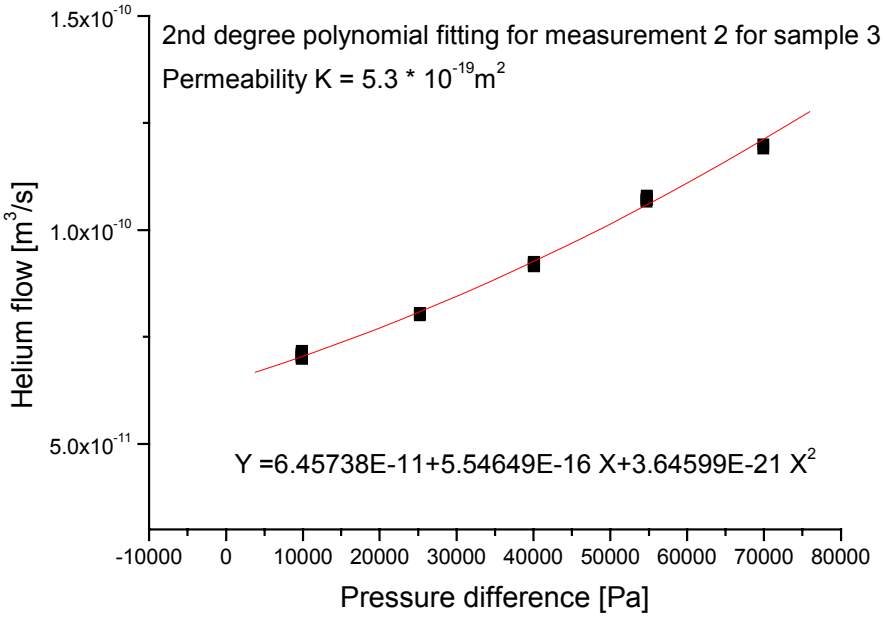
2nd degree polynomial fitting for measurement 2 for sample 3
Permeability K = 5.3 * 10-19m2
Helium flow [m3/s]
Pressure difference [Pa]
Y =6.45738E-11+5.54649E-16 X+3.64599E-21 X2
1.5x10-10
1.0x10-10
5.0x10-11
-10000
0
10000
20000
30000
40000
50000
60000
70000
80000

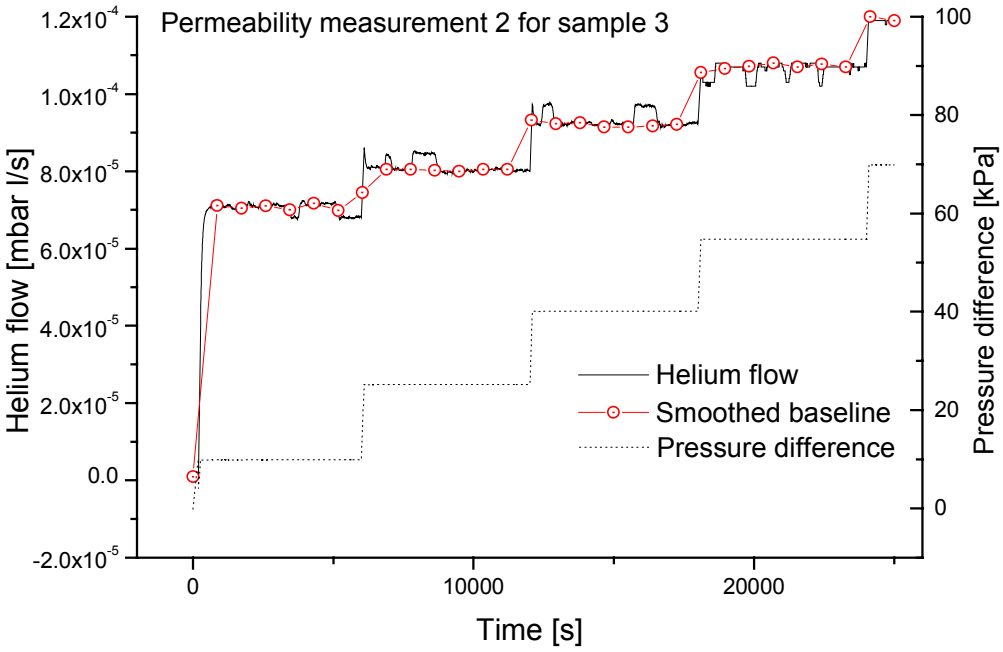
Permeability measurement 2 for sample 3
Helium flow [mbar l/s]
Pressure difference [kPa]
Time [s]
Helium flow
Smoothed baseline
Pressure difference
1.2x10-4
1.0x10-4
8.0x10-5
6.0x10-5
4.0x10-5
2.0x10-5
0.0
-2.0x10-5
100
80
60
40
20
0
0
10000
20000

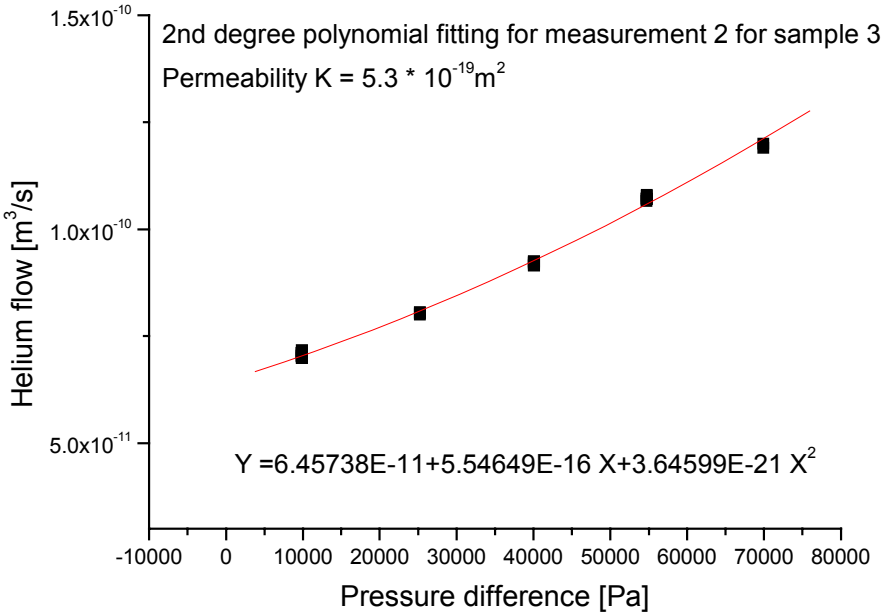
2nd degree polynomial fitting for measurement 2 for sample 3
Permeability K = 5.3 * 10-19m2
Helium flow [m3/s]
Pressure difference [Pa]
Y =6.45738E-11+5.54649E-16 X+3.64599E-21 X2
1.5x10-10
1.0x10-10
5.0x10-11
-10000
0
10000
20000
30000
40000
50000
60000
70000
80000

## Permeability curves for sample 4

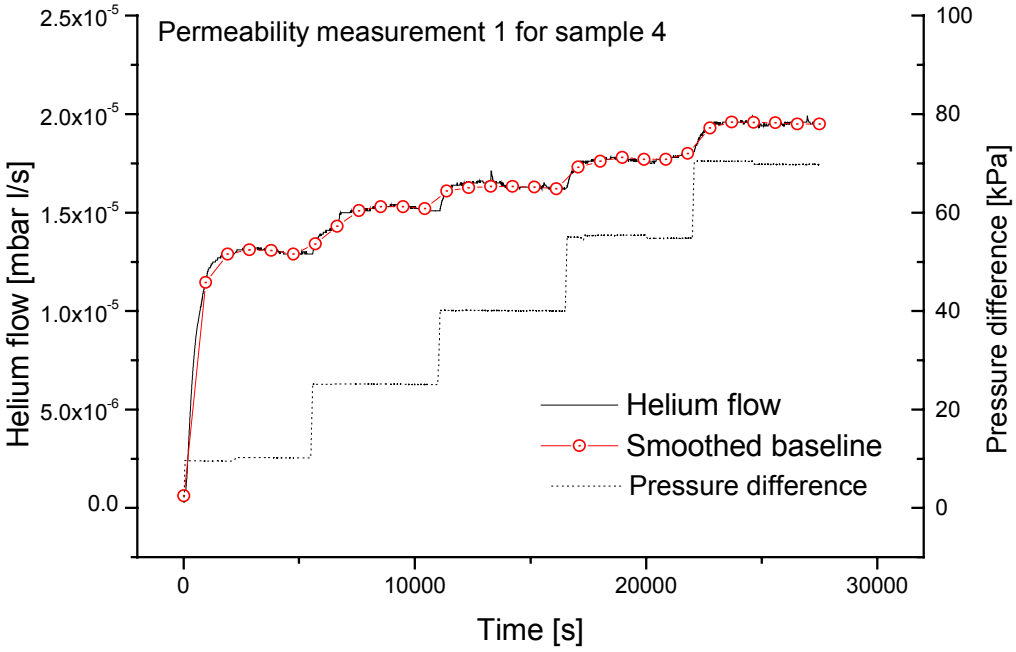


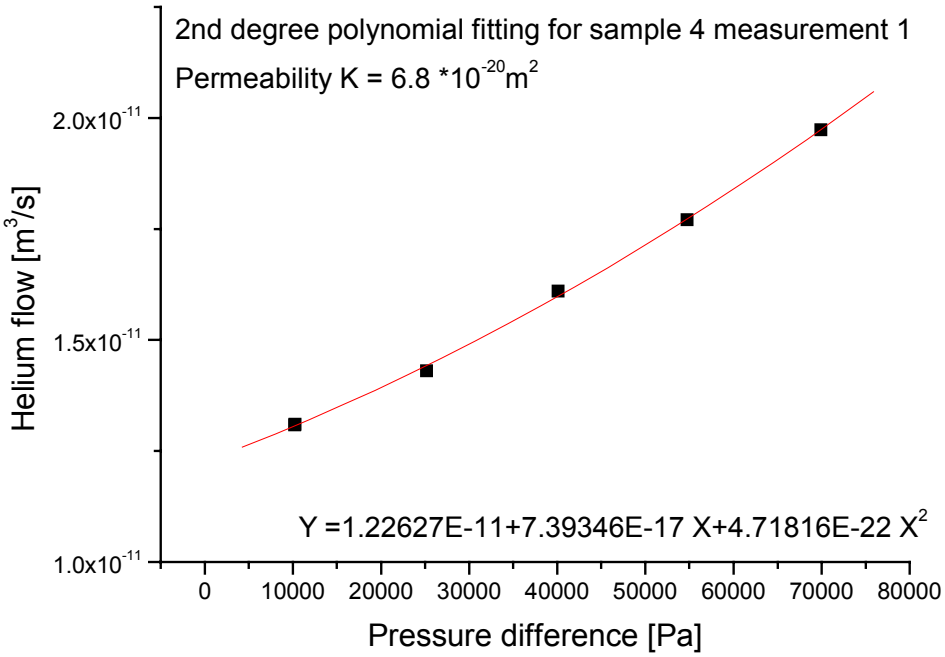

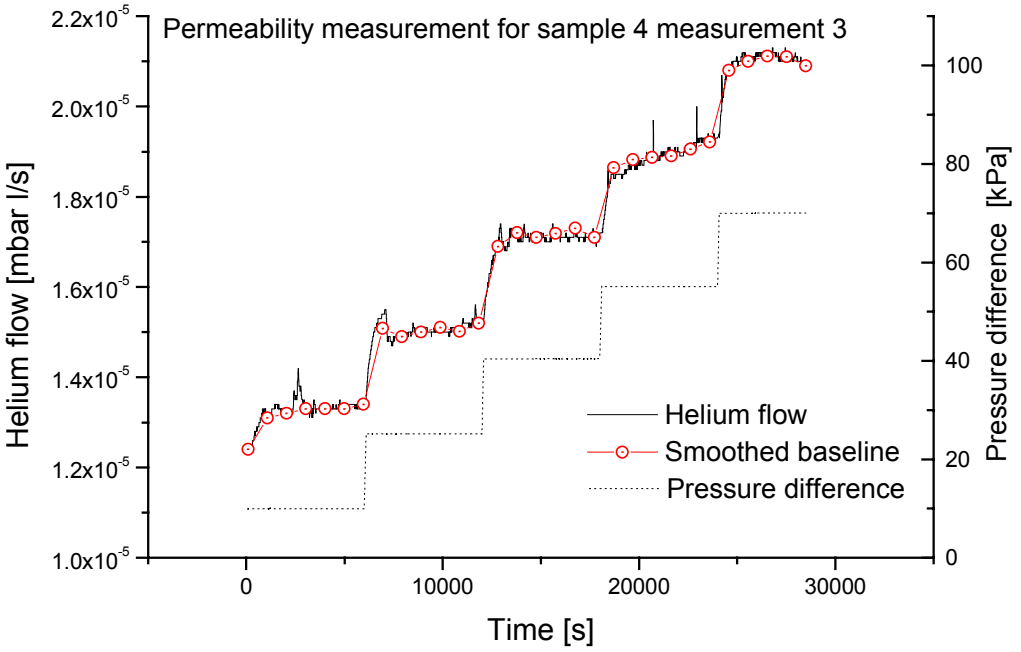
Permeability measurement for sample 4 measurement 3
Helium flow [mbar l/s]
Pressure difference [kPa]
Time [s]
Helium flow
Smoothed baseline
Pressure difference
2.2x10-5
2.0x10-5
1.8x10-5
1.6x10-5
1.4x10-5
1.2x10-5
1.0x10-5
100
80
60
40
20
0
0
10000
20000
30000

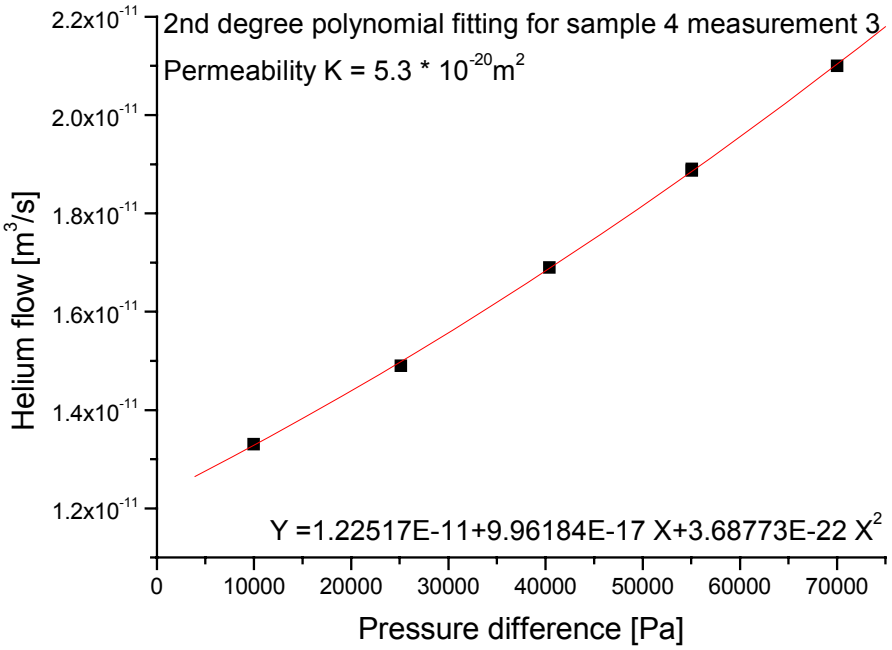
2nd degree polynomial fitting for sample 4 measurement 3
Permeability K = 5.3 * 10-20m2
Helium flow [m3/s]
Pressure difference [Pa]
Y =1.22517E-11+9.96184E-17 X+3.68773E-22 X2
2.2x10-11
2.0x10-11
1.8x10-11
1.6x10-11
1.4x10-11
1.2x10-11
0
10000
20000
30000
40000
50000
60000
70000

## Permeability curves for sample 5

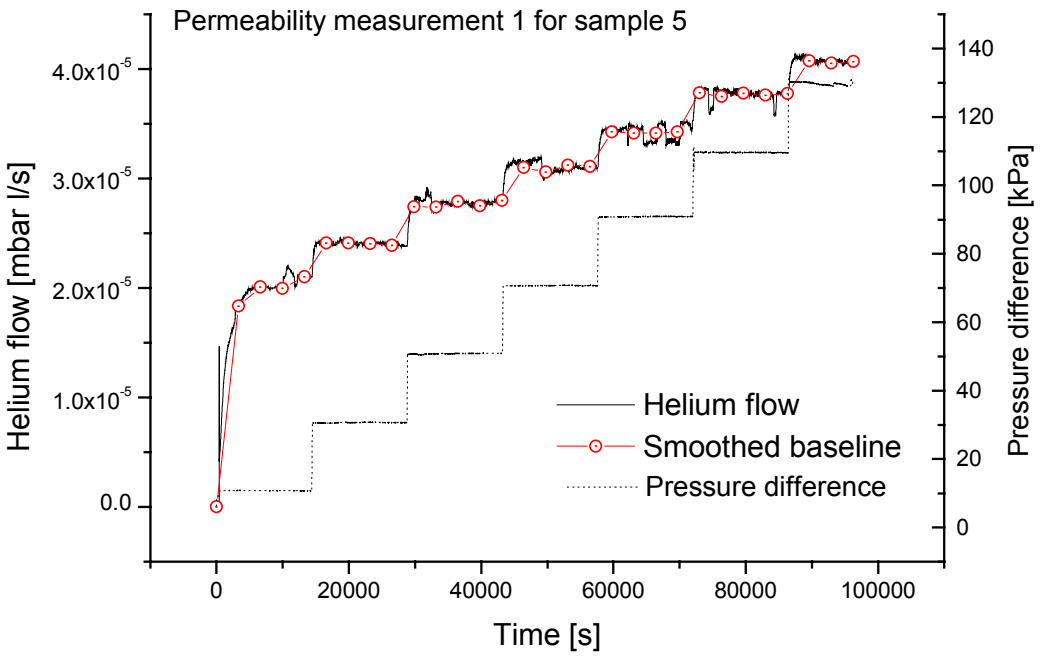


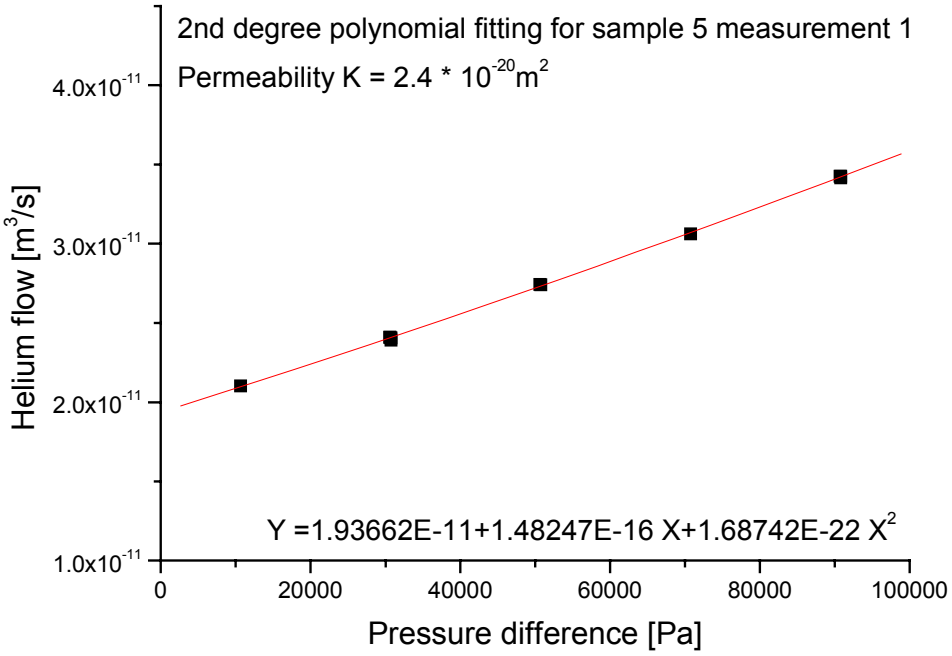

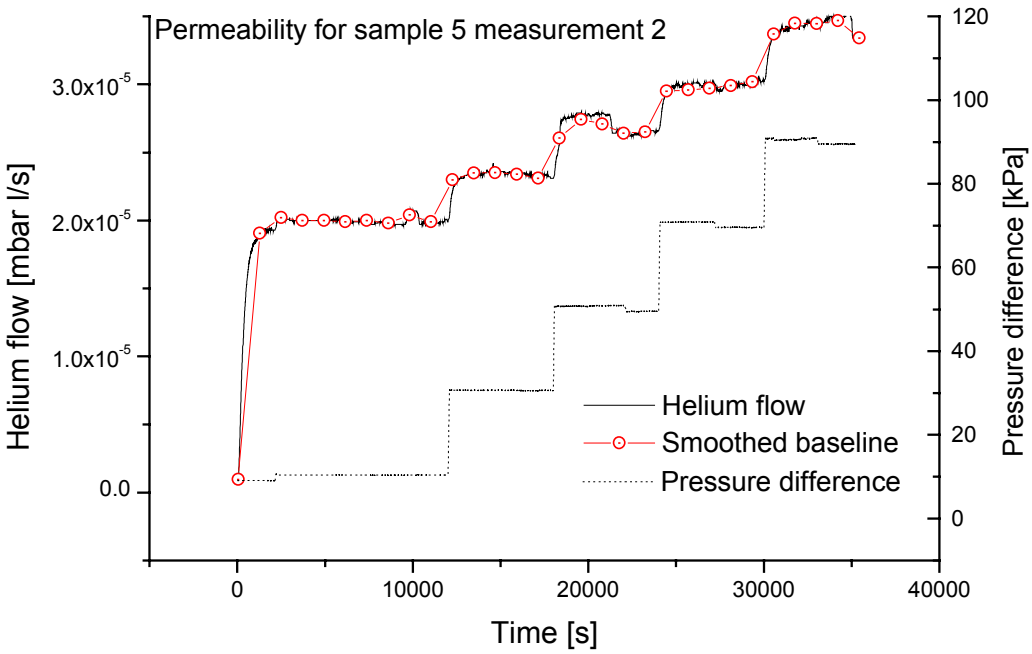
Permeability for sample 5 measurement 2
Helium flow [mbar l/s]
3.0x10-5
2.0x10-5
1.0x10-5
0.0
Pressure difference [kPa]
120
100
80
60
40
20
0
0
10000
20000
30000
40000
Time [s]
Helium flow
Smoothed baseline
Pressure difference

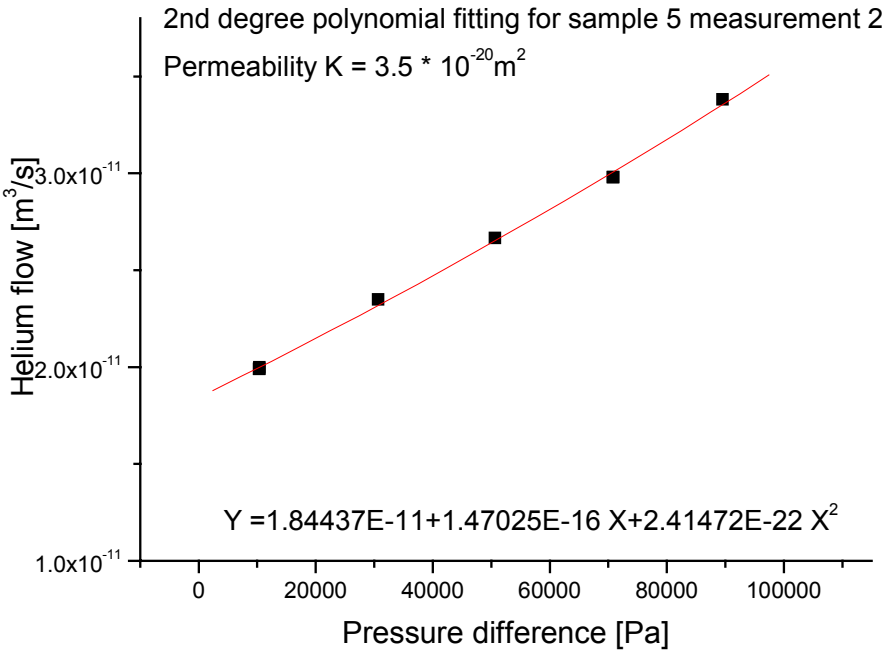
2nd degree polynomial fitting for sample 5 measurement 2
Permeability K = 3.5 * 10-20m2
Helium flow [m3/s]
3.0x10-11
2.0x10-11
1.0x10-11
Y =1.84437E-11+1.47025E-16 X+2.41472E-22 X2
0
20000
40000
60000
80000
100000
Pressure difference [Pa]

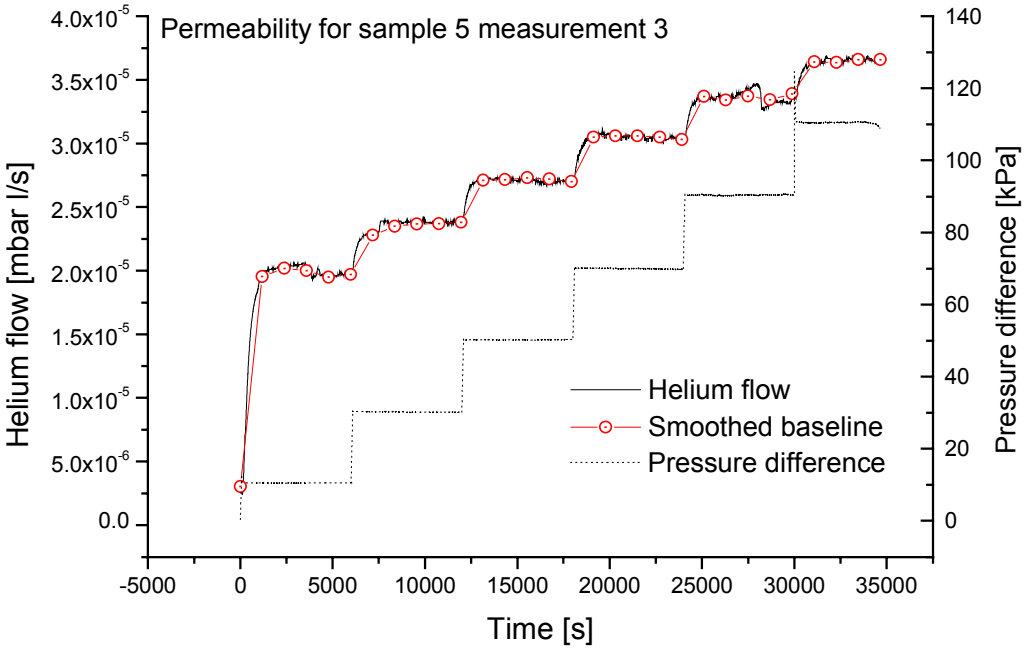
Permeability for sample 5 measurement 3
Helium flow [mbar l/s]
Pressure difference [kPa]
Time [s]
Helium flow
Smoothed baseline
Pressure difference
4.0x10-5
3.5x10-5
3.0x10-5
2.5x10-5
2.0x10-5
1.5x10-5
1.0x10-5
5.0x10-6
0.0
140
120
100
80
60
40
20
0
-5000
0
5000
10000
15000
20000
25000
30000
35000

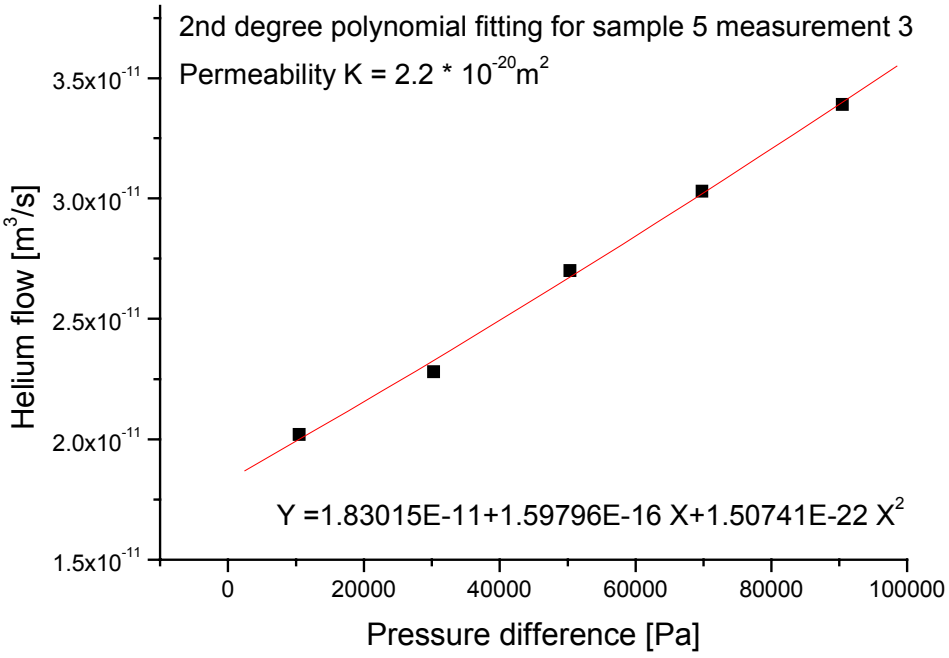
2nd degree polynomial fitting for sample 5 measurement 3
Permeability K = 2.2 * 10-20m2
Helium flow [m3/s]
Pressure difference [Pa]
Y =1.83015E-11+1.59796E-16 X+1.50741E-22 X2
3.5x10-11
3.0x10-11
2.5x10-11
2.0x10-11
1.5x10-11
0
20000
40000
60000
80000
100000

## Permeability curves for sample 6

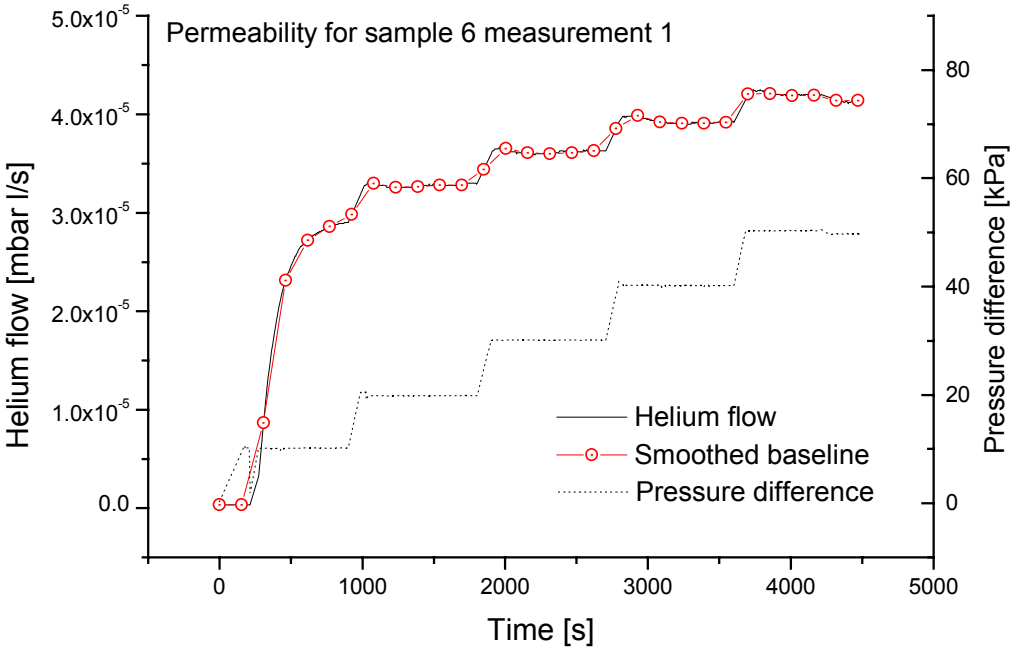


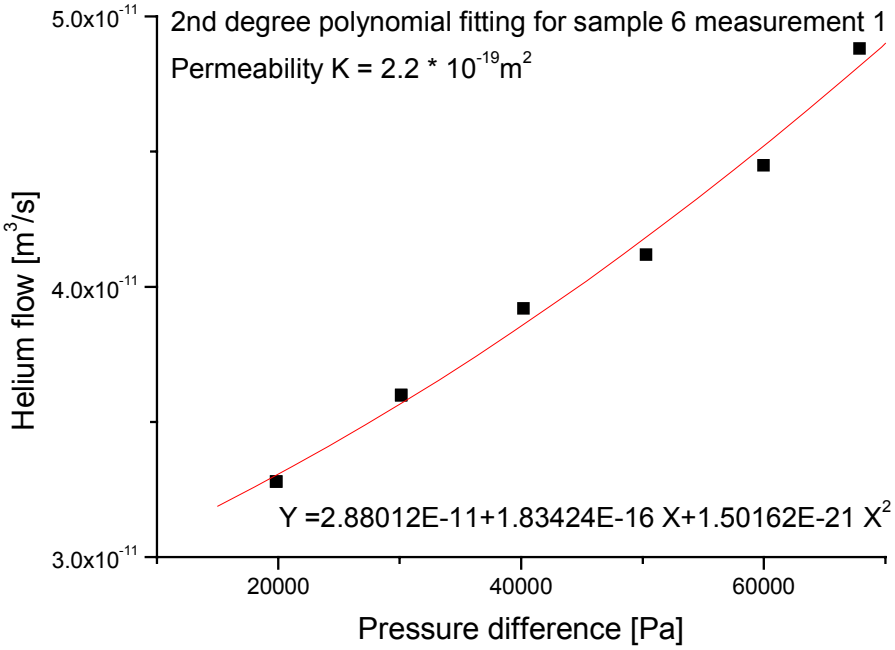

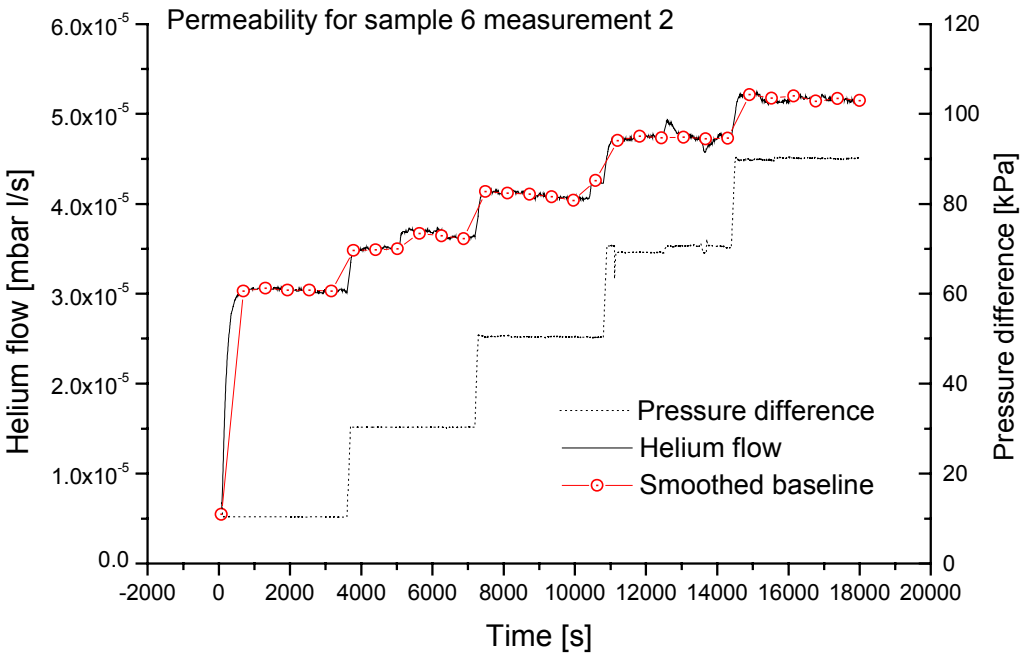
Permeability for sample 6 measurement 2
Helium flow [mbar l/s]
Pressure difference [kPa]
Time [s]
Pressure difference
Helium flow
Smoothed baseline
6.0x10-5
5.0x10-5
4.0x10-5
3.0x10-5
2.0x10-5
1.0x10-5
0.0
120
100
80
60
40
20
0
-2000
0
2000
4000
6000
8000
10000
12000
14000
16000
18000
20000

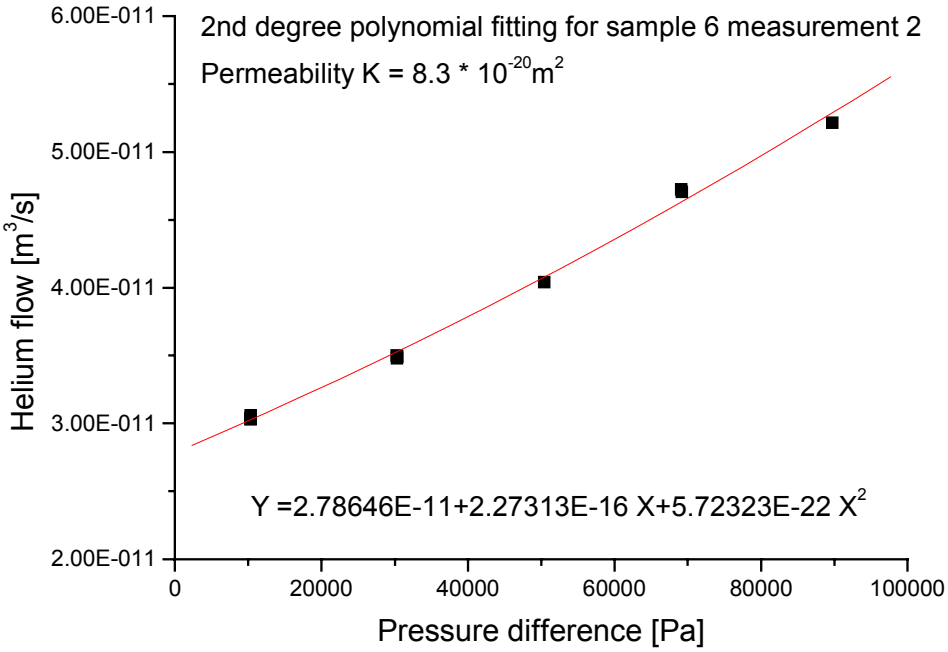
2nd degree polynomial fitting for sample 6 measurement 2
Permeability K = 8.3 * 10-20m2
Helium flow [m3/s]
Pressure difference [Pa]
Y =2.78646E-11+2.27313E-16 X+5.72323E-22 X2
6.00E-011
5.00E-011
4.00E-011
3.00E-011
2.00E-011
0
20000
40000
60000
80000
100000

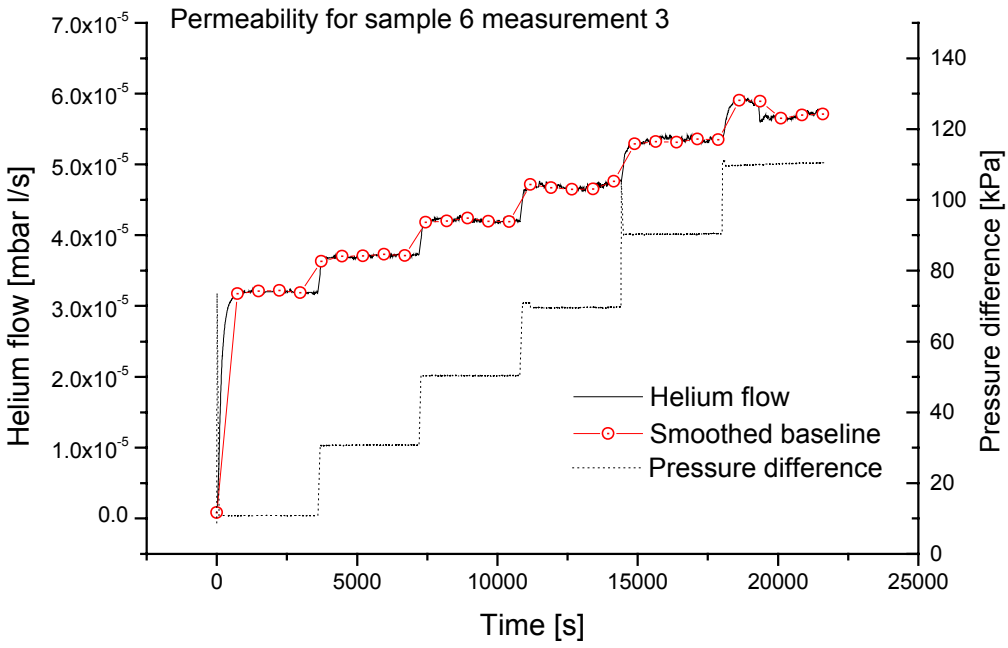
Permeability for sample 6 measurement 3
Helium flow [mbar l/s]
Pressure difference [kPa]
Time [s]
Helium flow
Smoothed baseline
Pressure difference
7.0x10-5
6.0x10-5
5.0x10-5
4.0x10-5
3.0x10-5
2.0x10-5
1.0x10-5
0.0
140
120
100
80
60
40
20
0
0
5000
10000
15000
20000
25000

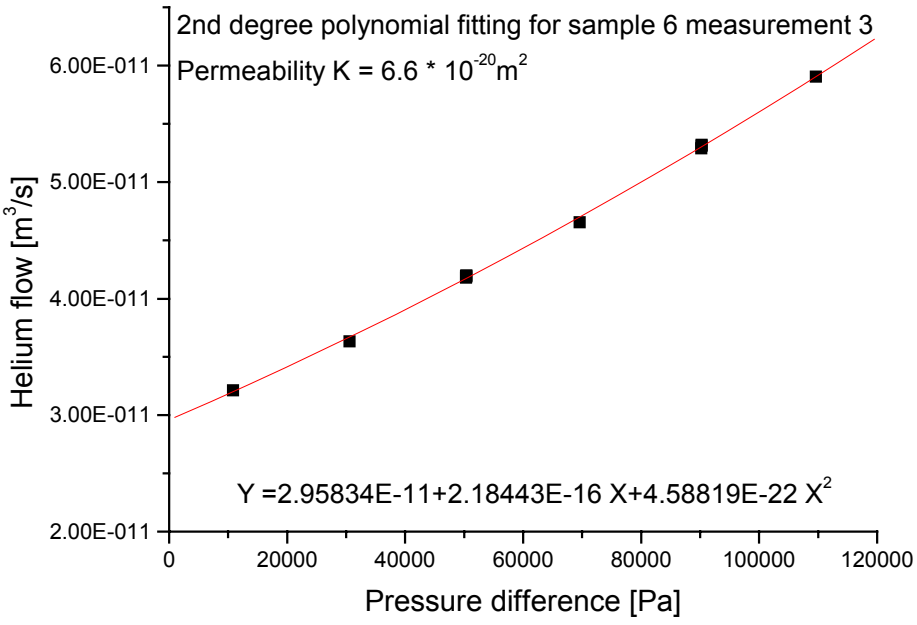
2nd degree polynomial fitting for sample 6 measurement 3
Permeability K = 6.6 * 10-20m2
Helium flow [m3/s]
Pressure difference [Pa]
Y =2.95834E-11+2.18443E-16 X+4.58819E-22 X2
6.00E-011
5.00E-011
4.00E-011
3.00E-011
2.00E-011
0
20000
40000
60000
80000
100000
120000

## Permeability curves for sample 8

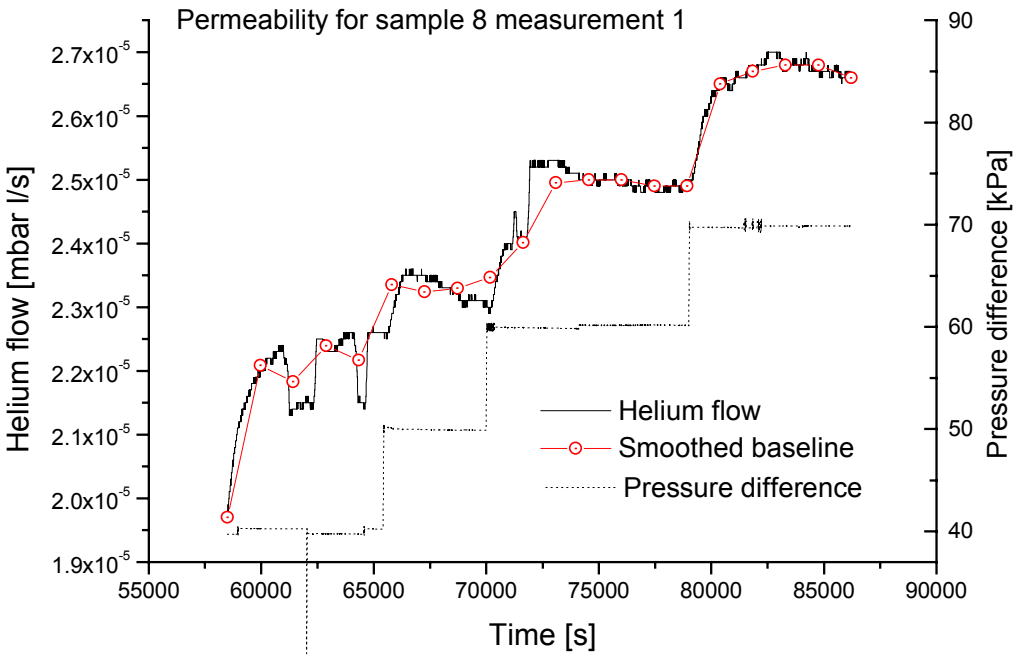


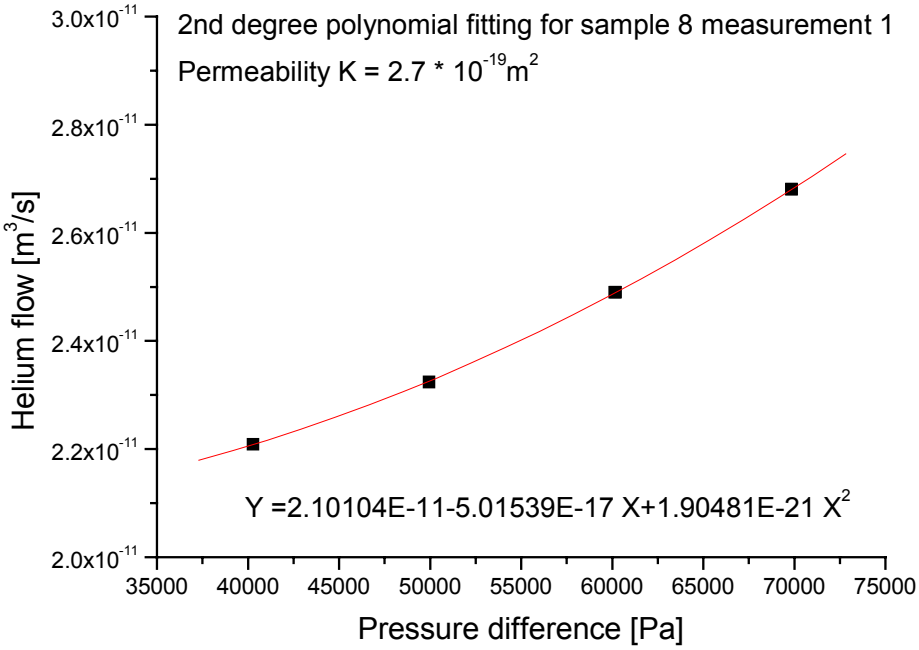

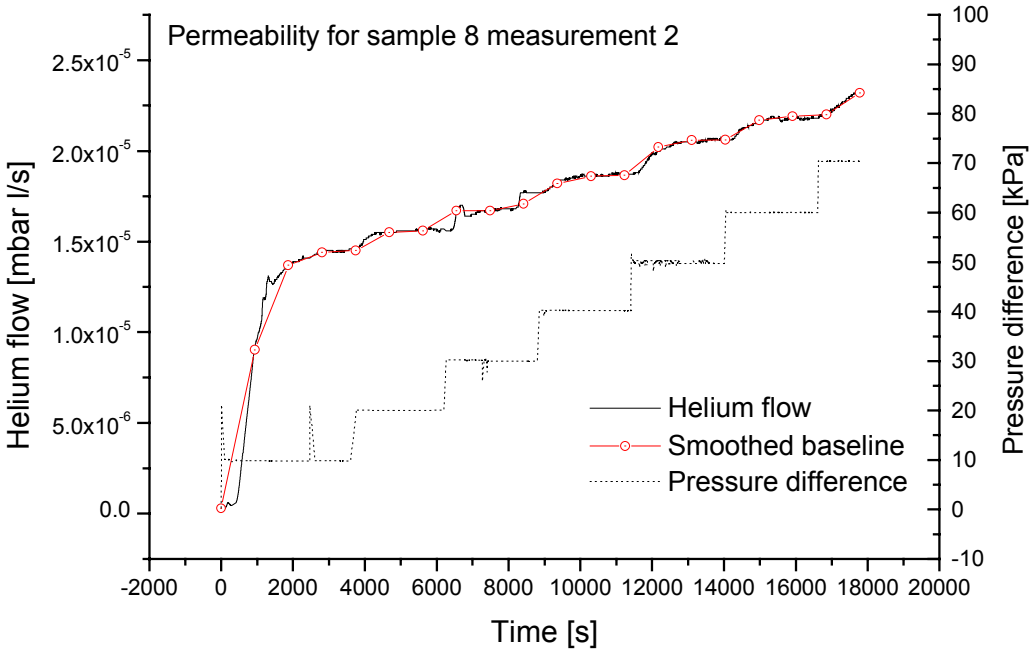
Permeability for sample 8 measurement 2
Helium flow [mbar l/s]
Pressure difference [kPa]
Time [s]
Helium flow
Smoothed baseline
Pressure difference
2.5x10-5
2.0x10-5
1.5x10-5
1.0x10-5
5.0x10-6
0.0
100
90
80
70
60
50
40
30
20
10
0
-10
-2000
0
2000
4000
6000
8000
10000
12000
14000
16000
18000
20000

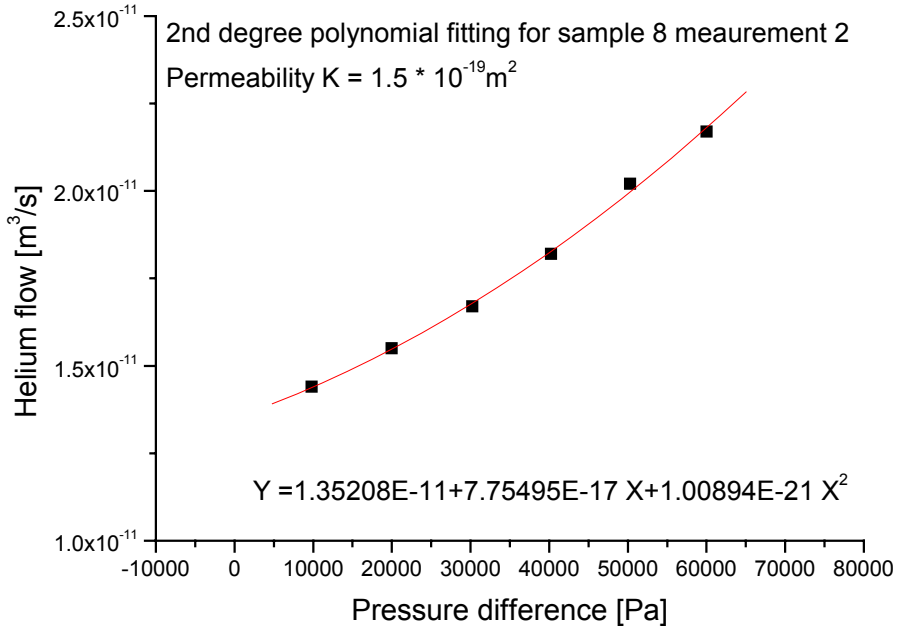
2nd degree polynomial fitting for sample 8 meaurement 2
Permeability K = 1.5 * 10-19m2
Helium flow [m3/s]
Pressure difference [Pa]
Y =1.35208E-11+7.75495E-17 X+1.00894E-21 X2
2.5x10-11
2.0x10-11
1.5x10-11
1.0x10-11
-10000
0
10000
20000
30000
40000
50000
60000
70000
80000

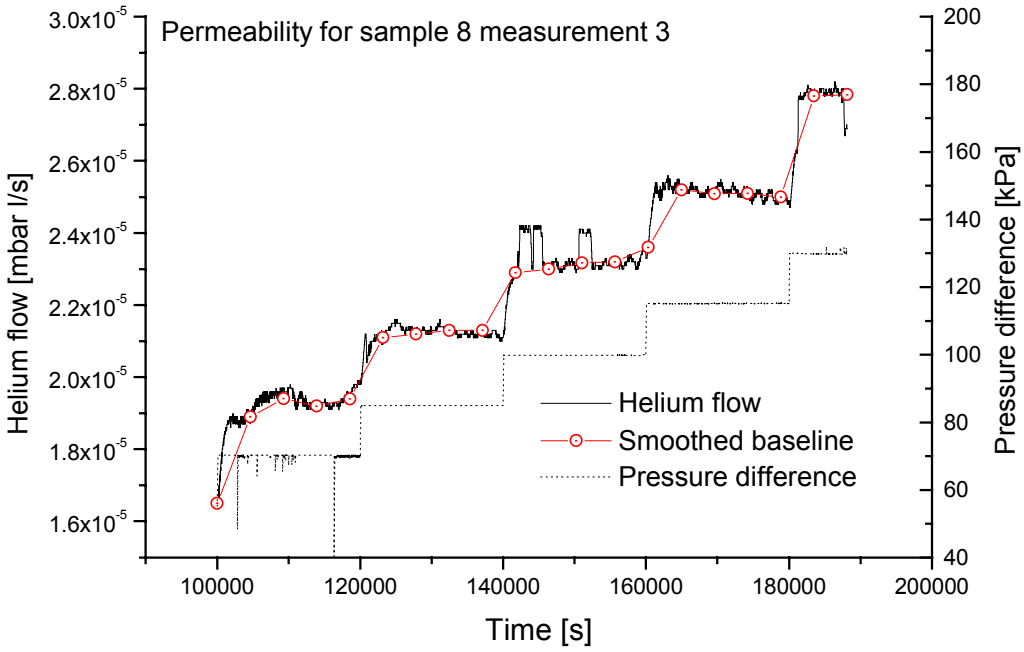
Permeability for sample 8 measurement 3
Helium flow [mbar l/s]
Pressure difference [kPa]
Time [s]
Helium flow
Smoothed baseline
Pressure difference
3.0x10-5
2.8x10-5
2.6x10-5
2.4x10-5
2.2x10-5
2.0x10-5
1.8x10-5
1.6x10-5
200
180
160
140
120
100
80
60
40
100000
120000
140000
160000
180000
200000

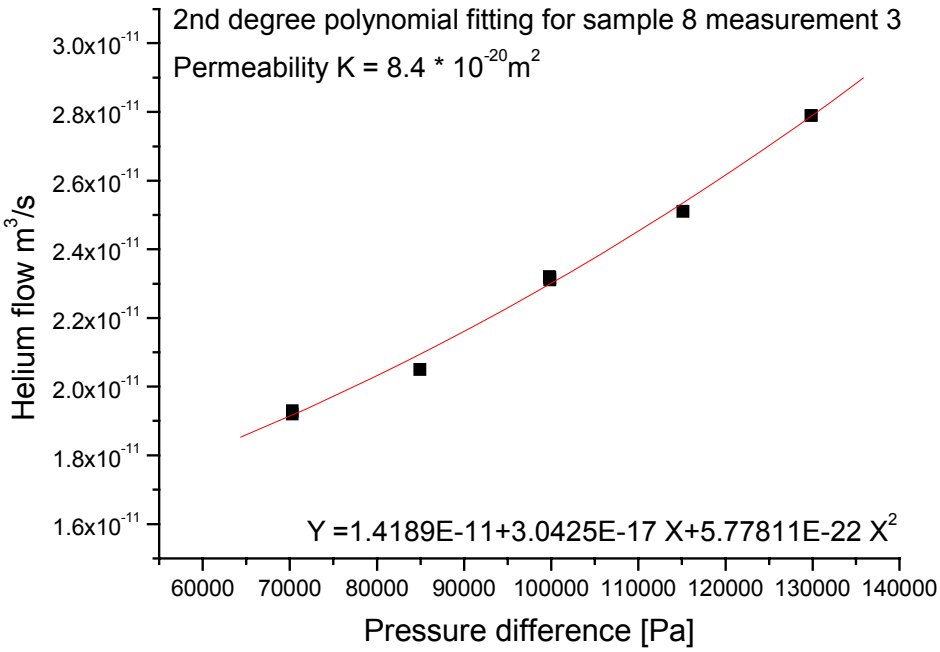
2nd degree polynomial fitting for sample 8 measurement 3
Permeability K = 8.4 * 10-20m2
Helium flow m3/s
Pressure difference [Pa]
Y =1.4189E-11+3.0425E-17 X+5.77811E-22 X2
3.0x10-11
2.8x10-11
2.6x10-11
2.4x10-11
2.2x10-11
2.0x10-11
1.8x10-11
1.6x10-11
60000
70000
80000
90000
100000
110000
120000
130000
140000